1994

Development of fast pulsed electrochemical detection of carbohydrates separated by liquid chromatography and capillary electrophoresis

Richard Earl Roberts
Iowa State University

INFORMATION TO USERS

This manuscript has been reproduced from the microfilm master. UMI films the text directly from the original or copy submitted. Thus, some thesis and dissertation copies are in typewriter face, while others may be from any type of computer printer.

The quality of this reproduction is dependent upon the quality of the copy submitted. Broken or indistinct print, colored or poor quality illustrations and photographs, print bleedthrough, substandard margins, and improper alignment can adversely affect reproduction.

In the unlikely event that the author did not send UMI a complete manuscript and there are missing pages, these will be noted. Also, if unauthorized copyright material had to be removed, a note will indicate the deletion.

Oversize materials (e.g., maps, drawings, charts) are reproduced by sectioning the original, beginning at the upper left-hand corner and continuing from left to right in equal sections with small overlaps. Each original is also photographed in one exposure and is included in reduced form at the back of the book.

Photographs included in the original manuscript have been reproduced xerographically in this copy. Higher quality 6" x 9" black and white photographic prints are available for any photographs or illustrations appearing in this copy for an additional charge. Contact UMI directly to order.

UMI

University Microfilms International
A Bell & Howell Information Company
300 North Zeeb Road, Ann Arbor, MI 48106-1346 USA
313/761-4700 800/521-0600

Order Number 9503589

Development of fast pulsed electrochemical detection of carbohydrates separated by liquid chromatography and capillary electrophoresis

Roberts, Richard Earl, Ph.D.

Iowa State University, 1994

U·M·I
300 N. Zeeb Rd.
Ann Arbor, MI 48106

Development of fast pulsed electrochemical detection of carbohydrates separated by liquid chromatography and capillary electrophoresis.

by

Richard Earl Roberts

A Dissertation Submitted to the

Graduate Faculty in Partial Fulfillment of the

Requirements for the Degree of

DOCTOR OF PHILOSOPHY

Department: Chemistry
Major: Analytical Chemistry

Approved:

Signature was redacted for privacy.

In Charge of Major Work

Signature was redacted for privacy.

For the Major Department

Signature was redacted for privacy.

For the Graduate College

Iowa State University
Ames, Iowa

1994

TABLE OF CONTENTS

GENERAL INTRODUCTION

Explanation of dissertation format. The four main sections of this dissertation consist of papers that were submitted to various electrochemical and analytical journals. The content of this thesis deals with the development of fast-pulsed electrochemical detection (PED) waveforms for liquid chromatography (LC) and capillary electrophoresis (CE). The four papers are preceded by a general introduction and followed by general conclusions and acknowledgements. References for the introduction and general conclusion will appear together following the general conclusion. The four papers are written in accordance with the guidelines of the journals to which they were submitted.

The research for this dissertation began in January of 1989, and was performed under the direction of Professor Dennis C. Johnson. Paper 1 is an investigation of the formation and dissolution of surface oxide at gold electrodes in 0.1 M NaOH. Paper 2 describes oxide formation and dissolution at platinum electrodes in 0.1 M NaOH. These studies were used to guide the development of fast-PED waveforms to be used with LC and CE. Paper 3 details the application of fast-PED waveforms for the detection of carbohydrates separated by anion-exchange LC. Paper 4 describes the optimization of fast-PED waveform for detection of carbohydrates separated by CE, and discusses the uses and limitations of these waveforms.

Importance of carbohydrates. Carbohydrates comprise the bulk of organic substance on the earth and play many roles in biological systems (1,2,3). They are important as sources of chemical energy, and are readily used by living organisms in their metabolic pathways. Plants and animals also can store this chemical energy as the polysaccharides starch and glycogen respectively. Other polysaccharides such as cellulose in plant, and chitin in arthropods provide structure for these organisms. The sheer number of plants and arthropods makes these the most abundant sources of naturally-occurring carbohydrates. The sugars ribose and deoxy ribose are also a major component of DNA and RNA.

There are many industrial uses for carbohydrates, and a nation's production of sucrose has been suggested to be a measure of its wealth (2). Sugars and starches have many uses in the food and beverage industry and are used as sweeteners and food additives. Carbohydrates such as agar and carrageenans are used to add viscosity and texture to food and cosmetics (2,4). Fermentation of sugars in grains and fruit is also used in the production of wine, beer, spirits and vinegars. In addition, carbohydrates such as starch and cellulose are important to the textile and paper industries (5).

Carbohydrates are useful in the pharmaceutical industry, where sugars are used to increase the palatability of medicines, and starches are used as binders in pills and capsules(6). Popular antibiotics, such as streptomycin and erythromycin, contain sugar moieties and act by interfering with protein metabolism in many bacteria. (7,8). The anticoagulant heparin is also a polysaccharide and is used to prevent blood clotting (9).

Recently, the sugar moieties on the surface of cells have been implicated in the disease process, and are used by bacteria and viruses to identify their hosts (10). Abnormal carbohydrate structures have also been noted in cancerous cells and in arthritis (10,11), and there is much interest in the development of carbohydrate-based drugs for the treatment of these diseases.

Sugars also have clinical significance, and their presence in body fluids and tissues is used in the diagnosis of disease. The most common disease associated with the presence of glucose in blood or urine is diabetes. Over 11 million Americans have diabetes (12), and blood sugar analysis is important in diagnosis and effective management of this disease. Melituria is a general category of disease arising from an enzymatic deficiency that leads to the inability to metabolize certain sugars (13). For example, the melaturia known as fructosuria arises from an absence of the enzyme fructokinase and results in the accumulation of fructose in the blood and urine. The presence of abnormal amounts of specific sugars in urine is diagnostic for these diseases.

Classical methods for analysis of carbohydrates mixtures. Carbohydrates lack extensive π-bonding, and they are not easily detected by direct photometric techniques such as UV-vis or fluorescence methods. However, many researchers have used chemical derivatization to allow quantitation of carbohydrate derivatives. To resolve individual sugars in complex mixtures of carbohydrates, they must be separated before

analysis. Recent developments in the separation and detection of carbohydrates recently have been reviewed (14).

Until the mid-1980s, carbohydrates frequently were determined by thin layer chromatography (TLC) and paper chromatography (PC), and comprehensive treatments of these techniques have been published (15,16,17). Although these methods are semi-quantitative at best, they are still prescribed as methods for analysis of carbohydrate mixtures (18). This probably is due to the simplicity of analysis and the modest instrumental requirements. Once carbohydrates are separated by either TLC of PC, derivatization is required for visualization. Ammoniacal silver nitrate is one of the most popular reagents for visualization of carbohydrate bands (19).

Gas chromatography (GC) also has been used for the analysis of carbohydrate mixtures. However, most carbohydrates are not volatile, and they decompose in the injection port of the GC (20). Therefore, carbohydrates must be derivatized to produce volatile, thermally stable products for GC analysis. A comprehensive review of derivatization techniques for GC determination of carbohydrates has been published (21). The most frequently used dervatizations are the conversion of carbohydrates to trimethyl silyl derivatives and alditol acetates.

Liquid chromatography of carbohydrates also has been used in conjunction with common detectors such as UV-vis and conductivity. Carbohydrates have low photometric activity, and require derivatization for detection by UV-vis or fluorometric methods. Phenylisocyanate is one of the more popular derivatives for UV-vis detection

of carbohydrates, and allows detection of ca. 10 pmol of most monosaccharides (22). Acyl derivatives of carbohydrates using benzoyl chloride (23) and p-nitrobenzoyl chloride (24) also are used. Although carbohydrates are not detected directly by conductivity, their borate complexes are acidic enough to allow detection by conductometric detection (25).

Nearly all of the techniques mentioned above require extensive preinjection or postcolumn sample preparation before analysis. This is time consuming, and may lead to errors caused by formation of multiple derivatization products, or in postcolumn reaction it may cause extra column broadening. Therefore, the direct and sensitive detection of carbohydrates (or any other analyte) will always be preferred.

Pulsed electrochemical detection. Typically, carbohydrates have been believed to have little amperometric response under constant potential detection at Au and Pt electrodes. However, they have been found to undergo surface-catalyzed oxidations at the surface of these electrodes resulting in the accumulation of adsorbed reaction products and inert oxides at the electrode surface. This causes attenuation of the amperometric signal, and has lead to the belief that these electrodes are not active for detection of carbohydrates. Hughes and Johnson developed a pulsed-potential waveform for detection of carbohydrates at Pt electrodes that maintains activity by application of anodic and cathodic potential steps to clean the electrode surface between detection steps (26). Gold electrodes have been found to have greater sensitivity for the detection of

carbohydrates than Pt electrodes and are used in most applications. PED waveforms also can be designed for Au which give virtually no response for the reduction of dissolved O_2. During the detection step, current is sampled over an integration period, and analytical signal is usually reported as an average current. Hence, this detection technique has become known as pulsed amperometric detection (PAD), and is applied at a frequency of *ca.* 1 Hz. Recently, coulometric detection schemes have been developed, and all techniques that incorporate potential-step waveforms are now referred to as pulsed electrochemical detection (PED) regardless of the mode of signal reporting.

Since its introduction, PED has become the preferred method for the detection of carbohydrates and polyalcohols. Pulsed detection schemes have also been devised for the detection of amines (27,28), amino-acids (29,30), sulfur containing compounds (31-34), and even arsenic (35). Several reviews of PED have been published that describe general principles and applications in liquid chromatography (36-39).

Capillary electrophoresis. Capillary electrophoresis is a rapidly developing separation technique, and has been the subject of several recent reviews (40,41) and textbooks (42 - 45). The primary allure of CE is the rapid and efficient separations (> 100,000 theoretical plates) which are possible. Additionally, the small sample volumes required (50 nl>) allow sampling of small microenvironments. In fact, CE has been used to analyze the contents of single cells (46 - 48). Separation in CE is achieved by applying a large voltage (10 - 40 kV) across a fused silica capillary, causing the

separation of molecules based upon their mass to charge ratio.

Detection methods developed for CE are similar to those used in LC. Most applications of capillary electrophoresis rely on UV-vis or fluorometric detection, because these are the only detectors available in commercial systems. Therefore, most applications of CE for the detection of carbohydrates require derivatization before analysis. Borate complexes of carbohydrates have been known to have a strong UV absorbance (49), and several researchers have exploited this by using borate in their running buffers for the detection of carbohydrates (50) and derivatized carbohydrates (51,52,53). Liu, Shirato and Novotony used 3-(4-Carboxybenzyl)-2-quinolinecarboxaldehyde as fluorescent label for the detection of carbohydrates (54). Additionally, carbohydrates have been detected by using indirect UV absorbance (55) and indirect fluorescence (56). Typically, photometric detections have high concentration detection limits (*ca.* 1 mM) because of the short path length in CE systems. As in LC investigations, derivatization is time consuming, and may lead to multiple derivatization products, and increased band broadening. Therefore, direct detection techniques are preferred, when available.

Electrochemical detection in CE is not dependent on the inner dimensions of the capillary, and significant developments in electrochemical detection for CE have been reviewed elsewhere (57,58). Most applications of electrochemical detection in CE use off-column detection to reduce noise caused by fluctuations in the high voltage power supply. Decoupling of the high-voltage power supply is achieved by forming a porous

junction a short distance from the detector. Several methods have been devised, that use porous glass (46, 59), or polymer (60) coated fractures in the capillary. When a decoupler is used, electrophoretic separation occurs up to the point of the porous junction, and the running buffer is swept over the remaining section of capillary by electroosmotic flow. Recently, Lu and Cassidy determined that use of decouplers may not be necessary for capillaries that have very small ($<< 25$ μm) inner diameters (61).

Electrochemical detection has been used primarily for the detection of easily oxidized or reduced species such as catechols (46,62), ascorbate (62), and neurotransmitters (63). However, the constant-potential detection of carbohydrates separated by CE has been described at conventional sized Cu electrodes (64) and Cu microwire electrodes (65). Although, LC applications for PED are well developed, few applications of CE-PED have appeared in the literature. A system for off-column CE-PED of carbohydrates, using a Nafion-coated decoupling junction and 300 - 350 $\times$ 50-μm Au microwire electrodes, was described by Lunte, O'Shea, and LaCourse (66). Lu and Cassidy (67) also described CE-PED of several carbohydrates using a Au microdisk electrodes with on-column PED of carbohydrates. In both of these studies, waveforms of *ca.* 1.6 Hz were used for the description of electrophoretic peaks.

Although 1-Hz waveforms commonly are used in liquid chromatography, we are concerned whether these are sufficient for detection of narrow elution peaks of carbohydrates separated by capillary electrophoresis. Guidelines for CE detection suggest that 25 - 30 points are sufficient for description of an analyte peak (68).

Therefore, a 10-s CE peak would require a PED waveform frequency of *ca.* 2.5 - 3.0 Hz for reproducible results.

Electrode current in PED routinely is sampled over an integer multiple (n) of 16.7 ms (1/60 Hz) to discriminate against 60-Hz line noise (*i.e.*, integration time = 16.7n ms). Neuberger and Johnson (69) reported a significant increase in the signal to noise ratio (S/N) for PED as the value of n is increased. Typically, a 200-ms integration period (n = 12) is recommended to provide optimal discrimination against both 50 and 60-Hz line noise. LaCourse and Johnson also used pulsed-voltammetry experiments at a Au rotated-disk electrode (RDE) to determine the optimum PED waveform parameters for detection of carbohydrates separated by LC (70). Their work suggests that a 1-Hz waveform with a 200-ms integration period will provide optimum sensitivity for the detection of carbohydrates.

To achieve frequencies greater than 1 Hz, the time periods for each step in the PED waveform need to be minimized. Because oxide formation and reduction are significant features of the PED waveform, decreasing the time spent cleaning the electrode surface is necessary in the development of fast-PED. The first two chapters of this work describe kinetic investigations of oxide formation and reduction at Au and Pt electrodes. These studies are then used as guidelines for design of fast-PED waveforms for detection of carbohydrates separated by LC and CE. The last two chapters describe the applications of fast PED for LC and CE, and discuss practical considerations, and limitations of increased PED waveform frequency.

PAPER 1.

FAST PULSED AMPEROMETRIC DETECTION AT NOBLE METAL ELECTRODES: A STUDY OF OXIDE FORMATION AND DISSOLUTION AT GOLD IN 0.1 M NaOH[1]

[1]Reprinted with permission from R.E. Roberts and D.C. Johnson, *Electroanalysis, 4* (1992) 741.

ABSTRACT

The anodic charge (q_a) for oxide formation, obtained by potential-step chronocoulometry at a Au minidisk electrode, is nearly a linear function of log(t/ms) for t = ca. 3-30 ms with a slope proportional to the applied overpotential for oxide formation. It was demonstrated that, contrary to popular opinion based on voltammetric observation at slow scan rates (ϕ), the anodic current for oxide formation obtained using a linear potential-scan waveform is not a linear function of ϕ at large values of ϕ. It was also demonstrated that a reverse potential-step waveform can be used to interrupt the rapid oxide growth and, perhaps, inhibit the conversion of the hydrous oxide (AuOH) to the inert oxide (AuO). This result has probable significance for decreasing the background current during anodic pulsed amperometric detection of amines and sulfur compounds whose oxidation mechanisms are believed to be catalyzed by AuOH but not by AuO. The cathodic charge (q_c) for oxide dissolution is approximately a linear function of t with a slope that is proportional to the applied potential.

INTRODUCTION

Extensive research in our laboratory is directed toward the development of pulsed amperometric detection (PAD) at noble-metal electrodes for application in liquid chromatography (LC) [1]. Emphasis has been placed on the detection of polar aliphatic compounds at Au electrodes in alkaline media (pH $\geq$ *ca.* 13). Compounds of primary interest are polyalcohols and carbohydrates. Whereas detection of these compounds at Au electrodes held at constant potential is not satisfactory because of rapid loss of electrode activity, reproducible and sensitive detection can be achieved easily using pulsed potential-time (*E-t*) waveforms [2]. Pulsed waveforms at Pt electrodes also are useful for sensitive detection of simple alcohols and glycols in acidic media [3].

The PAD waveform most commonly applied to Au electrodes at pH $\geq$ *ca.* 13 comprises three potential steps, as is illustrated in Figure 1A. In this so-called normal-PAD waveform (N-PAD), detection occurs at E_1 = 0.0 - +0.2 V, with measurement of the amperometric signal following a delay of *ca.* 100 - 200 ms. Very little surface oxide is formed on Au for E_1 values in this range. Efficient oxidative cleaning of the Au surface occurs at E_2 > *ca.* +0.6 V, typically applied for a period of *ca.* 50 - 200 ms, which corresponds to rapid formation of surface oxide (AuO) with oxidative desorption of adsorbed carbonaceous species. Reductive reactivation occurs at E_3 < -0.6 V, typically applied for a period of *ca.* 200 - 500 ms, with rapid cathodic conversion of the oxide-covered surface back to the clean and reduced metal. As described, frequencies of N-PAD waveforms are in the range of 0.5 - 1 Hz. Detection limits for N-PAD applied

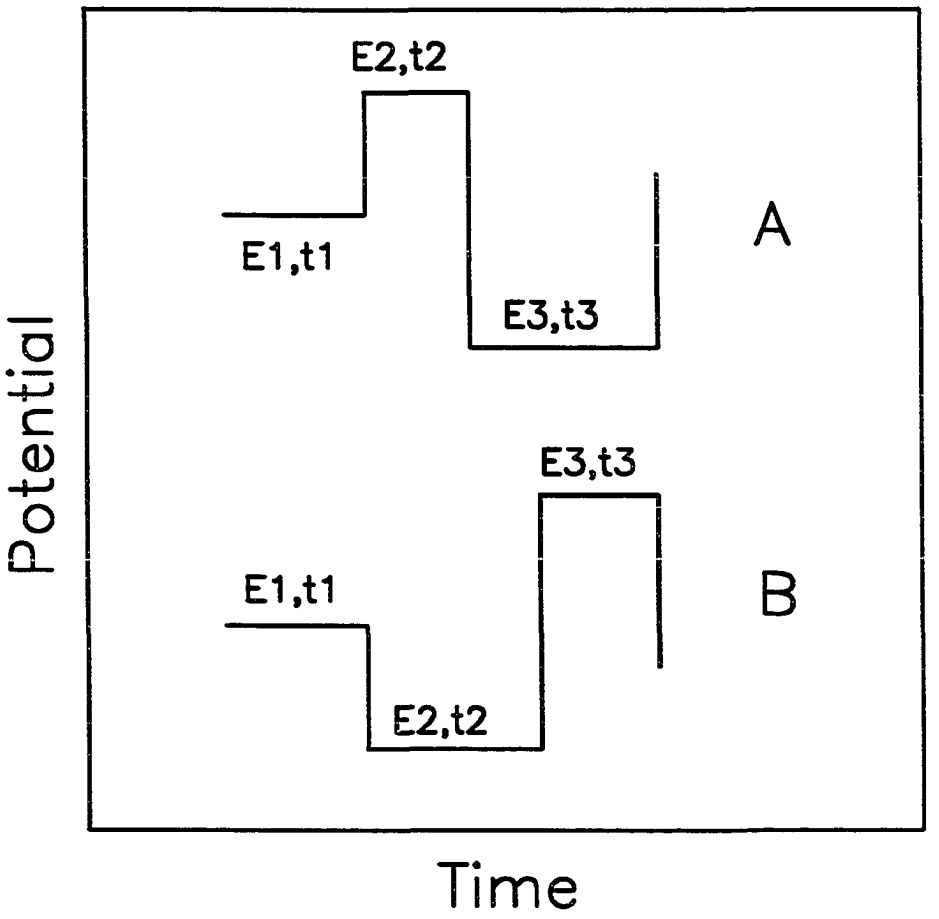

Figure 1. Pulsed amperometric detection (PAD) potential-time waveforms. (A) normal-PAD, (B) reverse PAD.

for monosaccharides separated by LC are presently at the picomole level [2].

We have growing interest in application of PAD at noble metal electrodes for aliphatic amines, including amino acids, and for inorganic and organic sulfur compounds. Detection of these compounds by N-PAD at Au electrodes (pH $\geq$ *ca.* 13) requires a waveform with E_1 in the range +0.2 - +0.6 V, corresponding to the formation of surface oxide. A major component of the anodic signal for amines and sulfur compounds results from the oxide-catalyzed oxidative desorption of analyte previously adsorbed at the oxide- free Au surface at E_3 < -0.6 V in the N-PAD waveform. The catalytic form of oxide is believed to be the hydrous oxide (AuOH), which is formed as a short-lived intermediate species in the production of the inert surface oxide.

A significant difficulty associated with application of N-PAD for amines and sulfur compounds, following their separations by LC, is the large background signal associated with oxide formation at E_1 > +0.2 V. In addition to the difficulty of detecting small LC peaks on a large background signal, complications can result in calibration of N-PAD response because the true background for the peak response is likely to be smaller than that observed before and after the LC peak. This can result because of inhibition of the oxide formation kinetics by adsorbed analyte. Furthermore, the background is observed to increase slowly as a result of a gradual increase in the true surface area of the electrode caused by surface reconstruction as a consequence of the repeated cycles for oxide formation and dissolution. The alternate waveform shown in Figure 1B was suggested by Polta and Johnson [4] to decrease the background signal

for detection of some inorganic sulfur species. In this so-called reverse-PAD waveform (R-PAD), the order of application of E_2 and E_3 is reversed from that in the N-PAD waveform. It was suggested [4] that the rate of oxide growth at E_1 is substantially decreased because of the prior, more rapid oxide growth at $E_3 > E_1$; however, no direct experimental evidence was presented in support of this supposition. Further exploration of this concept is a goal of this report.

We are also concerned with increasing the frequency of PAD waveforms. Whereas frequencies presently typical of PAD (0.5 - 1 Hz) ar compatible with present separations of carbohydrates using high-performance anion-exchange chromatography, they are not adequate to follow the sharp elution peaks obtained in reverse-phase and capillary-column chromatography, as well as capillary electrophoresis. Hence, we have initiated a study of those factors that ultimately limit the high-frequency of PAD waveforms applied at noble metal electrodes having small dimensions consistent with ultimate application for the separation techniques named. Because of the significance of anodic formation of oxide in PAD, our initial attention is focussed on the kinetics of these reactions. Results are reported here for Au electrodes in 0.1 M NaOH.

Gilroy [5,6] studied the kinetics of oxide formation at Pt electrodes in 1 M H_2SO_4. Values for the anodic charge (q_a) were determined as a function of time (t) following positive steps of potential (E) into the voltammetric region corresponding to oxide formation at reduced Pt surfaces. Plots of q_a vs. $\log(t/t_o)$ were linear, as described by Equation 1, where t_o is a time constant that corresponds to the units for t. Values of the intercept (A_a)

$$q_a = A_a + B_a \log\left\{\frac{t}{t_o}\right\} \tag{1}$$

were not discussed; however, from Figures 2 and 3 [5], it is apparent that A_a is not zero and is potential dependent. The slope (B_a) is reported to be proportional to the applied overpotential for oxide formation, as given by Equation 2, where $E_{o,a}$ is the potential corresponding to the onset of oxide formation.

$$B_a = C_a(E_a - E_{o,a}) \tag{2}$$

Our estimate of C_a from Figure 4 [5] is 18.6 μC V^{-1} or, with normalization for surface area (0.38 cm^2), we estimate 48.8 μC V^{-1} cm^{-2}. Gilroy demonstrated that the growth of oxide on Pt electrodes in 1 M H_2SO_4 can be temporarily halted when E is stepped from a value $E_1 >> E_{o,a}$ back to a value E_1' described by the relationship $E_1 > E_1' > E_{o,a}$. Then, at a value of t for which the q_a accumulated at E_1 equals q_a predicted by Equation 1 for E_1', q_a again increases according to Equation 1 for E_1'.

Gilroy and Conway [7], and Angerstein-Kozlowska, Conway, *et al.* [8 - 10] also arrived at logarithmic growth laws for Pt [7-9] and Au [10] electrodes in acidic media that are in agreement with the form of Equation 1. Using fast negative scans, after holding the electrode potential in the region of oxide formation, Conway et al. also demonstrated that multiple peaks can be obtained for oxide reduction at Pt electrodes [8 - 10]. This was attributed to the presence of multiple states for adsorbed oxygen. The kinetics of oxide growth also were discussed by Roscoe and Conway [9] in relation to the kinetics of Cl_2 evolution.

EXPERIMENTAL

Equipment. Data were obtained using a Au rotated minidisc electrode (Pine Instrument) with a geometric area (A_{geo}) of 0.00785 cm^2. Potentiostatic control was maintained by a model 173 potentiostat/galvanostat with a model 176 current follower (EG&G Princeton Applied Research). Potential Waveforms were applied and data acquisition achieved using a DT2821 interface (Data Translation) in conjunction with a Zenith 286 computer. Programs for pulsed-potential control and data processing were prepared using Asyst software (Data Translation). Fast linear-scan voltammetry was performed using a Au microdisk electrode (A_{geo} = 78 μm^2, Koslow) with waveforms generated by a Model 175 universal programmer (EG&G Princeton Applied Research). A miniature SCE (Fisher Scientific) was used as the reference electrode and potential values were reported in V *vs.* SCE. The counter electrode was a coiled Pt wire (*ca.* 2 cm^2). The reference and auxiliary electrodes in the electrolysis cell were separated from the working electrode by porous glass disks.

Reagents. The NaOH was reagent grade (Fisher Scientific), and all water was purified by passage through two D-45 demineralizing cartridges (Culligan) with further treatment in a Milli-Q system (Millipore). Solutions were deaerated by dispersed $N_2(g)$, and an inert atmosphere was maintained over the solutions during experimentation

Procedures. Data were obtained at ambient temperature (25° $\pm$ 2° C). Electrodes were polished with 0.05-μm alumina in water on microcloth (Buehler) and then rinsed with deionized water. Polished electrodes were preconditioned voltammetrically for 30 minutes in the test solutions by cycling the potential between values for anodic discharge of H_2O to produce O_2 (+0.65 V) and cathodic discharge of H_2O to produce H_2 (-1.40 V) at a scan rate (ϕ) of 5 mV ms^{-1}.

The waveforms applied (Figure 2) are similar to those used by Gilroy [5,6] and Gilman [11] in that electrode surfaces were activated by repeated potential alternations between values for anodic formation and cathodic dissolution of surface oxide. Following 10 alternate applications (i.e., n = 10 in Figure 2) of E_2 = +0.8 V (t_2 = 50 ms) and E_3 = -0.8 V (t_3 = 200 ms), the potential was stepped from E_3 to E_1, and the recording of *i-t* data was initiated. The waveform in Figure 2A is similar to the N-PAD waveform (Figure 1A) because of the positive potential step at the oxide free electrode for E_3 to E_1 >> E_3, and *i-t* data were recorded throughout the period t_1. The waveform in Figure 2B is similar to the R-PAD waveform (Figure 1B) because of the reverse potential step at the partially oxide-covered electrode from E_1 >> E_3 to E_1' < E_1, and *i-t* data were recorded throughout the combined periods $t_1 + t_1$'. In both waveforms, *i-t* data were recorded for a total period of 1000 ms, and *q-t* data were generated by digital integration of *i-t* data.

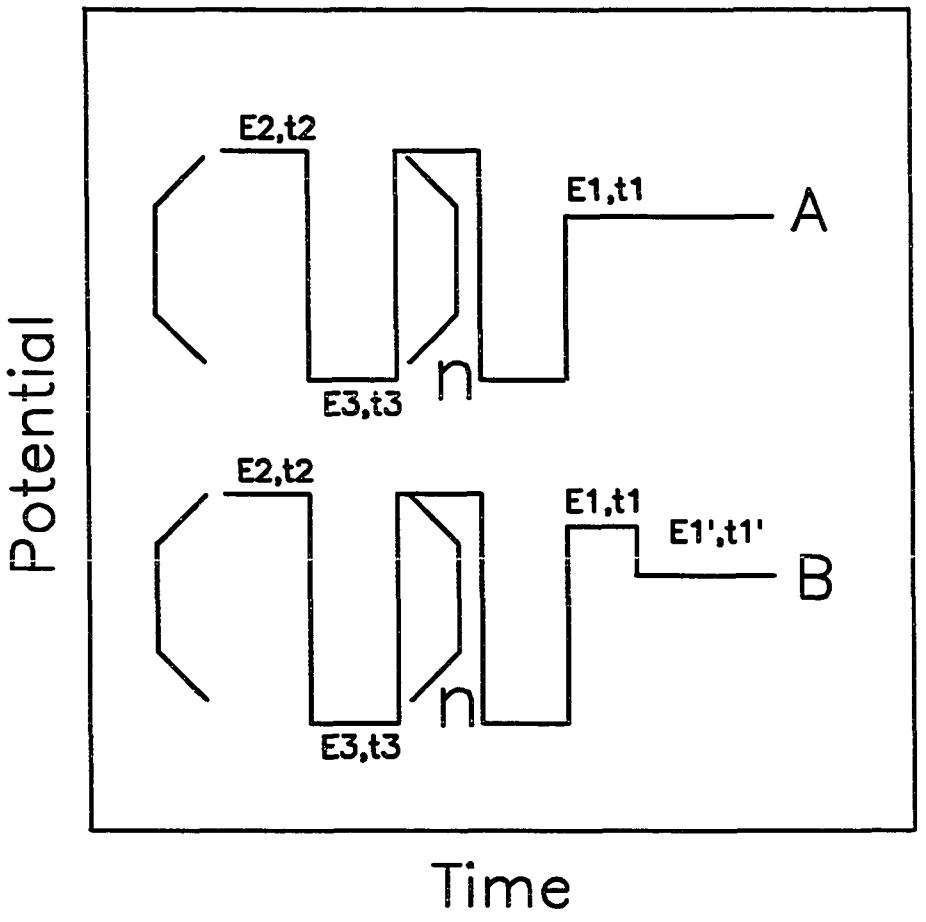

Figure 2. Potential-step waveforms used in studies of oxide formation. (A) Normal potential-step waveform: n = 10, E_2 = +0.8 V, t_2 = 50 ms, E_3 = -0.8 V, t_3 = 200 ms, E_1 = +0.3-+0.7 V, t_1 = 1000 ms. (B) Reverse potential-step waveform: n = 10, E_1 +0.55 V, t_1 = 5 ms, E_1' = +0.40 V, t_1 = 195 ms; other parameters as in A.

RESULTS AND DISCUSSION

Residual voltammetric response. Current-potential (*i-E*) curves obtained by cyclic voltammetry for the Au minidisk electrode in 0.1 M NaOH are shown in Figure 3 for three values of ϕ in the range of 0.1 - 0.4 Mv ms^{-1}. These curves are briefly interpreted on the basis of descriptions of similar curves obtained in acidic media [12,13]. During the positive scan, anodic formation of surface oxides (AuOH and AuO) occurs at $E >$ *ca.* +0.15 V, and the onset of O_2 evolution corresponds to the sharp current increase for $E >$ *ca.* +0.65 V. For the subsequent negative scan, the anodic current quickly decreases to zero at *ca.* +0.6 V, and there is no evidence of further oxide formation in the region E = +0.6-+0.3 V. This voltammetric evidence indicates that the waveforms in Figures 1B and 2B can result in cessation of oxide growth with the step from $E_1 >>$ +0.6 V back to $E_1' <$ +0.6 V. The cathodic peak , for $E <$ +0.3 V corresponds to cathodic dissolution of surface oxide.

There is evidence in the residual *i-E* curves in Figure 3 that a small amount of surface oxide, presumably AuOH, forms during the positive scan in the region E = -0.50 - +0.15 V (see curve c). Numerous anodic processes are observed to be initiated at *ca.* -0.5 V during the positive scan, and the implications of a catalytic role by this surface process have been discussed by Vitt *et al.* [14]. Throughout the region E = -1.50 - -0.50 V, the electrode is believed to be virtually free of oxide, and this is commonly known as the double-layer region. Based on the curves in Figure 3, values of E_2 and E_3 in Figure 2 were chosen at +0.80 and -0.80 V, respectively.

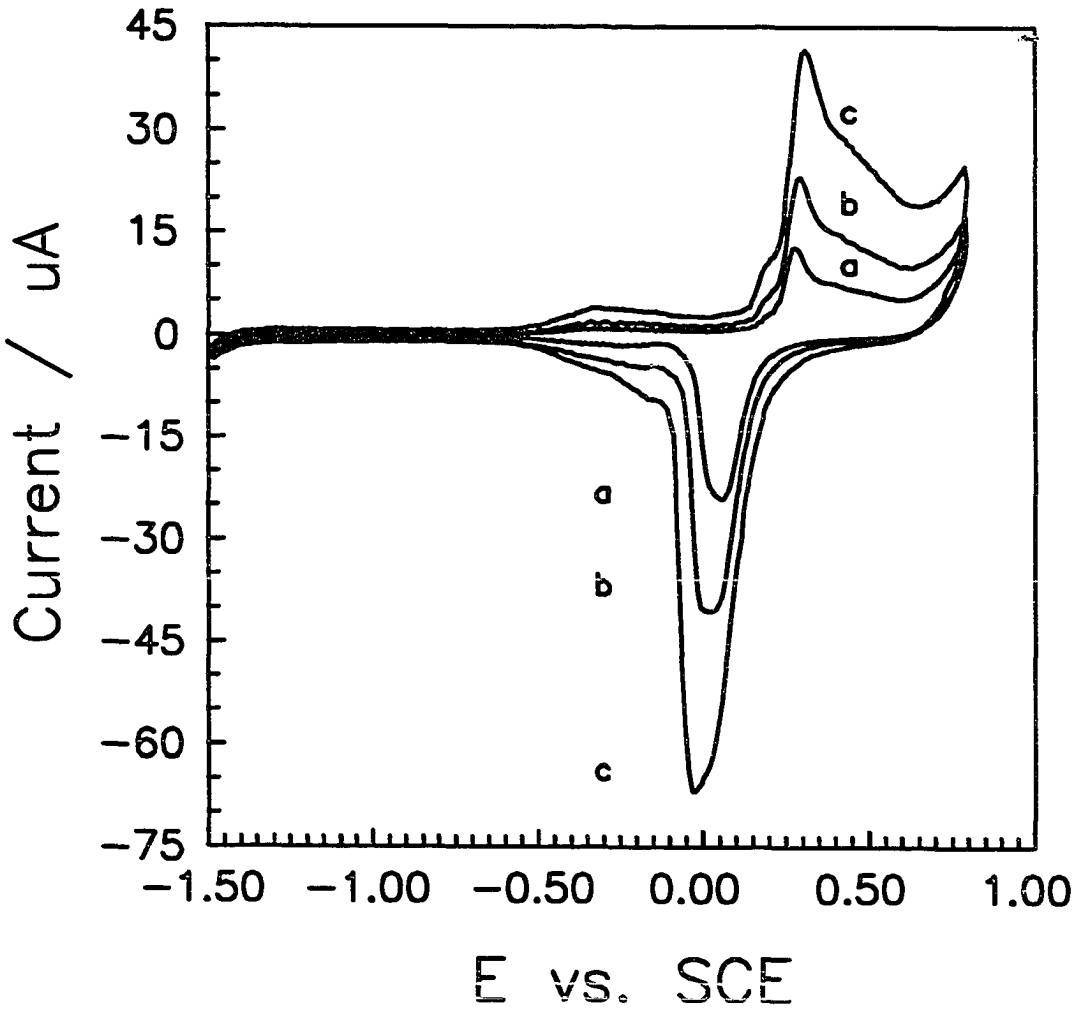

Figure 3. Residual voltammetric response for the Au minidisk electrode in 0.1 M NaOH under slow cyclic potential scan. Scan rate (mV ms^{-1}): (a) 0.10, (b) 0.20, (c) 0.40.

It is apparent in Figure 3 that the maximum current observed for oxide formation, during the positive scan in the region *ca.* +0.25 - +0.30 V, is approximately a linear function of ϕ. This is commonly interpreted as a typical result for surface-controlled processes involving passage of a constant charge within a fixed potential range. As will be demonstrated, this conclusion is not appropriate for large ϕ values when the time spent in the region of oxide formation is not sufficient to allow the oxide coverage to come to equilibrium.

Surface roughness and double-layer capacitance. The Au minidisk electrode (A_{geo} = 0.00785 cm^2) was polished and preconditioned in the prescribed manner and the true surface area (A_{true}) determined by voltammetric stripping of adsorbed iodide according to the procedure of Rodriguez *et al.* [15]. The results correspond to A_{true} = *ca.* 0.060 cm^2, that is, a surface roughness of *ca.* 7.7. Based on this value for A_{true} and the value of 400 $\mu C\ cm^{-2}$ for formation of a monolayer of AuO [16,17], the coulombic charges for formation of monolayers of AuOH and AuO are 12 μC and 24 μC, respectively, on the Au minidisk electrode.

The specific double layer capacitance (C°_{dl} of the minidisk electrode was estimated to be 18 $\mu F\ cm^{-2}$ from residual currents at *ca.* -1.0 V, which is close to reported values of 20-22 $\mu F\ cm^{-2}$ in $HClO_4$ media [12]. Cell resistance (R_{cell}) was estimated at 100 ohms; hence, the cell time constant ($R_{cell}\ C^\circ_{dl}\ A_{true}$) was *ca.* 0.1 ms, and double-layer charging was complete within 1 ms following the potential steps. Data are

corrected for the double-layer charge calculated by $q_{dl} = \Delta E C^{\circ}_{dl} A_{true}$, where ΔE is the potential step.

Oxide formation under a normal-pulse waveform. Typical plots of q_a *vs.* t are shown in Figure 4 for the Au minidisk electrode in 0.1 M NaOH as a function of E_1 in the normal potential-step waveform of Figure 2A. It is apparent for $+0.30 \leq E_1 \leq +0.60$ V that q_a increases very rapidly for $0 < t < ca.$ 30 ms to an extent that appears approximately proportional to E_1. The rate of increase in q_a for $t > 20$ ms is much slower and appears to be independent of E_1. Based on Gilroy's results for Pt in 1 M H_2SO_4 [5,6], an attempt was made to linearize the $q_a t$ data in Figure 4 according to Equation 1, and the plots of q_a vs. $\log\{t/\text{ms}\}$ are shown in Figure 5. These plots are not linear over an extended range of t values, which is in sharp contrast to results for Pt in 1 M H_2SO_4 [5], for which the slope of the q_a $\log\{t/\text{ms}\}$ plot is constant for t increasing to *ca.* 1000 ms. The plots in Figure 5 for $E_1 = +0.30$-$+0.55$ V are characterized by three distinct regions; region I_a ($t < ca.$ 3 ms) corresponds to initiation of oxide growth; region II_a ($ca.$ $3 < t < 30$ ms) is approximately linear and corresponds to a rapid increase in q_a; and region III_a ($t > ca.$ 30 ms) also is approximately linear and corresponds to a very slow increase in q_a. Linear approximations to the q_a $\log\{t/\text{ms}\}$ plots in regions II_a and III_a are indicated in Figure 5 by dashed lines for $E_1 = +0.55$ V.

Values of the intercept (A_a) and slope (B_a) of the linear approximations to the

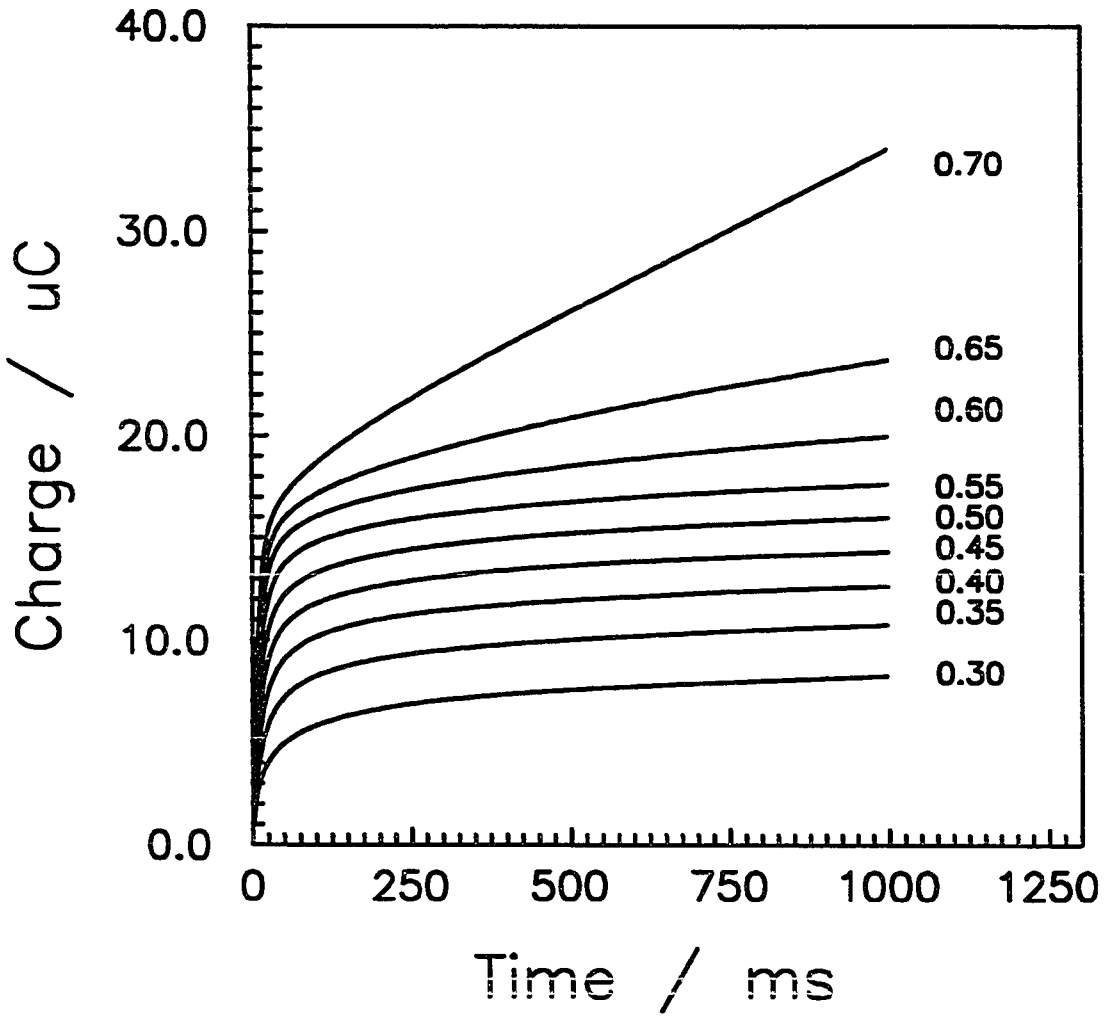

Figure 4. Plot of anodic charge (μC) versus time (ms) for formation of surface oxide at the Au minidisk electrode in 0.1 M NaOH. Values of E_1 in waveform of Figure 2A are shown as V vs. SCE.

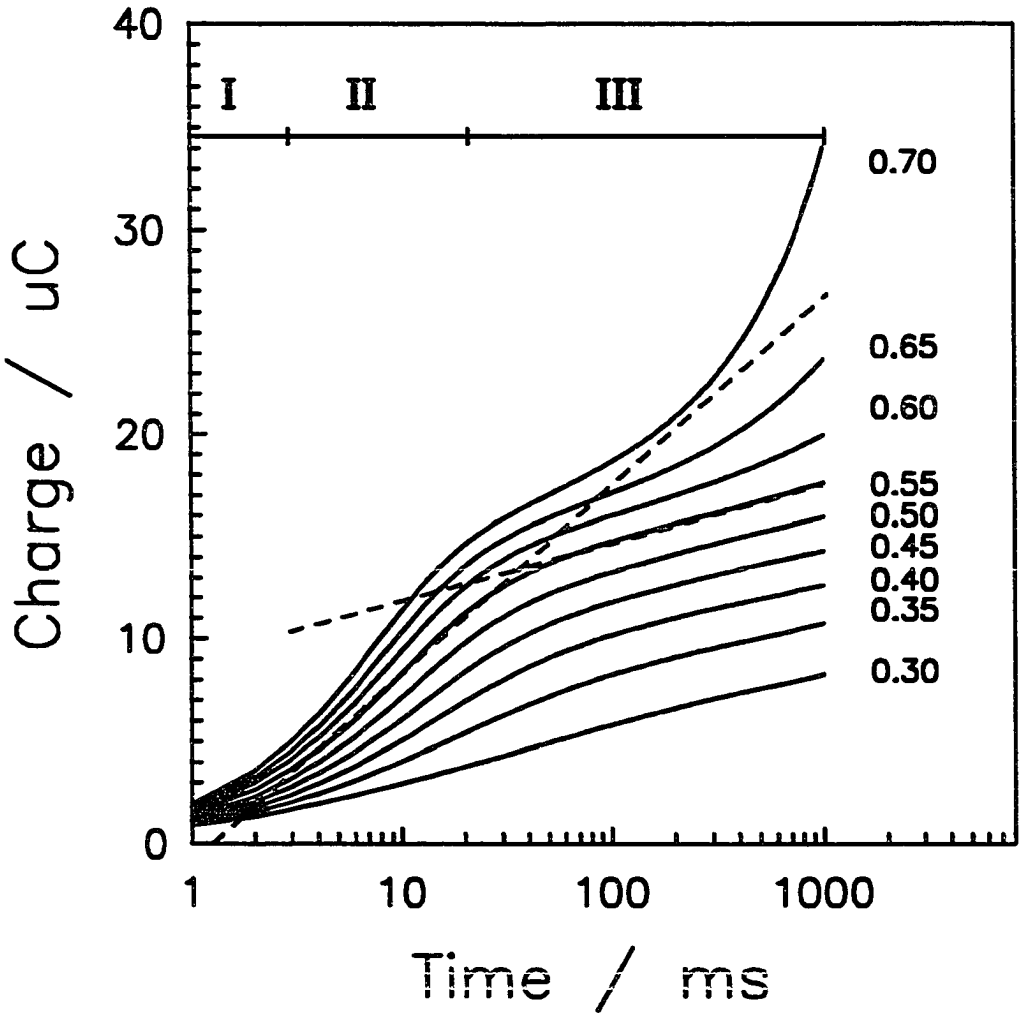

Figure 5. Plot of anodic charge (μC) versus log{time/ms} for oxide formation at the Au minidisk electrode in 0.1 M NaOH. Values of E_1 in waveform of Figure 2A are shown as V vs. SCE. Linear approximations (---) are indicate for regions II_a and III_a

curves for region II_a in Figure 5 are given in Table 1 as a function of E_1. Clearly, the values of A_a are not zero and are observed to vary with E_1. Values of B_a are virtually linear functions of E_1 in the range +0.30-+0.55 V, as shown in Figure 6. Hence, we conclude that B_a is a function of the applied overpotential as given by Equation 2. A linear regressions analysis of the data in Figure 6 for E_1 = +0.30 - +0.55 V according to Equation 2 gives C_a = 26.2 $\pm$ 0.15 μC V^{-1} (90% confidence), $E_{o,a}$ = +0.20 $\pm$ 0.03 V, and a correlation coefficient (R) equal to 0.9985. This estimate of $E_{o,a}$ is in good agreement with the potential for onset of oxide formation deduced from iE curves in Figure 3. Normalization of C_a for A_{true} yields the value 437 μC V^{-1} cm^{-2}. By comparison, we estimate a normalized value of 49 μC V^{-1} cm^{-2} for Pt in 1 M H_2SO_4 on the basis of data of Gilroy [5]. Clearly, the rate of oxide growth at Au in 0.1 M NaOH for t = 3 - 30 ms (region II_a) is much faster than at Pt in 1 M H_2SO_4.

Based on the data in Figure 5, we estimate for E_1 = *ca.* +0.6 V (i.e., E_1-$E_{o,a}$ = *ca.* +0.4 V) that sufficient charge is passed at t = *ca.* 20 ms to achieve formation of a virtual monolayer of AuOH (12 μC). Hence, we tentative conclude that the rapid process in region II_a corresponds to AuOH formation and the slower process in region III_a corresponds predominantly to the conversion of AuOH to AuO. Values of A_a and B_a for the linear approximations to q_a log {t/ms} plots in region III_a (Figure 5) are listed in Table 2, and B_a values are plotted versus E_1 in Figure 7. It is very apparent in Figures 5 and 7 that B values in region III_a are independent of E_1 in the range +0.30 - +0.55 V. The increase in B_a in region III_a for E_1 > +0.60 V is attributed to O_2 evolution,

Table 1. Values of intercept (A_a) and slope (B_a) for region II_a of plots of q_a vs. log{t/ms} shown in Fig. 5 for anodic formation of oxide on the Au minidisc electrode in 0.1 M NaOH.

$$q_a = A_a + B_a\log\{t/\text{ms}\}$$

Potential (E_1, V)	Intercept (A_a, μC)	Slope (B_a, μC)
0.30	0.47	2.53
0.35	0.01	4.14
0.40	-0.26	5.47
0.45	-0.50	6.74
0.50	-0.67	7.96
0.55	-0.73	9.15
0.60	-0.66	10.1
0.65	-0.54	10.8
0.70	-0.24	11.5

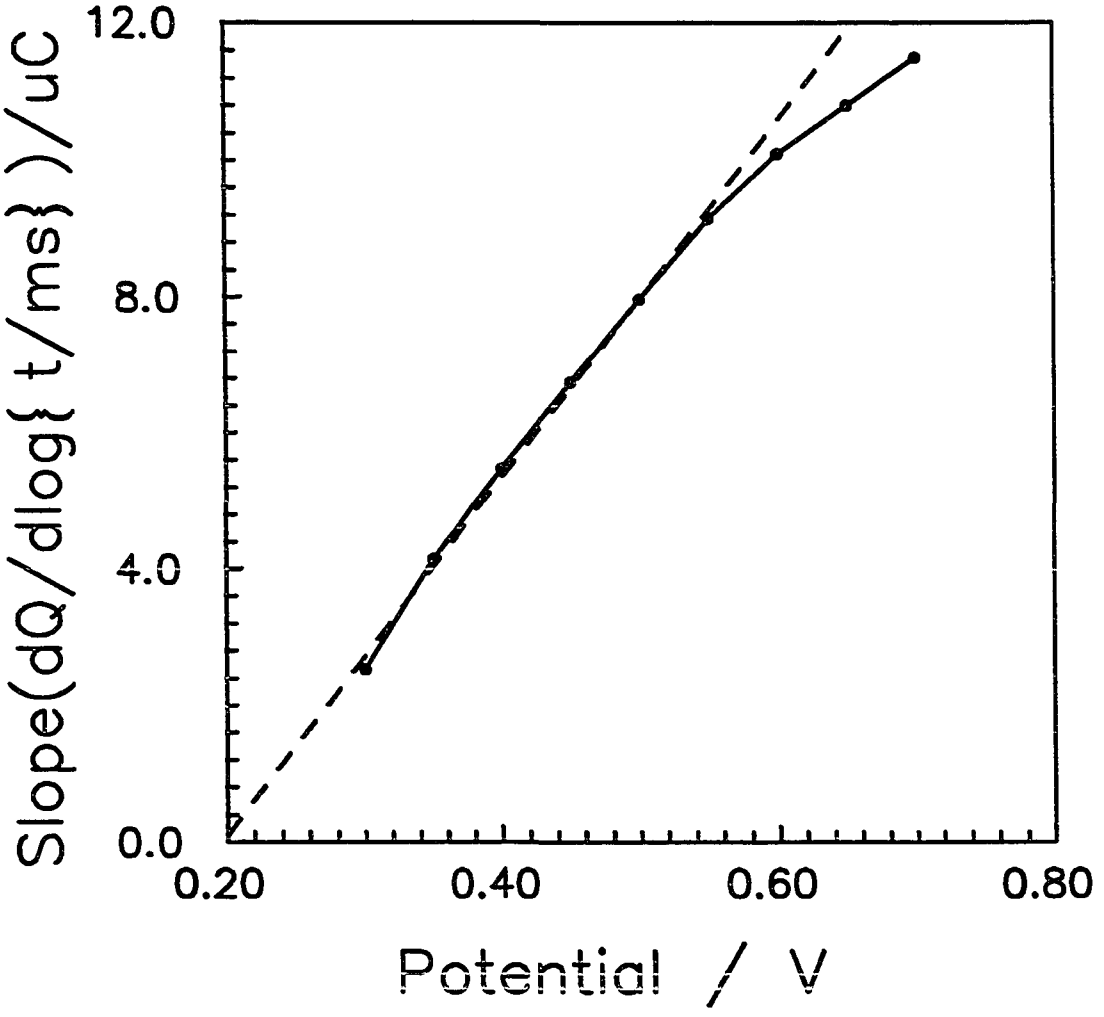

Figure 6. Plot of slopes (μC V-1) versus potential (V) for the linear approximations to the anodic response in region IIa of Figure 5.

Table 2. Values of intercept (A_a) and slope (B_a) for Region III_a of plots of q_a vs. $\log\{t/\text{ms}\}$ shown in Fig. 5 for anodic formation of oxide on Au minidisk electrode in 0.1 M NaOH.

$$q_a = A_a + B_a \log\{t/\text{ms}\}$$

Potential (E_1, V)	Slope (A_a, μC)	Intercept (B_a, μC)
0.30	1.01	2.44
0.35	3.29	2.51
0.40	5.25	2.49
0.45	6.64	2.60
0.50	7.84	2.74
0.55	9.00	2.88
0.60	8.90	3.54
0.65	8.63	4.28
0.70	6.77	6.01

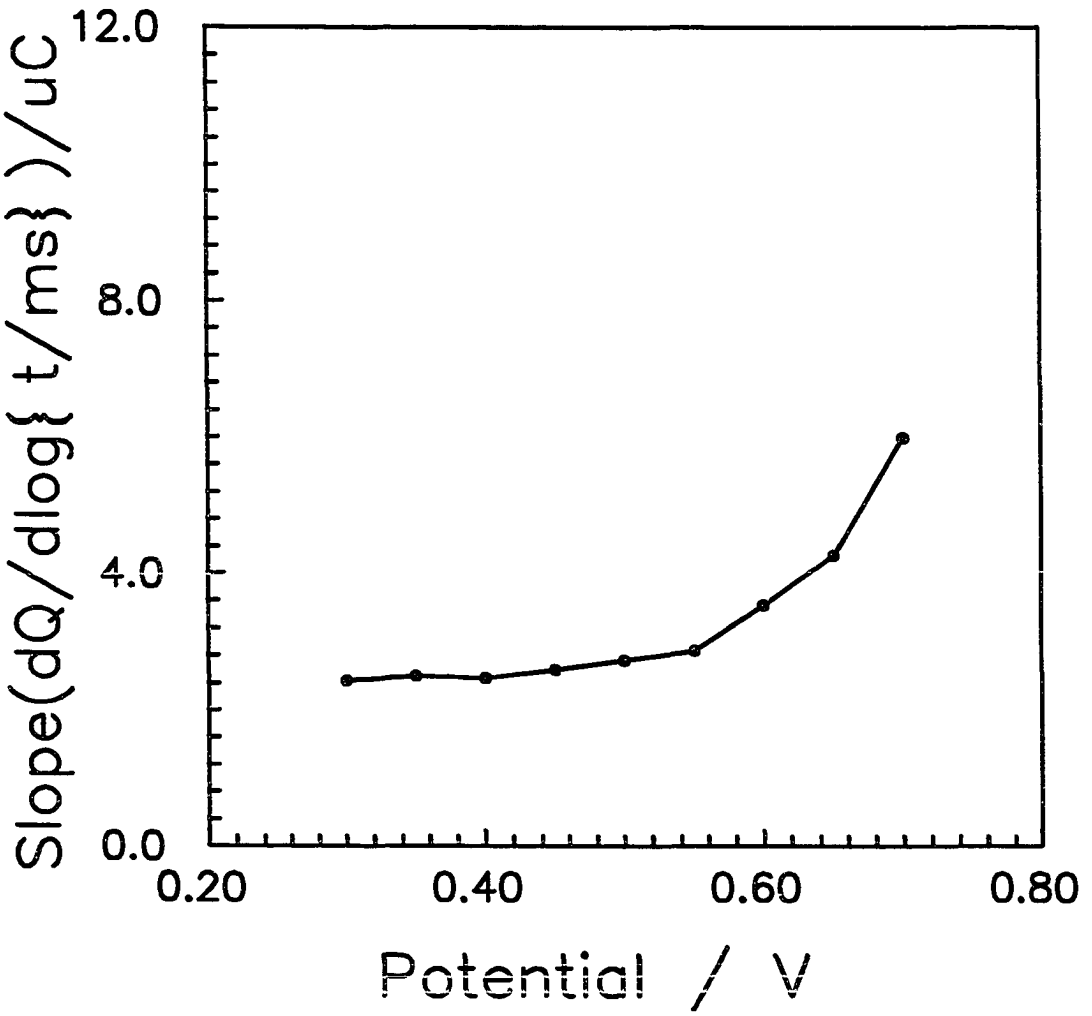

Figure 7. Plot of slopes (μC V-1) versus potential (V) for the linear approximations to the anodic response in region IIIa of Figure 5.

which is consistent with conclusions based on *Ie* curves in Figure 3 obtained by cyclic voltammetry at low ϕ values.

It is also observed in Figure 5 that the slope in region III_a for $E = +0.65$ V increases noticeably for $t > ca.$ 300 ms, whereas for $E = +0.70$ V a similar sharp increase occurs for $t > ca.$ 100 ms. These data are tentatively interpreted to indicate that O_2 evolution occurs only on regions of the surface where oxide growth has proceeded to the final form (AuO). As a consequence, we anticipate in fast PAD waveforms that very large values of E_2 can be applied for very short time periods to achieve rapid formation of AuOH without significant evolution of O_2.

Fast linear-sweep voltammetry. As was mentioned previously, it is commonly concluded from residual *Ie* data for low ϕ values, that the anodic current for oxide formation on Au electrodes varies approximately as a linear function of ϕ. However, in view of Equations 2 and 3, such a linear correspondence cannot be expected for large ϕ. This can be demonstrated more clearly by a prediction of the dependence of i on ϕ. We begin by differentiating Equation 1 after substitution for B_a from Equation 2 with the simplifying assumptions that A_a is constant and that $dE/dt = \phi$. The result is given by Equation 3.

$$\frac{dq_a}{dt} = i_a = \frac{C_a(E-E_{o,a})}{2.3t} + C_a\phi\log\left\{\frac{t}{t_o}\right\} \qquad (3)$$

It is also assumed here that i is measured at constant values of E-$E_{o,a}$. Hence, t in Equation 3 is substituted by $(E\text{-}E_{o,a})/\phi$ and, after division by ϕ and differentiation with respect to log $\{\phi\}$, Equation 4 predicts the slope of plots of i/ϕ vs. log $\{\phi\}$.

$$\frac{d(i/\phi)}{d\log\{\phi\}} = -C_a \qquad (4)$$

Representative plots of i/ϕ vs E are shown in Figure 8 for the minidisk electrode obtained at ϕ = 0.2, 20 and 200 Mv ms^{-1}. It is obvious that the maximum normalized current decreases dramatically with increasing large values of ϕ. Furthermore, the position of the apparent onset potential for the anodic wave is shifted to more positive values. This shift gives the appearance that the thermodynamic potential for the onset of oxide formation ($E_{o,a}$) is also shifted. Such an interpretation is not correct, however, and the appearance of a shift must be understood as a visual consequence of the fact that the potential axis is also a time axis and, therefore, the *Ie* plot at large ϕ displays kinetic rather than thermodynamic information. These data also indicate that the limit of the positive scan for large ϕ can be made very large without significant evolution of O_2. This interpretation is in agreement with the conclusion based on the q log$\{t$/ms$\}$ data in Figure 5 that O_2 evolution commences only following formation of AuO.

Values of the maximum current (i_{max}) in the anodic waves for oxide formation at the microdisk electrode are shown in Figure 9 plotted as i_{max}/ϕ vs. log $\{\phi\}$ for ϕ values in the range 0.2-500 mV ms^{-1}. These data demonstrate that i_{max}/ϕ decreases with

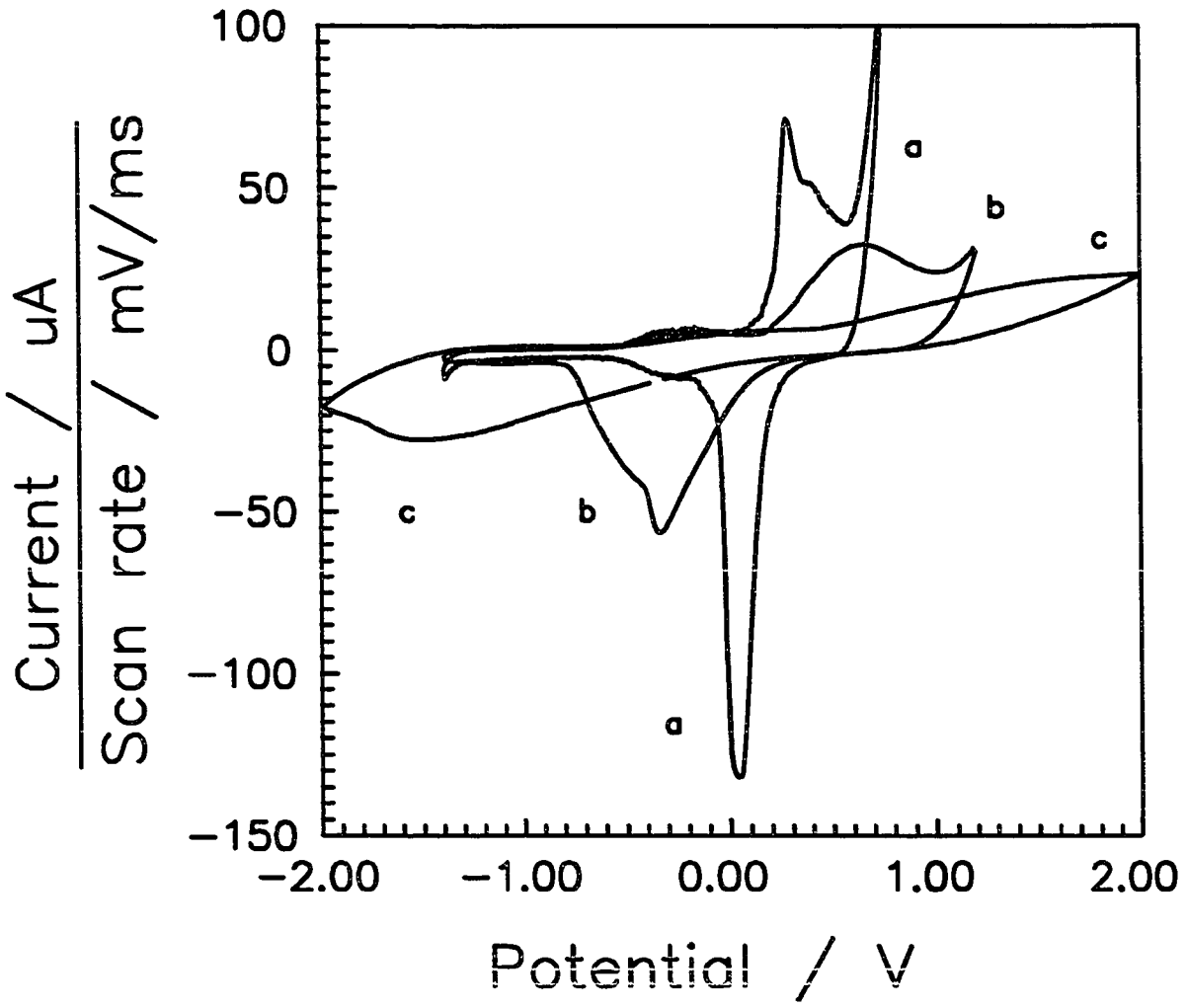

Figure 8. Residual voltammetric response for the Au minidisk electrode in 0.1 M NaOH under fast cyclic potential scans. Scan rate (mV ms^{-1}): (a) 0.20 (b) 20, (c) 200.

increasing ϕ, approaching zero for very large ϕ. For example, at 500 mV ms^{-1}, i_{max} is < 0.3% of the value for 0.2 mV ms^{-1}. For ϕ = 500 mV ms^{-1}, the scan period ($1/\phi$) is 2 ms V^{-1}, and it is understandable from Figure 5 that the rate and amount of oxide formed are very small during the positive scan at this ϕ value.

The dashed line in Figure 9 is drawn with a slope of C_a = -26 μC V^{-1}, as predicted by Equation 4. Clearly, the best fit for this predicted slope with the data exists for small ϕ values. It is not surprising that Equation 4 is not adequate over the entire range of ϕ shown in Figure 9. First, it was assumed in the derivation of Equation 4 that i_{max} values correspond to constant values of (E-$E_{o,a}$). This is not the case, as is evident from examination of the iE data in Figure 8. Second, it was assumed that A in Equation 1 is independent of potential. This also is not true, as is apparent from examination of data in Table 1.

Oxide formation under a reverse potential-step waveform. It is speculated that the benefit of using the R-PAD waveform in Figure 1B for amines and sulfur compounds following LC separation will come as a result of the rapid initial formation of the catalytically active hydrous oxide (AuOH) at $E_3 >> E_{o,a}$, with subsequent cessation of oxide growth with the step back to $E_1 > E_{o,a}$ for detection of analyte. Hence, the oxide-catalyzed detection mechanisms will be enabled; however, the analytical signal will be measured with a minimal background signal. Furthermore, it is expected for very small values of t_1, even at large values of E_1, that virtually no

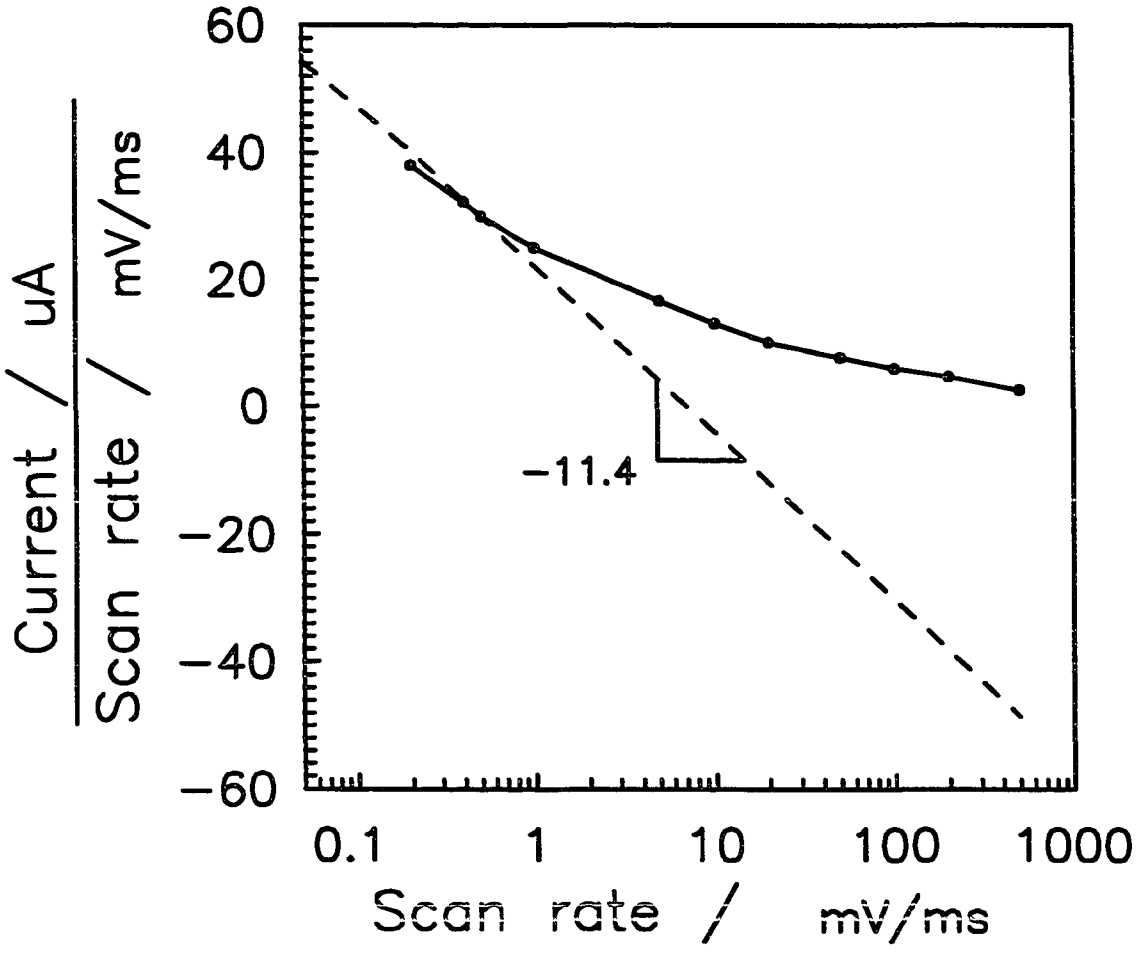

Figure 9. Plot of normalized maximum anodic peak current (μA ms mV^{-1}) versus scan rate (mV ms^{-1}) for the Au microdisk electrode in 0.1 M NaOH. Dashed line indicates slope of -26 μC V^{-1}.

hydrous oxide (AuOH) will be converted to inert oxide (AuO) and the electrode surface can have a maximum catalytic activity over the period of signal measurement at E_1.

This concept was tested by application of the reverse potential-step waveform in Figure 2B. Shown in Figure 10 by solid lines are plots of q_a vs. log {t/ms} obtained for E_1 = +0.55 V with reverse steps to E_1' = +0.40 V at t^1 = 40 ms (curve a) and 5 ms (curve b). It is readily apparent that the growth rate of q_a is decreased sharply in response to the reverse step from +0.55 V to +0.40 V. However, contrary to the expectation based on results for Pt in 1 M H_2SO_4 [5], the growth of q_a for the Au electrode does no completely cease following the reverse step. Also shown in Figure 10 by dashed lines are plots of q_a vs. log{t/ms} obtained using the normal potential-step waveform (Figure 2A) with E_1 = +0.55 V (curve c) and +0.40 V (curve d). Based on intercomparison of these and other plots for the normal and reverse potential-step waveforms, the following conclusions are appropriate; (i) The reverse step from E_1 to E_1' < E_1, when t_1 values for application of E_1 correspond to region II_a (Figure 5), causes an immediate and substantial decrease in the growth rate of q_a to a value that is characteristic of region III_a. (ii) If the q_a generated by the normal potential-step waveform using a value of E_1 in Figure 2A that is equal to E_1' in Figure 2B, q_a follows the q_a log {t/ms} plot generated by the normal potential-step waveform.

Cathodic oxide dissolution. The waveform in Figure 2B, using E_1 = +0.60 V and t_1 = 50 ms, was applied to determine the cathodic charge (q_c) for dissolution of

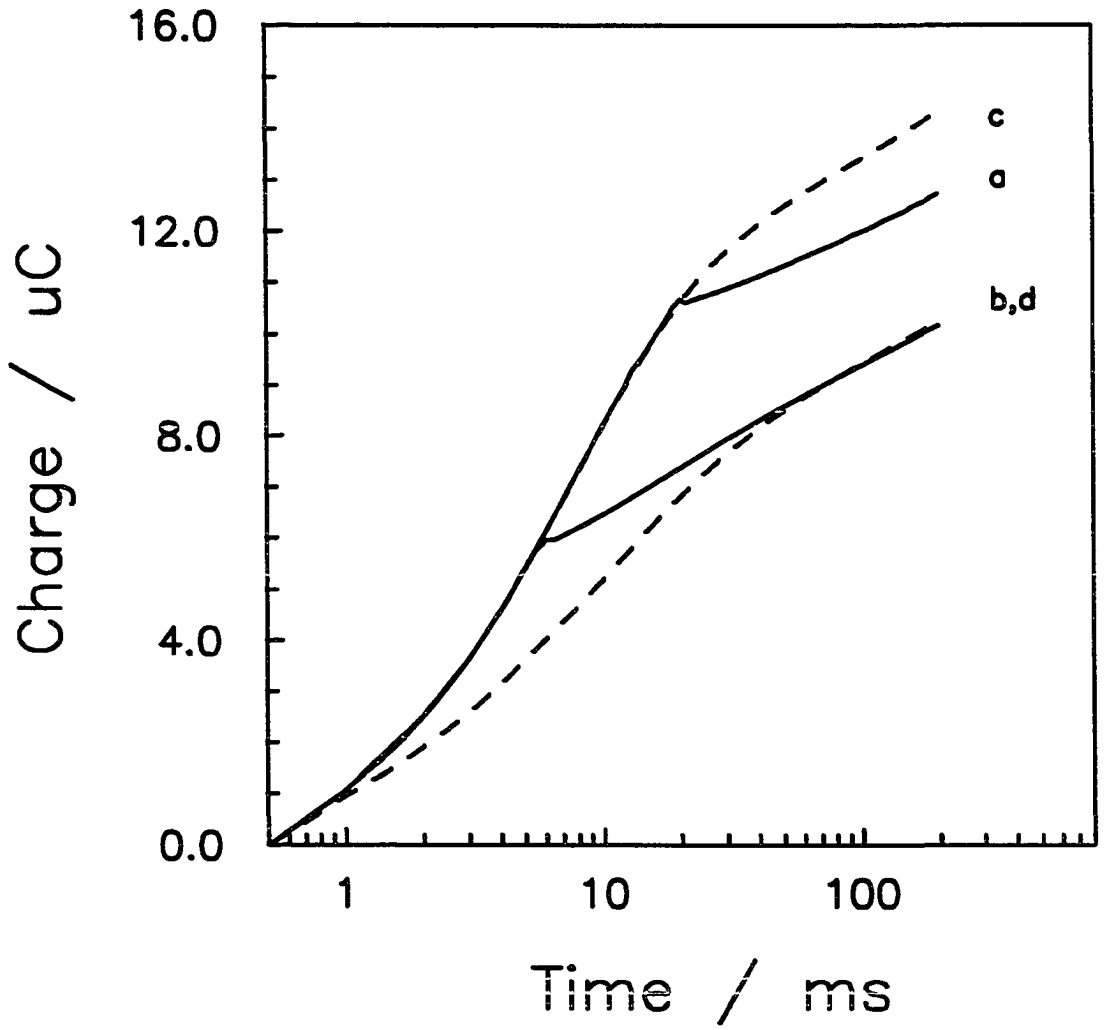

Figure 10. Plot of anodic charge (μC) versus log{time/ms} under the normal potential-pulse and reverse potential-pulse waveforms for oxide formation at the Au minidisk electrode in 0.1 M NaOH. Waveforms (----) Figure 2A, (—) Figure 2B. Curves: (**a**) E_1 = +0.55 V, t_1 = 40 ms, E_1' = +0.40 V, t_1' = 160 ms. (**b**) E_1 = +0.55 V, t_1 = 5 ms, E_1' = +0.40 V, t_1' = 195 ms, (c) E_1 = +0.55 V, t_1 = 200 ms, (**d**) E_1 = +0.40 V, t_1 = 200 ms.

surface oxide as a function of E_1' in the range -0.40 - -0.80 V. The results are plotted in Figure 11 as q_c vs. log {t/ms} for t = 0.2-200 ms. Three cathodic regions are designated: region I_c corresponds to initiation of oxide dissolution for t < *ca.* 2 ms, region II_c corresponds to rapid dissolution of q_c for t = *ca.* 2 - 10 ms, and region III_c corresponds to the subsequent slower increase in q_c for t > *ca.* 10 ms. The initial growth of q_c (region I_c) is virtually a linear function of t, as is evident from the $q_c t$ plots in Figure 12 and illustrated by the linear dashed line for E_1' = -0.40 and -0.80 V. Values of intercept and slope of the linear approximations to q_c-t plots for t < 2 ms are tabulated in Table 3. The slope is a linear function of E_1', as shown by the plot in Figure 13. The data in region I_c were analyzed by linear regression according to Equation 5 with small values of A_c = -0.89E_1'-0.74 μC, C_c = 4.14 $\pm$ 0.05 μC V^{-1} ms^{-1}, and $E_{o,c}$ = -0.09 $\pm$ 0.006 V. This value of $E_{o,c}$ is consistent with the potential for onset of oxide reduction estimated from the *it* curves in Figure 3.

$$q_c = A_c + C_c(E_1'-E_{o,c})\,t/ms \qquad (5)$$

In region IIc of Figure 11, q_c is a linear function of log{t/ms}, as indicated by the dashed line for E_1' = -0.40 and -0.80 V, but exhibits little dependence on E_1'. This indicates, for cathodic dissolution of the last 10% to 20% of the surface oxide (region IIc), that mechanistic steps up to and including the rate controlling step do not involve charge transfer. It is also interesting that the time required for complete cathodic dissolution of the surface oxide is *ca.* 20 ms and is relatively insensitive to variations in E_1' for E_1' < -0.50 V.

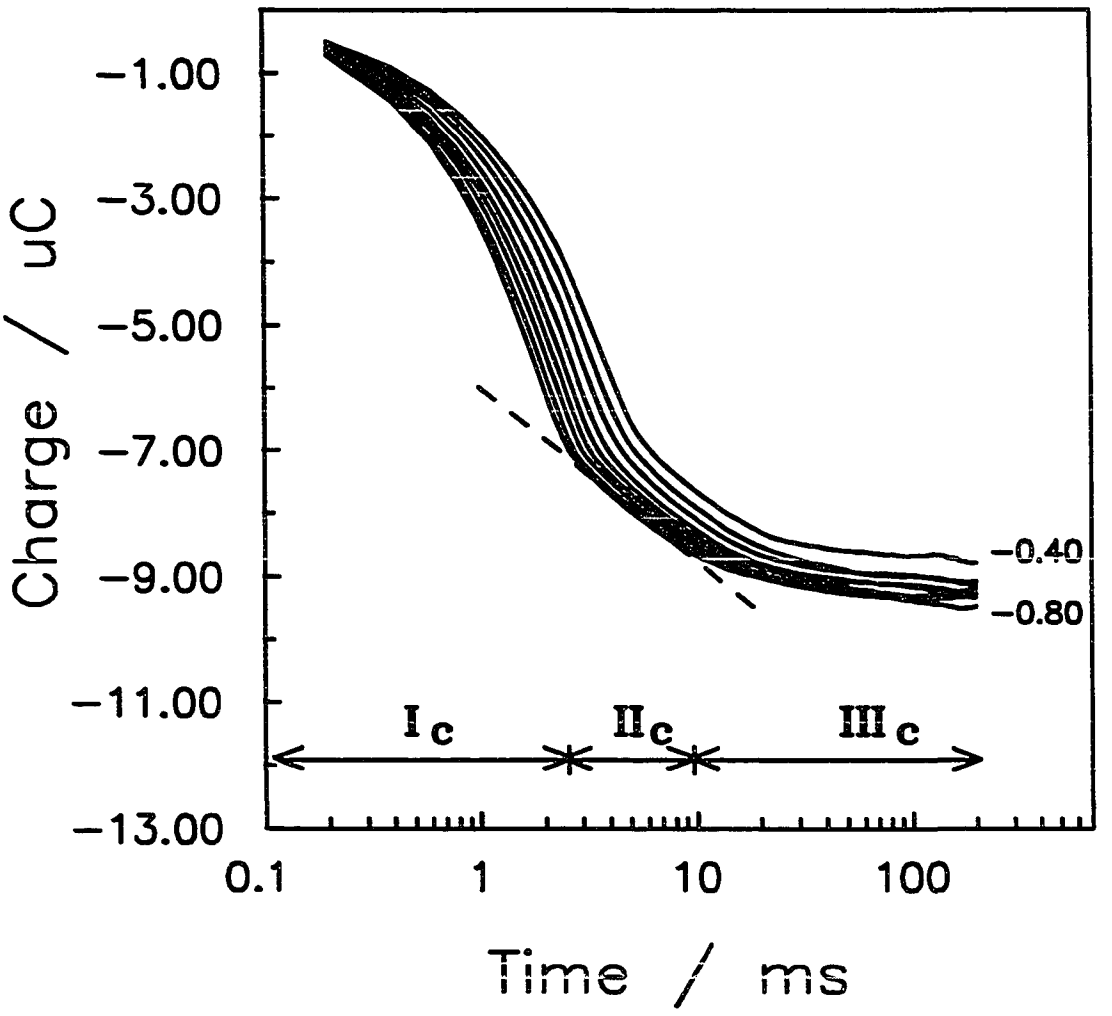

Figure 11. Plot of cathodic charge (μC) versus log{time/ms} for oxide dissolution at the Au minidisk electrode in 0.1 M NaOH using the reverse potential-pulse waveform of Figure 2B with E_1' varied by 50 mV intervals in the range -0.40--0.80 V. Linear approximations (---) are indicated in region II_c for E_1' = -0.40 V and -0.80 V.

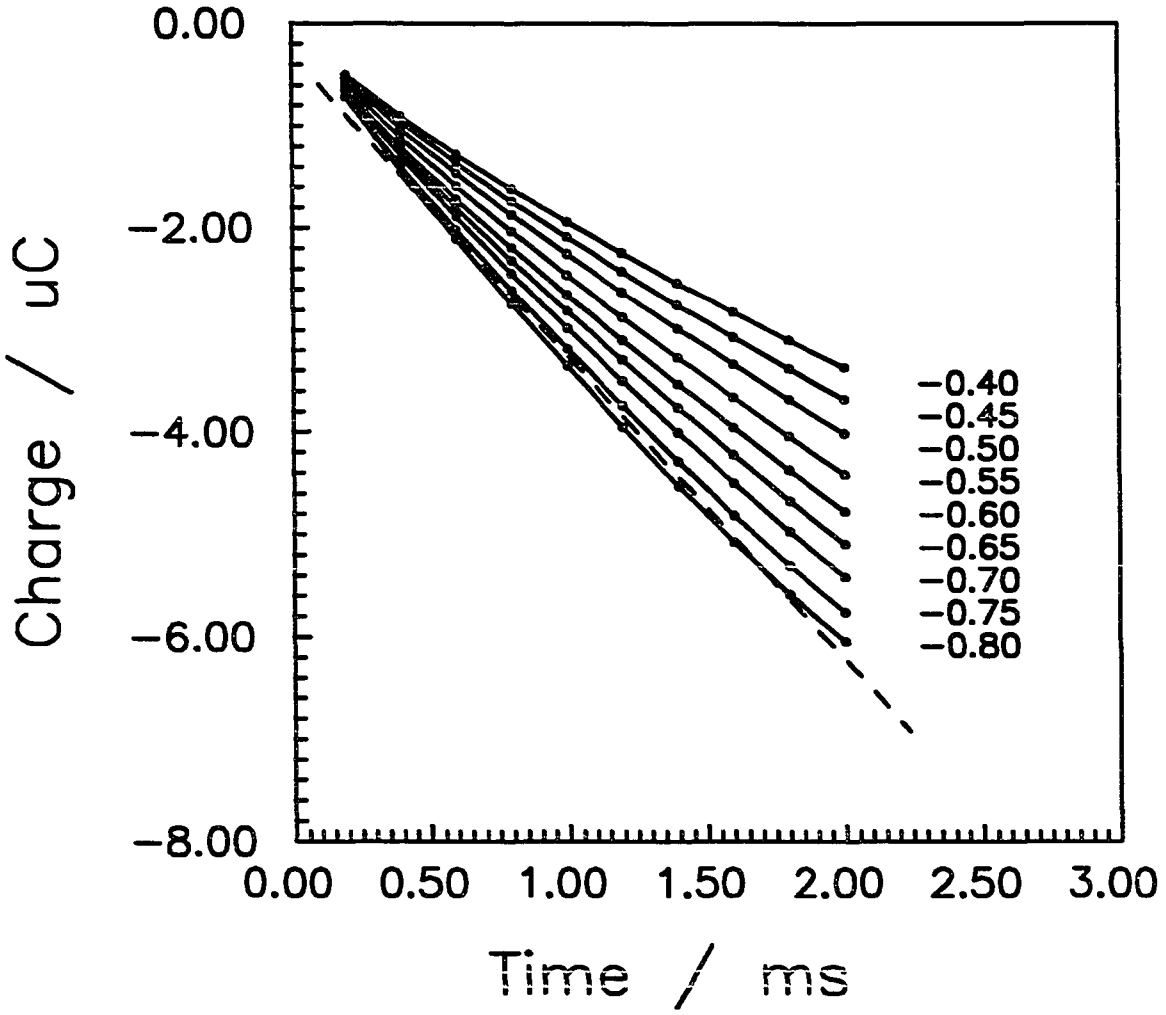

Figure 12. Plot of cathodic charge (qc,μC) versus time (ms) for cathodic oxide dissolution in region I_c of Figure 12. Values of E_1' in the waveform of Figure 2B are shown as V vs SCE. Linear approximations (---) are indicated for E_1' = -0.40 and -0.80 V.

Table 3. Values of intercept (A_c) and slope (B_c) for Region II_c of plots of q_c vs log{t/ms} shown in Fig. 12 for cathodic dissolution of oxide at the Au minidisk electrode in 0.1 M NaOH.

$$q_c = A_c + B_c\{t/\text{ms}\}$$

Potential (E_1', V)	Intercept (A_c, μC)	Slope (B_c, μC s^{-1})
-0.80	-0.296	-2.96
-0.75	-0.356	-2.73
-0.70	-0.363	-2.52
-0.65	-0.415	-2.31
-0.60	-0.456	-2.12
-0.55	-0.489	-1.90
-0.50	-0.475	-1.71
-0.45	-0.548	-1.49
-0.40	-0.632	-1.29

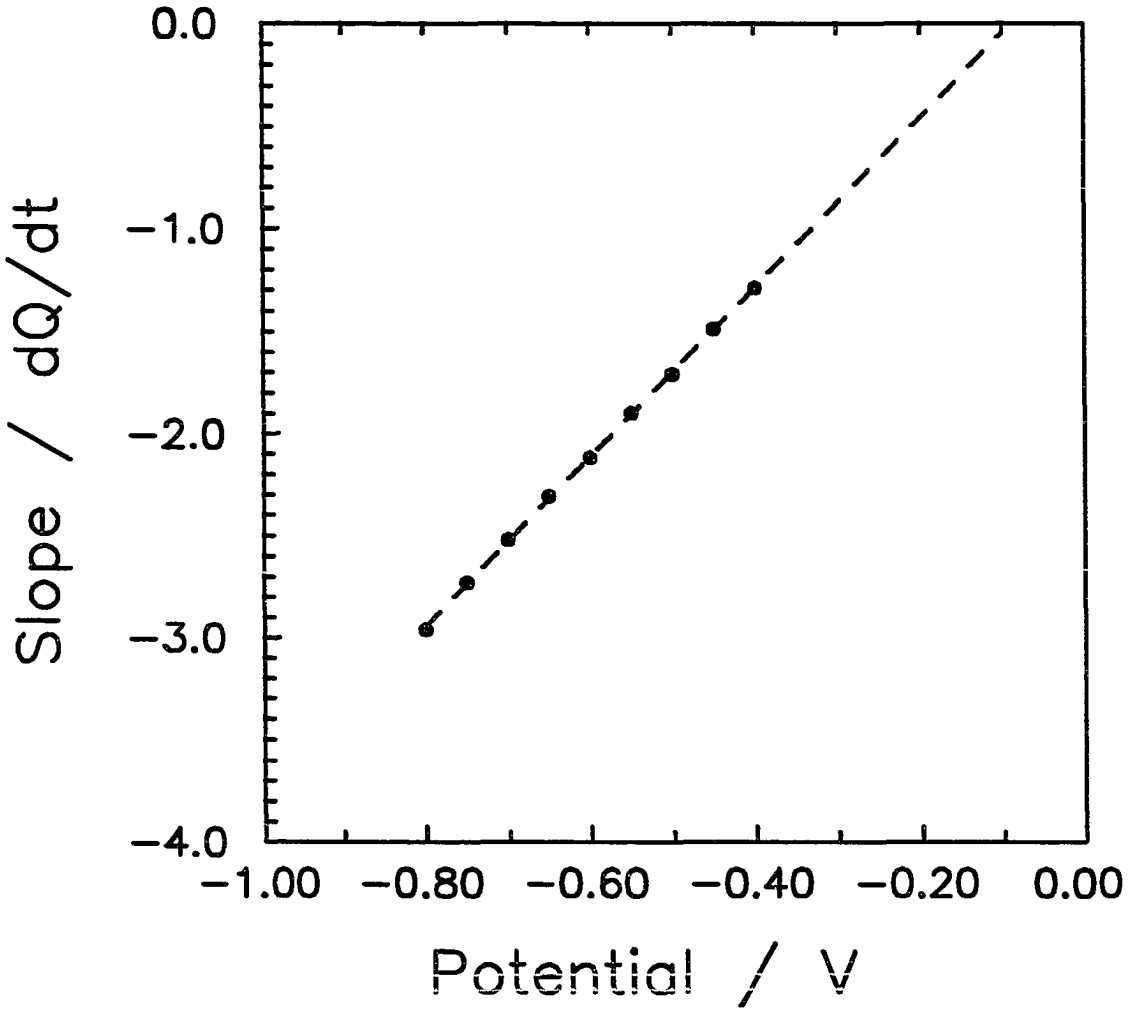

Figure 13. (plot of slopes (μC ms^{-1}) versus potential (V) for linear approximations to data in region I_c for Figure 12.

CONCLUSIONS

Anodic chronocoulometric ($q_a t$) data for a Au electrode in 0.10 M NaOH obtained with a normal potential-step waveform indicate a very rapid initial growth rate for surface oxide with a logarithmic dependence on t (region II_a in Figure 5). We tentatively conclude that this period corresponds to generation of the catalytically active hydrous oxide (AuOH) and that a potential step to $E = +0.50$ V for o.10 M NaOH produces a virtual monolayer of AuOH (12μC) within *ca.* 20 ms. We tentatively conclude also that conversion of AuOH to the inert surface oxide (AuO) occurs more slowly for $t >$ *ca.* 30 ms (region III_a in Figure 5) at a rate that is virtually independent of potential.

Data shown in Figure 10, generated using a reverse potential-step waveform (Figure 2B), are consistent with the observation by Polta and Johnson [4] that application of a three-step R-PAD waveform can result in a significant decrease in the background signal for pulsed amperometric detection of amine and sulfur compounds at Au electrodes in alkaline media. On the basis of data in Figure 5, we predict that maximum surface activity will occur when the surface activation potential (E_3 in Figure 1B) is applied for very short time periods (*i.e.*, $t_3 <$ 20 ms), so that very little AuOH is converted to AuO. Furthermore, for very small t_3 in the R-PAD waveform, the amount of adsorbed analyte lost by oxidative desorption prior to application of the detection potential (E_1 in Figure 1B) can be minimized. However, for the three-step R-PAD waveform (Figure 1B), the oxidative cleaning of the electrode surface is expected

to be minimal when t_3 is maintained at a small value. Hence, in future applications of the R-PAD concept for the oxide-catalyzed detection of amines and sulfur compounds, we anticipate that the optimum waveform will be modified from that in Figure 1B by the addition of a positive potential step for oxidative surface cleaning immediately following detection (E_1,t_1) and prior to cathodic reactivation (E_2, t_2).

The initial rate of cathodic dissolution of surface oxide (region I_c in Figure 11) is a linear function of E_1' in the waveform of Figure 2B. Nevertheless, the time required for virtual complete dissolution of oxide (ca. 20 ms) varies only slightly as a function of E_1'.

Based on the results shown here, we anticipate that suitable time periods for each of the steps in the three-step R-PAD waveform of Figure 1B are t_1 = 20 ms, with current sampling for 16.7 ms (1/60 Hz), t_2 = 20 - 30 ms and t_3 = 20 - 30 ms. Hence, we anticipate success for waveform frequencies approaching 15 Hz at Au electrodes in 0.1 M NaOH. Future publications will report on further development and application of fast PAD waveforms applied at Au microwire electrodes for detection in capillary chromatography and capillary electrophoresis.

ACKNOWLEDGEMENT

This work was supported by the National Science Foundation under contract CHE-8914700.

REFERENCES

1. D.C. Johnson and W.R. LaCourse, *Anal. Chem., 62* (1990) 589A.

2. W.R. LaCourse and D.C. Johnson, *Carbohydrate Res., 215* (1991) 159.

3 W.R. LaCourse, D.C. Johnson, M.A. Rey, and R.W. Slingsby, *Anal. Chem., 63* (1991) 134.

4. T.Z. Polta and D.C. Johnson, *J. Electroanal. Chem., 209* (1986) 159

5. D. Gilroy, *J. Electroanal. Chem., 71* (1976) 257.

6. D. Gilroy, *J. Electroanal. Chem., 83* (1977) 329.

7. D. Gilroy and B.E. Conway, *Can. J. Chem., 46* (1968) 87.

8. H. Angerstein-Kozlowska, B.E. Conway and W.B.A. Sharp, *J. Electroanal. Chem., 43* (1973) 9.

9. S.G. Roscoe and B.E. Conway, *J. Electroanal. Chem., 224* (1987) 163.

10. H. Angerstein-Kozlowska, B.E. Conway, K. Tellefsen, and B. Barnett, *Electrochim. Acta, 34* (1989) 1045.

11. S. Gilman, *Electrochim. Acta, 9* (1964) 1025.

12. H. Angerstein-Kozlowska, B.E. Conway, A. Hamelin, and L. Stoicovich, J. *Electroanal. Chem., 228* (1987) 429.

13. H. Angerstein-Kozlowska, B.E. Conway, A. Hamelin, and L. Stoicovich, *Electrochim. Acta*, Electrochim. Acta, *31* (1986) 1051.

14 J.E. Vitt, L.A. Larew, and D.C. Johnson, *Electroanalysis, 2* (1990) 21.

15. J.F. Rodreguez, T. Mebrahtu, and M.P. Soriaga, *J. Electroanal. Chem., 233* (1987) 283.

16. A.A. Michri, A.G. Pshchnichnitov, and R. Kh. Burshtein, *Electrochem., 8*

(1972) 351.

17. S.B. Brummer and A.C. Makrides, *J.Electrochem. Soc., 117* (1964) 1122.

PAPER 2.

FAST-PULSED AMPEROMETRIC DETECTION AT NOBLE METAL ELECTRODES: A STUDY OF OXIDE FORMATION AND DISSOLUTION AT PLATINUM IN 0.1 M NaOH[2]

[2]Reprinted with permission from R.E. Roberts and D.C. Johnson, *Electroanalysis*, 6 (1994) 193.

ABSTRACT

Results of a potential-step chronocoulometric study of oxide formation at a Pt rotated minidisc electrode (0.00785 cm^2) indicate that the anodic charge (q_a) grows approximately as a linear function of the log of time (t) for t = *ca.* 2 - 30 ms. Furthermore, the slope of the linear q_a-log{t/ms} plot is proportional to the applied overpotential for oxide formation. The anodic peak current observed during linear potential-scan voltammetric experiments is nearly a linear function of scan rate (ϕ) for small ϕ ($<$ 1000 mV s^{-1}) but shows substantial negative deviation from linearity for ϕ $>$ 1000 mV s^{-1}. The peak potential for oxide formation shifts in a positive direction for increasing values of ϕ, suggesting that this process is kinetically slow relative to large ϕ values. Reverse potential-step chronocoulometric measurements demonstrate that the background current in so-called "reverse pulsed amperometric detection (RPAD)" can be decreased by inhibiting the conversion of the hydrous oxide (PtOH) to the inert oxide (PtO). Data also indicate that the rate of cathodic dissolution of surface oxide is dependent on applied potential for t < 2 - 30 ms. Oxide reduction continues even for t $>$ 1000 ms.

INTRODUCTION

The kinetics of oxide formation on Pt electrodes in acidic media have been studied by Gilroy [1,2]. He concluded that the anodic charge (q_a) for oxide formation is a linear function of the log of time (t) as described by Equation 1, where t_o is a time constant corresponding to the units on t, A_a and B_a are constants. Although A_a was not

$$q_a = A_a + B_a \log\left\{\frac{t}{t_o}\right\} \tag{1}$$

discussed by Gilroy, it is apparent from Figures 2 & 3 in [1] that A_a has a non-zero value and is dependent on applied potential (E). Gilroy reported that the slope (B_a) of q_a-log$\{t/t_o\}$ plots is proportional to the applied overpotential for oxide formation (E - E_o), as given by Equation 2 where E_o is the potential corresponding to the onset of oxide formation. Our estimate of C_a from Figure 4 of [1] is 48.8 μC V^{-1} cm^{-2}.

$$B_a = C_a(E-E_o) \tag{2}$$

Gilroy also demonstrated for Pt in acidic media that a negative step from $E >> E_{o,a}$ to $E' > E_{o,a}$ can temporarily halt further oxide growth with subsequent resumption of oxide growth according to Equation 1 for $E = E'$. This is consistent with the observations of the residual voltammetric response for Pt in acidic media that the anodic current for oxide formation decreases rapidly to zero when the scan direction is reversed form positive to negative [3].

Recently, we reported results of kinetic studies of oxide formation and dissolution at Au electrodes in 0.1 M NaOH using potential-step chronocoulometry [4]. Plots of q_a vs. $\log\{t/t_o\}$ exhibited a nearly linear correspondence for t = *ca.* 3 - 30 ms, in agreement with Equation 1, with slopes (B_a) that were proportional to the applied overpotential (E - E_o). This linear region apparently corresponds to formation of AuOH. A second linear region in q_a-$\log\{t/t_o\}$ plots was observed for t > *ca.* 30 ms, provided E < +0.55 V vs. SCE so O_2 evolution did not occur. This region apparently corresponds to the conversion of AuOH to AuO and the observation B_a is independent of E indicates the slow step in this mechanism does not involve charge transfer. Data also indicate O_2 evolution occurs for E > +0.55 V vs. SCE, but only after formation of a virtual monolayer of AuO.

As had been shown for Pt in acidic media [1,2], we demonstrated for Au in 0.1 M NaOH that growth of surface oxide (AuOH plus AuO) can be temporarily halted by the application of a small negative step. This has possible practical consequence in that the background signal from oxide formation might be substantially decreased for anodic detection mechanisms that are facilitated by the presence of AuOH but not AuO on Au electrode surfaces.

The cathodic dissolution of oxide at Au electrodes in 0.1 M NaOH was also studied by potential-step chronocoulometry. Oxide dissolution occurs at a rate virtually independent of potential and is essentially completed (*ca.* 80%) within *ca.* 20 ms for E < *ca.* -0.5V *vs.* SCE.

These kinetic studies in our laboratory are motivated by the need to understand the fundamental processes that ultimately limit the upper frequency for so-called *pulsed amperometric detection* (PAD) based on application of multi-step *E-t* waveforms. Because the anodic formation and cathodic dissolution of surface oxide are fundamental aspects of PAD technology, a clear understanding of the kinetics of these processes is necessary to enable the design of fast PAD waveforms. Here, we describe results of kinetic studies for oxide formation and dissolution at Pt electrodes in 0.1 M NaOH.

EXPERIMENTAL

Equipment. Data were obtained using a Pt rotated minidisc electrode (0.00785 cm^2, Pine Instrument). All other apparatus and reagents were identical to that described previously [4].

Procedures. Data were obtained at ambient temperature (25 $\pm$ 2° C). Electrodes were polished with 0.05-μm alumina in water on microcloth (Buehler) and then rinsed with deionized water. After polishing, electrodes were conditioned in the test solutions for 30 minutes by cyclic potential scans at 1.0 V s^{-1} between the potential limits corresponding to anodic discharge of H2O to produce O_2 (+0.60 V vs. SCE) and cathodic discharge of H_2O to produce H_2 (-1.00 V vs. SCE).

The *E-t* waveforms applied in chronocoulometric measurements were virtually identical to those previously applied at Au electrodes and shown in Figure 2 of [4]. For the waveform in Figure 1A, which is similar to the so-called "normal" PAD waveform (NPAD), the Pt electrode was activated by ten (n = 10) alternate applications of potential values for oxide formation (E_2 = 0.8 V, t_2 = 50 ms) and dissolution (E_3 = -0.6 V, t_3 = 50). The potential was then stepped from E_3 to the detection potential (E_1) and the *i-t* response recorded digitally. The waveform in Figure 1B resembles the so-called "reverse" PAD waveform (RPAD) and involved a negative step from E_1 to $E_1' < E_1$. In this case, data were collected digitally during both periods t_1 and t_1'. For both experiments, *q-t* data were generated by digital integration of the *i-t* data.

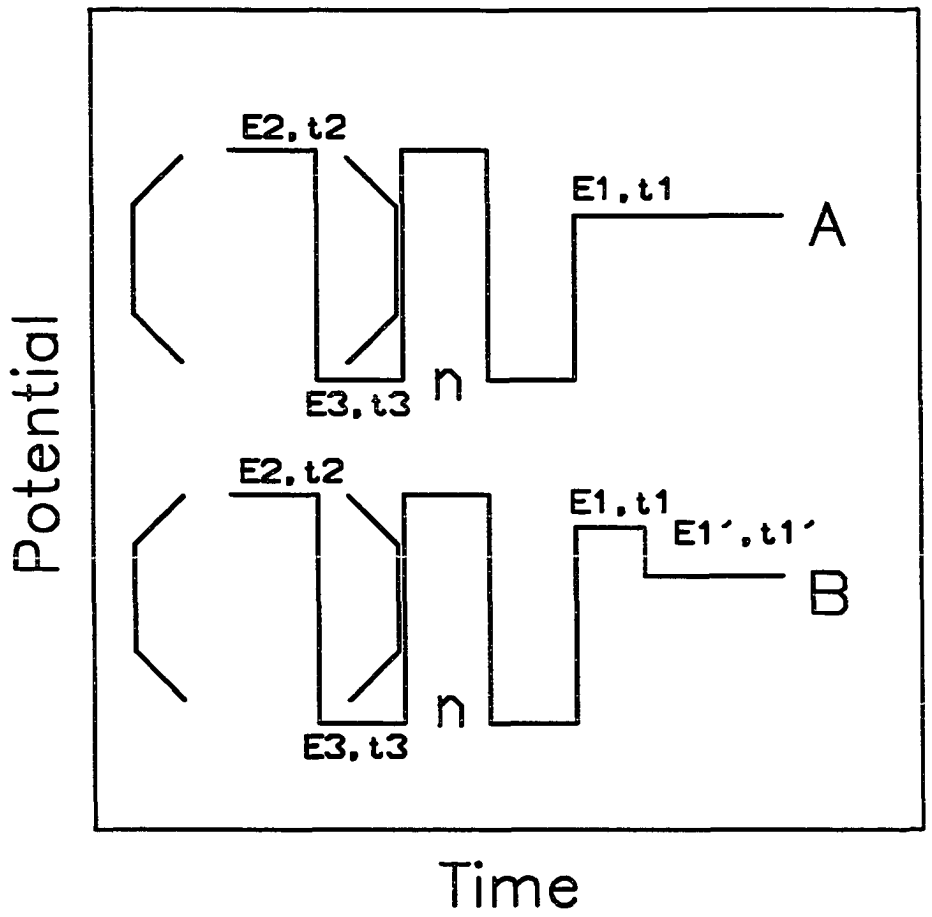

Figure 1. Potential-step waveforms used in studies of oxide formation. (A) Normal potential-step waveform: n = 10, E_2 = +0.60 V, t_2 = 50 ms, E_3 = -0.60 V, t_3 = 200 ms, E_1-0.2 - +0.7 V, t_1 = 1000 ms. (B) Reverse potential-step waveform: n = 10, E_1 = +0.50 V t_1 = 10 ms, E_1' = +0.20 V - +0.40 V, t_1' = 290 ms; other parameters as in A.

RESULTS AND DISCUSSION

Residual voltammetric response. Typical current-potential (*i-E*) curves obtained by cyclic voltammetry are shown in Figure 2 for the Pt minidisc electrode in 0.1 M NaOH using ϕ = 0.1, 0.2 and 0.5 mV ms^{-1}. The significant features of these curves can be interpreted in accordance with explanations of voltammetric curves obtained in acidic media [5 - 7]. During the positive scan from *ca.* -0.5 V, the anodic wave for $E >$ *ca.* -0.30 V corresponds to the formation of surface oxides (PtOH and PtO)and the sharp increase in anodic current for $E >$ *ca.* +0.50 V corresponds to the discharge of H_2O with evolution of dioxygen (O_2).

Upon scan reversal at +0.6 V, the anodic current decreases quickly to zero, as an indication that oxide formation ceases. With continued negative scan, a large cathodic peak appears in the region *ca.* 0.0 to -0.6 V corresponding to dissolution of the surface oxide formed during the preceding positive scan. The cathodic peak in the region *ca.* -0.6 to -0.9 V corresponds to cathodic discharge of H_2O to generate adsorbed hydrogen atoms ($\cdot H_{ads}$). Hoare [7] noted that only one peak is obtained in alkaline solutions for this process whereas there are multiple peaks observed in acidic media. The sharp increase in cathodic current at $E <$ -0.9 V, is the result of generation of dihydrogen (H_2). Scan reversal at -1.0 V results in the appearance of anodic peaks in the region -1.0 to -0.6 V corresponding to ionization of adsorbed hydrogen. On the basis of the *i-E* curves in Figure 2, values of E_2 and E_3 in Figure 1 were chosen to be +0.60 and -0.60 V, respectively.

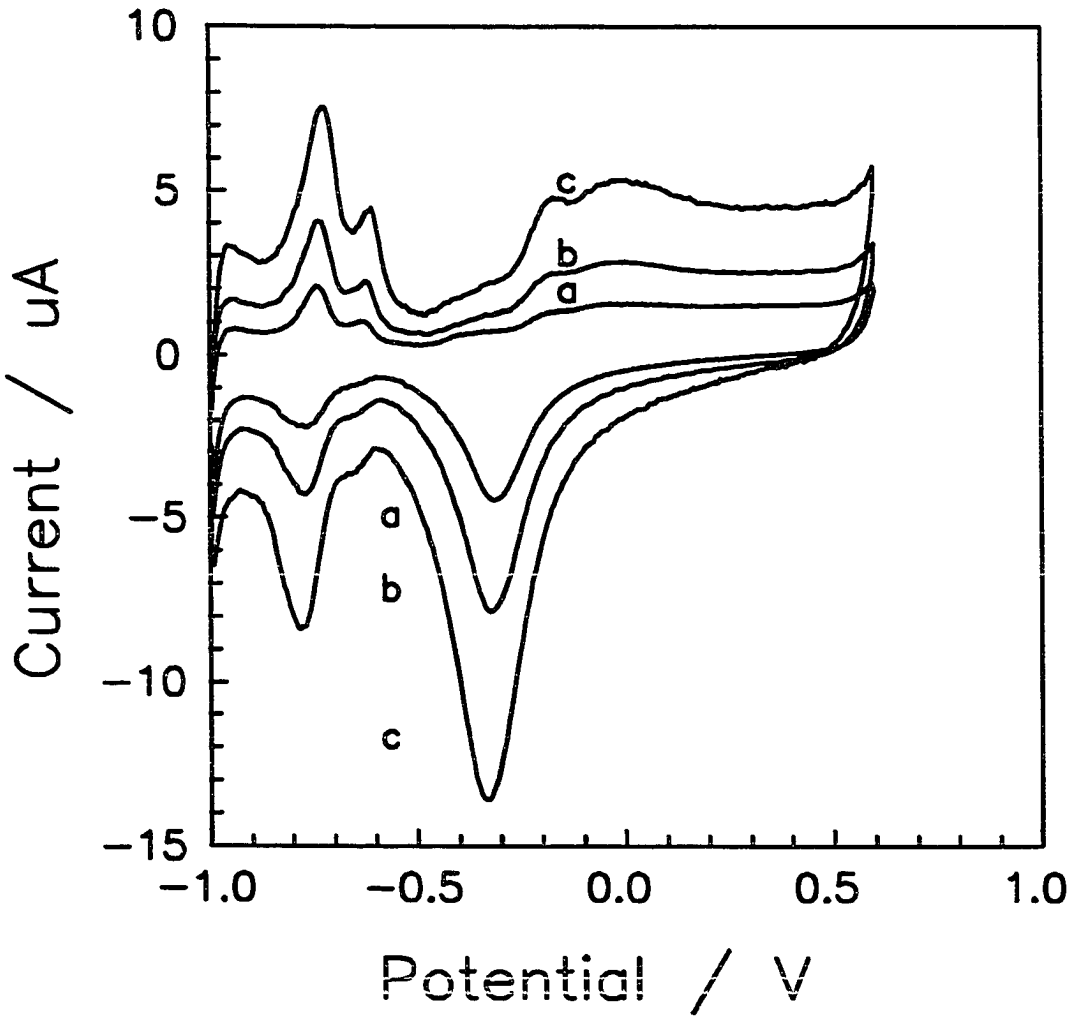

Figure 2. Residual voltammetric response for the Pt minidisc electrode in 0.1 M NaOH under slow cyclic potential scan. Scan rate (mV ms^{-1}): (a) 0.1, (b) 0.2, (c) 0.5.

Surface roughness and double-layer capacitance. The Pt minidisc electrode was polished and preconditioned in the prescribed manner, and the anodic charge associated with the desorption of adsorbed hydrogen was determined to be 4.8 $\pm$ 0.1 μC. Based on a literature value of 220 μC cm^{-2} for cathodic adsorption of hydrogen [3], the true area (A_{true}) of the electrode was calculated to be *ca.* 0.022 cm^2. This corresponds to a surface roughness of *ca.* 2.8. The anodic charge for hydrogen desorption was used instead of the cathodic charge for hydrogen adsorption to minimize the contribution from reduction of surface oxide cause by a slight overlap of the two cathodic peaks in alkaline media. Based on the calculated value for A_{true}, the coulombic charges for formation of monolayers of PtOH and PtO on the minidisc electrode are 4.8 and 9.6 μC, respectively.

Values of specific double-layer capacitance ($C_{o,dl}$) for Pt electrodes have been reported in the range 20 - 70 μC cm^{-2} [8]. Using the approximately values of 50 μC cm^{-2} for C°_{dl} and 100 Ω for the cell resistance (R_{cell}), the cell time constant ($R_{cell}C^{\circ}_{dl}A_{true}$) was calculated to be *ca.* 0.11 ms. Hence, double-layer charging is estimated to be virtually complete within a 1 ms period following all steps in the applied potential. All *q-t* data shown have been corrected for the double layer charge by $q_{dl} = EC^{\circ}_{dl}A_{true}$, where E is the potential step.

Oxide formation under a normal-pulse waveform. Plots of q_a vs. log(t/ms) are shown in Figure 3 as a function of E_1 in the normal potential-step waveform of Figure 1A for the Pt minidisc electrode in 0.1 M NaOH. As was done for Au electrodes

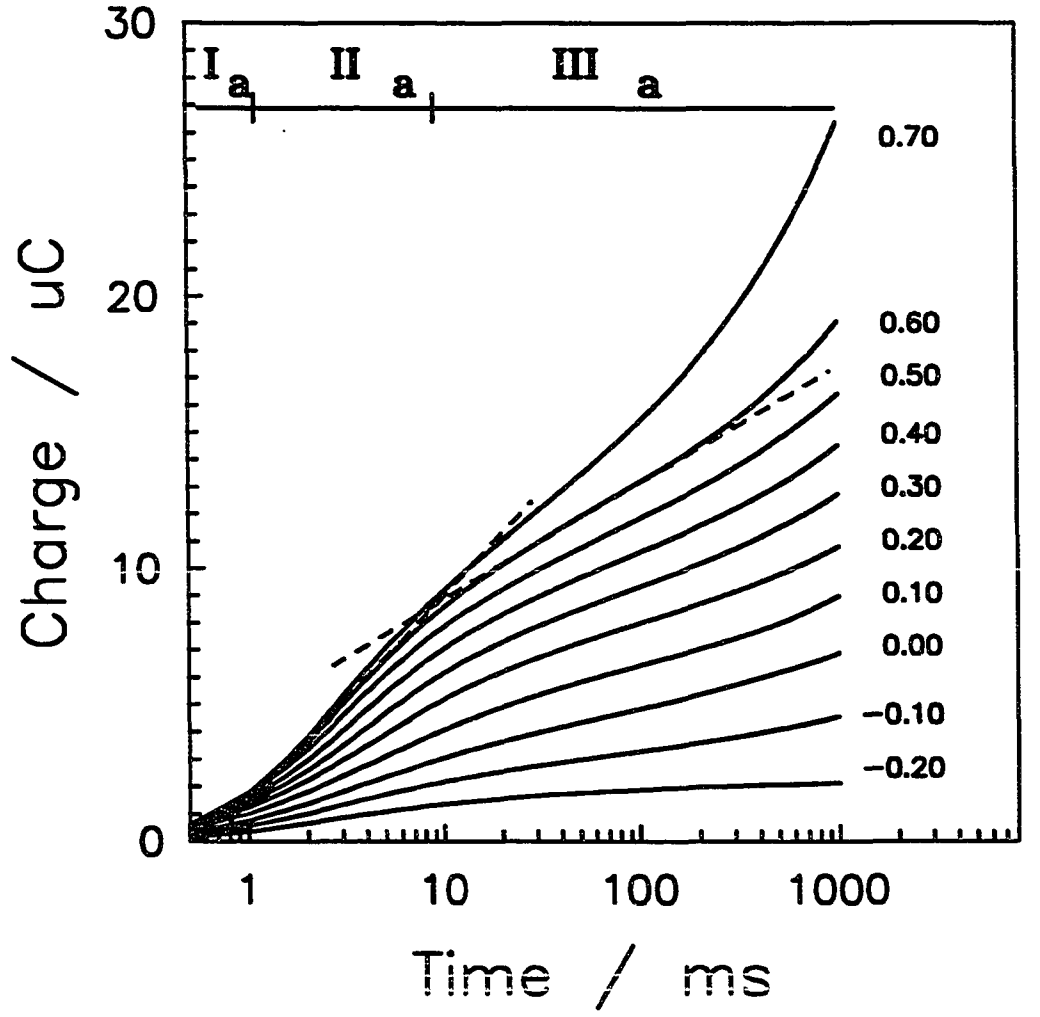

Figure 3. Plot of anodic charge (μC) versus log{time/ms} for oxide formation at the Pt minidisc electrode in 0.1 M NaOH. Values of E_1 in the waveform of Figure 1A are shown as V *vs.* SCE. Linear approximations (---) are indicated for Regions II_a and III_a at E_1 = +0.60 V.

in 0.1 M NaOH [4], we divide these plots into three distinct regions. Region I_a ($t < 2$ ms) corresponds to the initiation (i.e., nucleation) of oxide growth. Region II_a ($2 \leq t \leq 10$ ms) shows a rapid and approximately linear increase in q_a with a slope that increases with increasing potential for $-0.20 < E_1 < 0.60$ V. As was observed for Au in 0.1 M NaOH [4], we speculate that region II_a corresponds to anodic formation of PtOH. Region III_a ($t > 10$ ms) shows a much slower rate of increase for q_a and, as was done for Au in 0.1 M NaOH, we speculate that Region III_a corresponds to conversion for PtOH to PtO. The slope of the q_a-log{t/ms} plots in region III_a was independent of potential for Au; however, for Pt (Fig. 4) the slope clearly increases for increased applied potential.

Linear approximations to the q_a-log{t/ms} data in Region II_a were made and values of the intercept (A_a) and slope (B_a) are presented as a function of E_1 in Table 1. Clearly, A_a is not zero and is observed to increase with increasing values of E_1. Values of B_a are plotted vs E_1 in Figure 4 and B_1 is seen to be virtually a linear function of E_1, in the region $-0.20 < E_1 < +0.70$ V, which is consistent with Equation 2. A linear regression of the data in Figure 4 gives $C_a = 7.6 \pm 0.3$ μC V^{-1} (90% confidence), $E_{o,a} = -0.33 \pm 0.02$ V, and a correlation coefficient (r) equal to 0.9985. This estimate of $E_{o,a}$ is in good agreement with the potential for onset of oxide formation inferred from the i-E curves in Figure 2. Normalization of C_a for A_{true} gives the value of 690 μC V^{-1} cm^{-2}, which is *ca.* 13 times larger than the value estimated from Gilroy's data in H_2SO_4 (see above). This suggests that the rate of oxide formation at Pt is much faster

Table 1. Values of intercept (A_a) and slope (B_a) for region II_a of plots of q_a vs. $\log\{t/\text{ms}\}$ shown in Fig. 3 for anodic formation of oxide on the Pt minidisc electrode in 0.1 M NaOH.

$$q_a = A_a + B_a \log\{t/\text{ms}\}$$

Potential (E_1, V)	Intercept (A_a, μC)	Slope (B_a, μC)
-0.2	0.41	0.98
-0.1	0.56	1.67
0.0	0.73	2.37
0.1	0.94	3.16
0.2	1.10	4.10
0.3	1.24	4.96
0.4	1.41	5.72
0.5	1.63	6.34
0.6	1.68	7.03
0.7	1.50	7.63

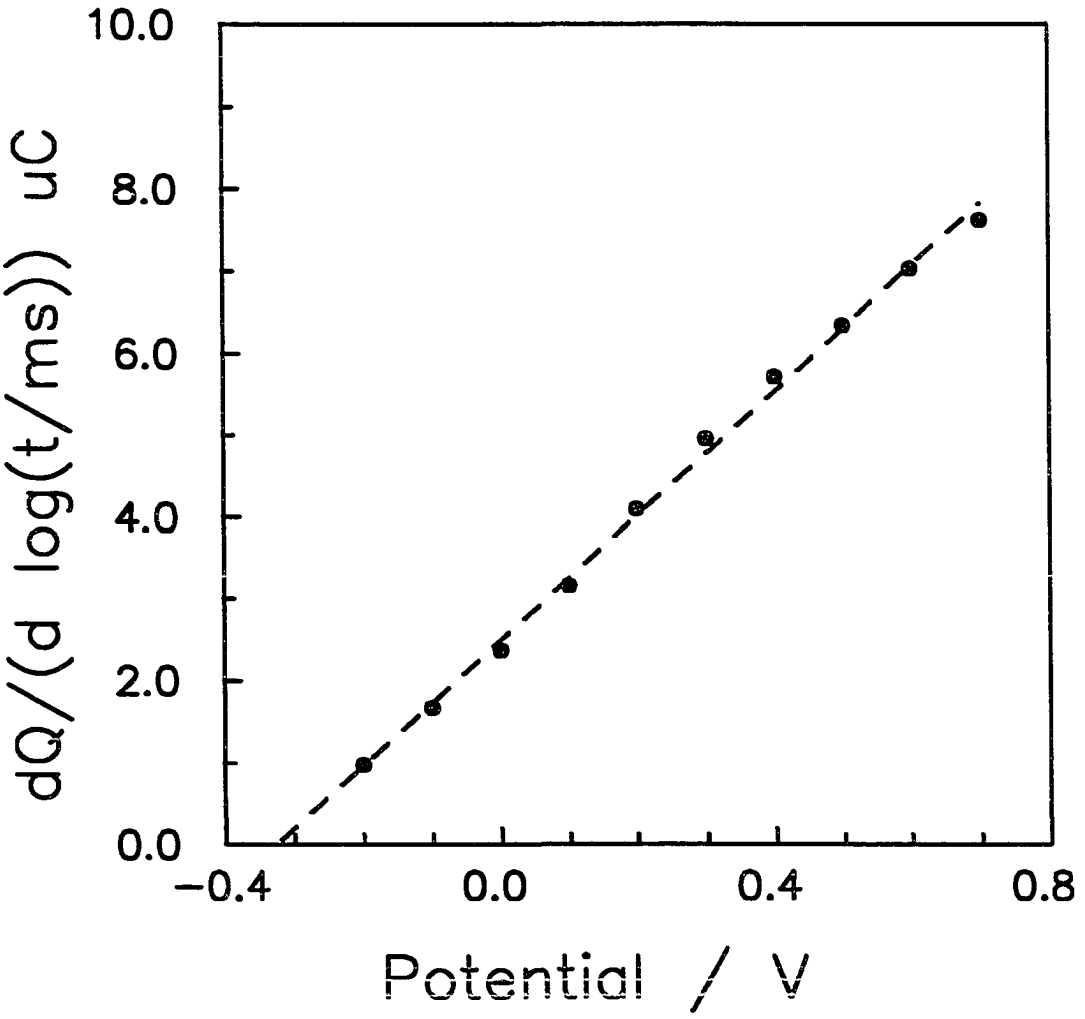

Figure 4. Plot of slopes (μC) versus potential (V vs. SCE) for the linear approximations to the anodic response in Region II_a of Figure 3.

in 0.1 M NaOH than in H_2SO_4. Based on the data in Figure 3, we estimate for E_1 = +0.2 V (i.e., E_1 - $E_{o,a}$ = *ca.* +0.53 V) that ample charge has been passed at t = *ca.* 10 ms to achieve the formation of a virtual monolayer of PtOH (4.8 μC). Because the charge in this region increases beyond 4.8 μC, we must conclude that Region II_a corresponds to multilayer growth of PtOH and, perhaps, some conversion of PtOH to PtO.

We speculate that Region III_a in Figure 3 corresponds primarily to the conversion of PtOH to PtO. Values of A_a and B_a for linear approximations to the plots in Region III_a are given in Table 2, and B_a are plotted vs. E_1 in Figure 5 for E_1 = 0.0 to +0.5 V. It is apparent from Figure 5 that the B_a is virtually a linear function of E_1 within the range indicated. This suggests that the rate controlling step in the conversion of PtOH to PtO involves charge transfer. This is in marked contrast to Region III_a of the q_a-log{t/ms} plots for Au in 0.1 M NaOH wherein B_a is independent of E_1 [4]. The rapid increase in B_a in region III_a observed here in Figure 3 for t > *ca.* 100 ms at E_1 > 0.5 V is attributed to the evolution of O_2 which commences following formation of a virtual monolayer of PtO. Hence, as previously concluded for Au in 0.1 M NaOH, it should be possible to apply large values of E_2 for very short time periods in NPAD to achieve rapid formation of PtOH without significant evolution of O_2 prior to the negative step from E_1 to E_1 < E_2.

Fast linear-sweep voltammetry. Figure 6 shows the residual voltammetric response obtained using a triangular waveform with ϕ = 0.1, 1.0, 10, and 50 mV ms^{-1}.

Table 2. Values of intercept (A_a) and slope (B_a) for Region III_a of plots of q_a vs. log{t/ms} shown in Fig. 3 for anodic formation of oxide on Pt minidisc electrode in 0.1 M NaOH.

$$q_a = A_a + B_a \log\{t/\text{ms}\}$$

Potential (E_1, V)	Intercept (A_a, μC)	Slope (B_a, μC)
-0.2	1.18	0.35
-0.1	1.28	1.01
0.0	1.46	1.69
0.1	2.41	2.01
0.2	3.28	2.36
0.3	3.82	2.76
0.4	4.34	3.13
0.5	4.46	3.68
0.6	4.35	4.41
0.7	2.21	6.58

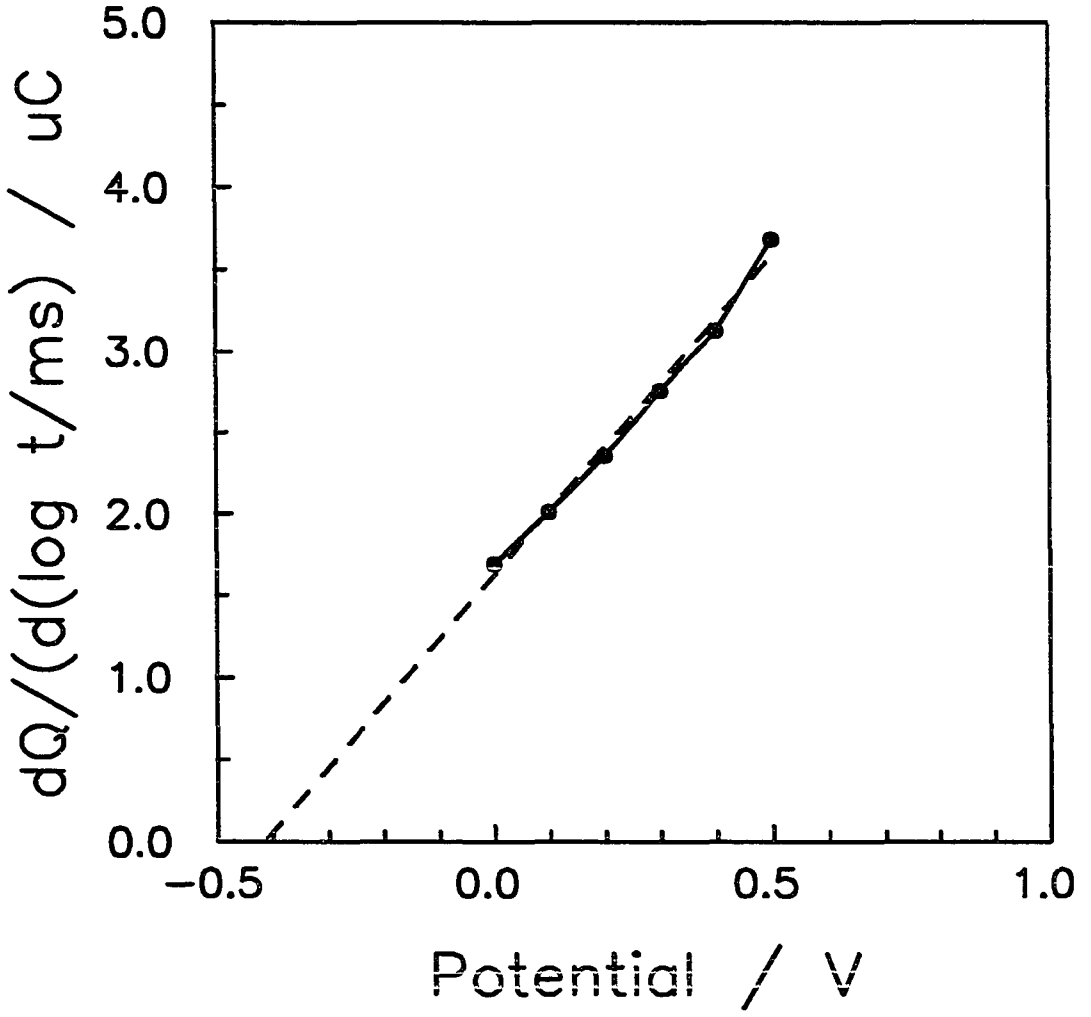

Figure 5. Plot of slopes (μC) versus potential (V *vs.* SCE) for the linear approximations to the anodic response in Region III_a of Figure 3.

The values of current plotted have been normalized for the scan rate (i/ϕ). Thus, if the heterogeneous rate constants are infinitely large for oxide formation (positive scan in the region -0.3 to +0.6 V) and for oxide dissolution (negative scan in the region 0.0 to -0.6 V), then the i/ϕ values in Figure 6 are expected to be superimposed throughout these regions. Conversely, a decrease in i/ϕ is readily observed in Figure 6 for both oxide formation and oxide dissolution as a result of increased ϕ. This is evidence for finite kinetics for these surface processes.

Furthermore, because the potential axis is also a time axis in figure 6, the onset of waves corresponding to processes occurring with slow heterogeneous kinetics are shifted in the direction of larger overpotential (longer time) as ϕ is increased. Such shifts are evident in Figure 6 for both oxide formation and oxide dissolution. It is also apparent for ϕ = 100 mV ms^{-1} that O_2 evolution does not occur even at +0.8 V during the positive scan, whereas onset of O_2 evolution for ϕ = 0.1 mV ms^{-1} is clearly evident at +0.6 V. This observation is consistent with the conclusion based on q_a-log{t/ms} plots in Figure 3 that O_2 evolution does not commence until a virtual monolayer of PtO is formed.

Oxide formation under a reverse potential-step waveform. We believe that formation of hydrous oxide at Au and Pt electrodes (AuOH and PtOH) is beneficial for the detection of numerous compounds, including many amines and sulfur compounds. These reactions involve anodic transfer of oxygen from H_2O to the oxidation products

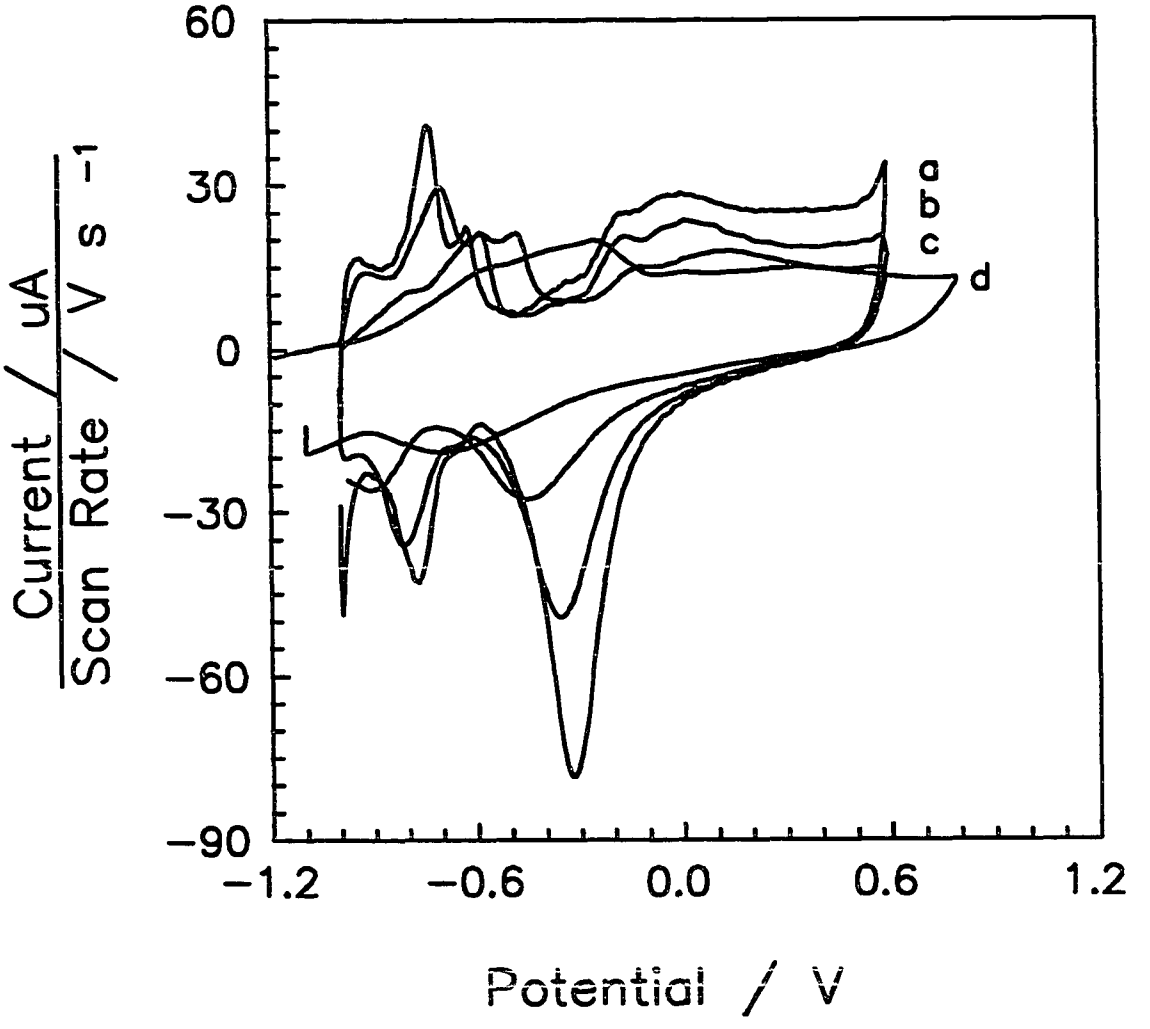

Figure 6. Residual voltammetric response for the Pt minidisc electrode in 0.1 M NaOH under fast cyclic potential scans. Scan rate (mV ms^{-1}): (a) 0.1, (b) 1.0, (c) 10, (d) 50.

and AuOH or PtOH are believed to represent the "activated" state of oxygen in these reaction mechanisms. Williams and Johnson [9] tested various multi-step waveforms to determine their benefit for activating Pt for the detection of As(III) in acidic media according to the reaction:

$$As(OH)_3 + H_2O \rightarrow OAs(OH)_3 + 2H^+ + 2e^-$$

This reaction is observed to occur concomitantly with oxide formation (PtOH and PtO) but does not occur at a surface covered with inert oxide (PtO). A reverse pulse waveform similar to that in Figure 1B was discovered to yield a transport-limited anodic signal with a virtual zero background. In this case, a large positive potential step applied for 100 ms produced the reactive PtOH and the subsequent negative step prior to current measurement prevented significant conversion of PtOH to PtO during the measurement process.

The reverse potential-step waveform illustrated in Figure 1B was applied at the Pt electrode in).1 M NaOH and representative plots of q_a *vs.* log(t/ms) are shown in Figure 7. The solid lines (—) correspond to data for an initial step to E_1 = + 0.5 V (t_1 = 10ms) with subsequent steps to E_1' = 0.4 (**a**) and 0.2 V (**b**). The dashed lines (----) correspond to the normal potential-step experiments for E_1 = 0.5 (**c**), 0.4 (**d**), and 0.2 V (**e**). The growth curves for q_a in the reverse potential-step experiments (**a** and **b**) are observed to make a transition from a rate of growth corresponding to E_1 = +0.50 V to that curve for the subsequent value of E_1'. In the case where E_1 - E_1' = 0.10 V (**a**), the rate of growth for q_a decreases and follows the dashed line for E_1 = +0.40 V

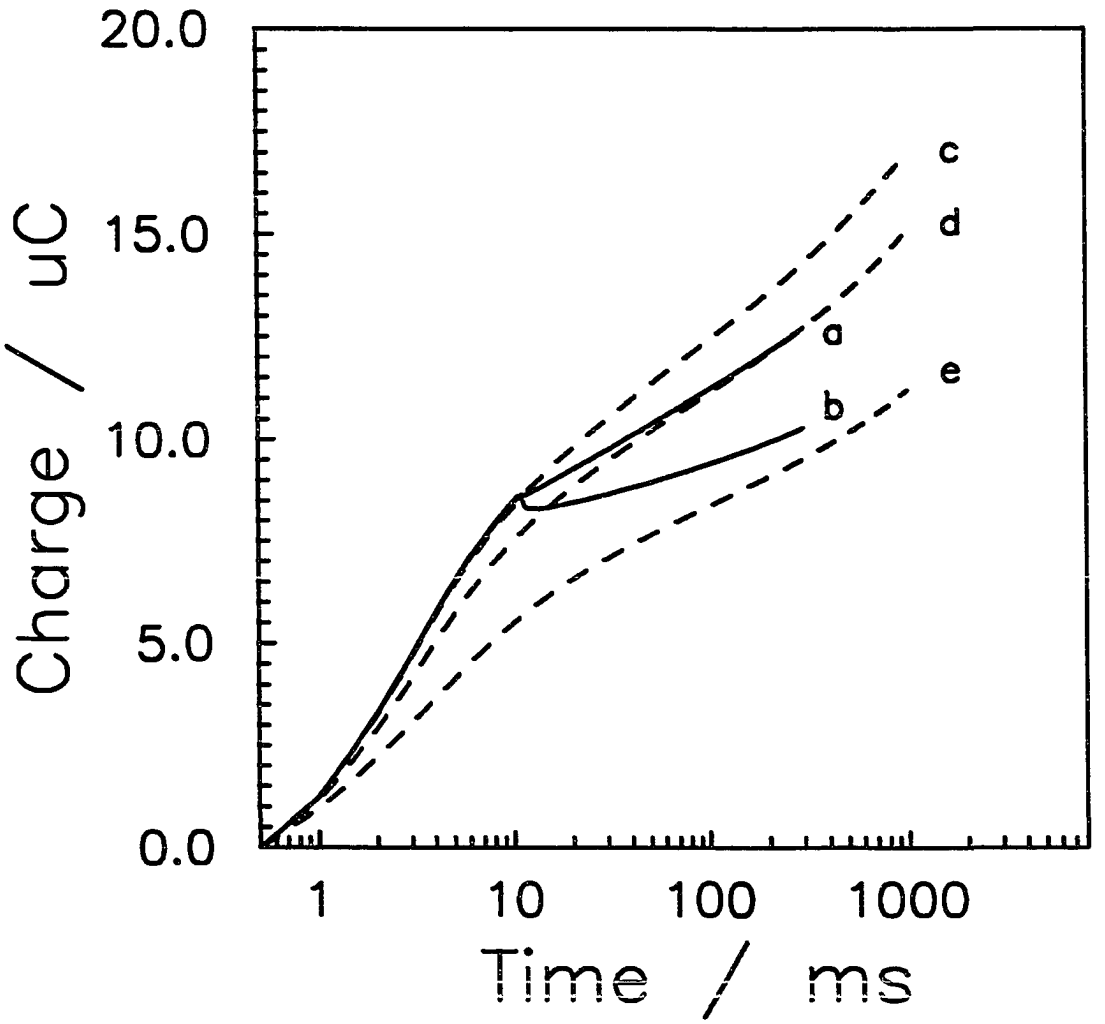

Figure 7. Plot of anodic charge (μC) versus log{time/ms} under normal potential-pulse and reverse potential-pulse waveforms for oxide formation at the Pt minidisc electrode in 0.1 M NaOH. Waveforms: (———) Figure 1A; (- - -) Figure 1B. Curves: (a) E_1 = +0.50 V, t_1 = 10 ms, E_1' = +0.40 V, t_1' = 290 ms; (b) E_1 = +0.50 V, t_1 = 10 ms, E_1' = +0.20 V, t_1' = 290 ms; (c) E_1 = +0.50 V, t_1 = 1000 ms; (d) E_1 = +0.40 V, t_1 = 1000 ms; (e) E_1 = 0.20 V, t_1 = 1000 ms.

(**d**). However, for the E_1 - E_1' = 0.30 V (**b**), the negative step results in a virtual zero slope for the growth curve during the period t = ca 10 - 50 ms. The slope gradually increases in anticipation of q_a following the dashed line for E_1 = +0.20 V (**e**).

Cathodic oxide dissolution. The waveform in Figure 1B, with E_1 = +0.40 V and t_1 = 50 ms, (*i.e.*, q_a = *ca.* 12 μC) was applied to study the cathodic dissolution of surface oxide as a function of E_1' in the range of -0.25 to -0.60 V. Chronoamperometric data (*i-t*) were collected during the period t_1' and digitally integrated to obtain q_c-t data. The q_c-log{t/ms} plots are shown in Figure 8 for $t \leq$ 1000 ms. Three cathodic regions are designated: Region I_c (t < 2 ms) corresponds to the initiation of oxide dissolution: Region II_c (2 < t < 10 ms) corresponds to a rapid and nearly linear growth in q_c at a rate which is potential dependent; and Region III_c (t > 10 ms) corresponds to a slower but nearly linear increase in q_c that appears to be relatively insensitive to E_1' for E_1' < -0.3 V. It also appears that the oxide dissolution is not complete, even for t > 1000 ms. This might imply that the surface monolayer of oxide is stripped quickly in Region II_c and that Region III_c corresponds to a slower reduction of the "bulk" oxide. Linear approximations to the curves in Regions II_c and III_c are shown by dashed lines (----) in Fig. 8.

The linear segments of plots in Regions IIc in Figure 8 were analyzed by linear regression and the values of the intercept (A_c) and slope (B_c) are presented in Table 3,

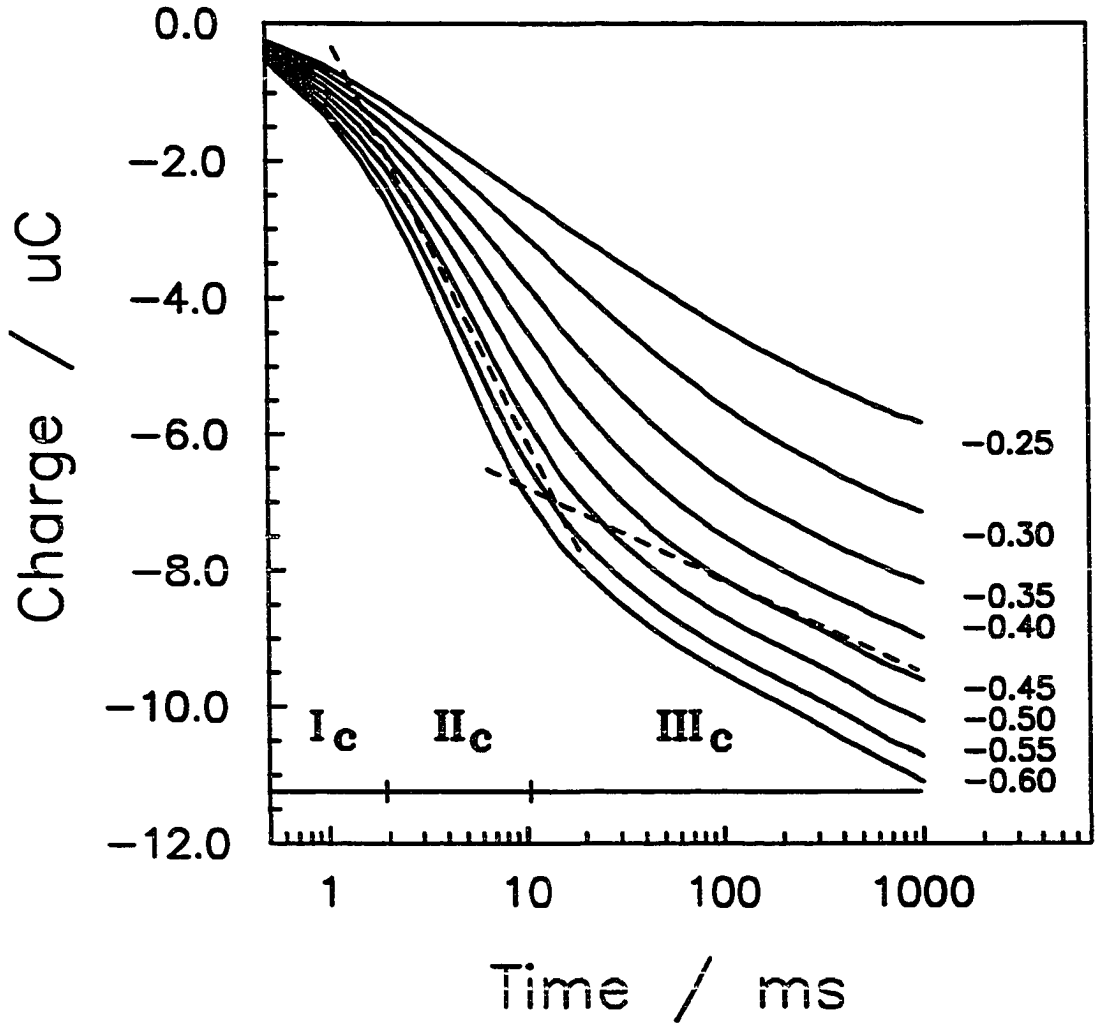

Figure 8. Plot of cathodic charge (μC) versus log{time/ms} for oxide dissolution at the Pt minidisc electrode in 0.1 M NaOH using the reverse potential-pulse waveform of Figure 1B with E_1' varied by 50 mV intervals in the range -0.2 - -0.6 V.

and B_c plotted in Figure 9, as a function of E_1'. It is apparent from Figure 9 that B_c is a linear function of the reduction overpotential as described by:

$$B_c = -C_c(E_1' - E^o) \tag{2.3}$$

Based on results of linear regression analysis of the data in Figure 9, $C_c = 12.3 \pm 0.7$ μC V^{-1} and $E_{o,c} = -0.08 \pm 0.02$ V. This value of $E_{o,c}$ corresponds well with the potential value in the *i-E* data in Figure 3 corresponding to onset of cathodic oxide dissolution.

Table 3. Values of intercept (A_c) and slope (B_c) for Region II_c of plots of q_c vs $\log\{t/\text{ms}\}$ shown in Fig. 8 for cathodic dissolution of oxide at the Pt minidisc electrode in 0.1 M NaOH.

$$q_c = A_c + B_c\log\{t/\text{ms}\}$$

Potential (E_1', V)	Intercept (A_c, μC)	Slope (B_c, μC)
-0.60	-0.71	-6.17
-0.55	-0.51	-5.85
-0.50	-0.37	-5.35
-0.45	-0.33	-4.73
-0.40	-0.34	-4.06
-0.35	-0.38	-3.35
-0.30	-0.45	-2.61
-0.25	-0.49	-2.02
-0.20	-0.50	-1.54

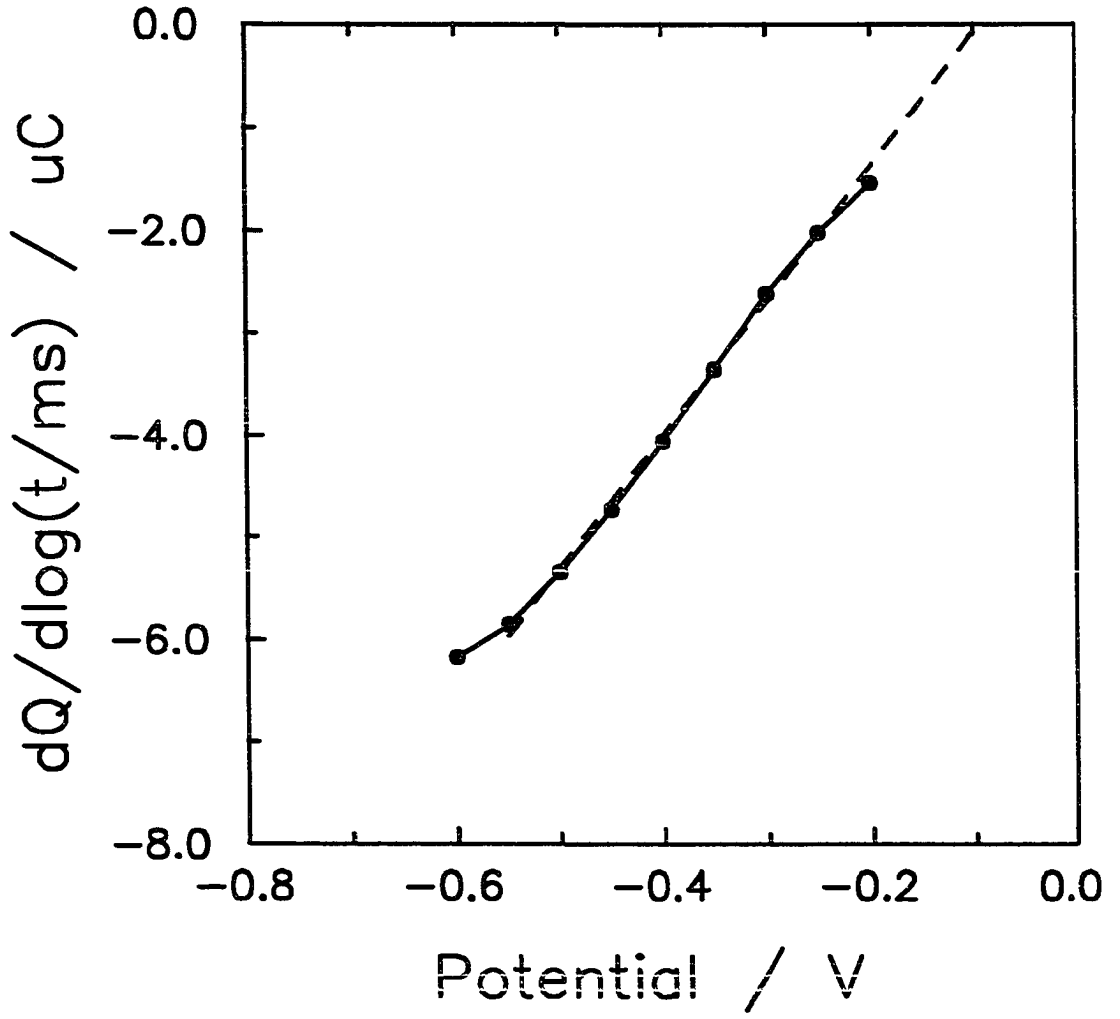

Figure 9. Plot of slope (μC) versus potential (V *vs.* SCE) for linear approximations to data in Region II_c for Figure 8.

CONCLUSIONS

Chronocoulometric (q-t) data obtained for a Pt minidisc electrode in 0.1 M NaOH with a normal potential-step waveform indicate a very rapid, potential dependent, growth rate of surface oxide, characterized by a logarithmic dependence on of q_a on t in Region II_a (see Fig. 3). This is region is concluded to correspond to the formation of multi-layers of hydrous oxide (PtOH). This is in contrast to the data for Au which showed only monolayer growth of AuOH in the corresponding region of the q_a-log{t/ms} plots. A virtual monolayer of PtOH may be formed by applying a potential step of $E_1 = +0.2$ V for *ca.* 10 ms. We also conclude that Region III_a of the q_a-log{(t > 10 ms)} corresponds to the conversion of the bulk PtOH to PtO at a much slower rate which is potential dependent.

Data in Figure 8 show that the growth of oxide can be temporarily decreased by using a reverse potential-step waveform. This observation is consistent with previous observations for Au electrodes in 0.1 M NaOH [4], and with prior conclusions by Polta and Johnson [10]. The practical consequence of this fact in RPAD is the significant decrease in background signal for the detection of sulfur compounds at both Pt and Au electrodes.

Oxide dissolution studies indicate that the initial stages of oxide dissolution are rapid (Region II_c, Fig. 9). However further reduction of bulk oxide occurs more slowly at a rate which is independent of potential. This suggests that Pt might not satisfy our desire for increased PAD signal frequency, since the frequency in this case will be limited by the dissolution of oxide.

ACKNOWLEDGEMENT

This work was supported by the National Science Foundation under contract CHE-8914700.

REFERENCES

1. D. Gilroy, *J. Electroanal. Chem.*, *71* (1976) 257.

2. D. Gilroy, *J. Electroanal. Chem.*, *83* (1977) 329.

3. H. Angerstein-Kozlowska, B.E. Conway and W.B.A. Sharp, *J. Electroanal. Chem.*, *43* (1973) 9.

4. R. Roberts and D.C. Johnson, *Electroanal.*, *4* (1992) 741.

5. G. Belanger and A.K. Vijh, in *Oxides and Oxide Films*, A.K. Vijh Ed., Marcell Dekker: New York, (1977), Vol. 5, Ch.1.

6. L.D. Burke and M.E.G. Lyons, in *Modern Aspects of Electrochemistry*, R.E. White, J.O'M. Bockris, B.E. Conway, Eds., Plenum Press, New York, 1986, Vol. 18, Ch. 4.

7. J.P. Hoare, in *Advances in Electrochemistry and Electrochemical Engineering*, P. Delahay, Ed., Interscience, New York, 1967, Vol.6, pp 201-288.

8. A.J. Bard, Ed., of *Encyclopedia of Electrochemistry of the Elements*, Marcell Dekker: New York, (1976), Vol. 6, p. 196.

9. D.G. Williams and D.C. Johnson, *Anal. Chem.*, *63* (1993) 1785.

10. T.Z. Polta and D.C. Johnson, *J. Electroanal. Chem.*, *209* (1986) 159.

PAPER 3.

FAST-PULSED ELECTROCHEMICAL DETECTION AT NOBLE METAL ELECTRODES: A STUDY OF THE FREQUENCY-DEPENDENT RESPONSE FOR CHROMATOGRAPHICALLY SEPARATED CARBOHYDRATES[3]

[3]Reprinted with permission from R.E. Roberts and D.C. Johnson, *Electroanalysis, 6* (1994) 269. Copyright 1994 VCH Publishers, Inc.

ABSTRACT

Waveforms used in pulsed electrochemical detection (PED) have frequencies of *ca.* 1 Hz when optimized to give a maximum signal-to-noise ratio (S/N) for carbohydrates. However, higher frequencies are desired for applications of PED to capillary electrophoresis (CE) and microcolumn liquid chromatography (MLC) which can produce narrow elution peaks. Minimization of the time periods for oxidative cleaning and reductive reactivation in PED waveforms generated by the Dionex Pulsed Electrochemical Detector allows the increase in waveform frequency to *ca.* 3 Hz without change in the traditional time period of 200 ms prescribed for integration of anodic current. However, further increase in frequency requires a decrease in the integration period with a corresponding loss of signal strength.

INTRODUCTION

Research in our laboratory is devoted to the development of electrochemical detection for polyalcohols, carbohydrates, amines, amino acids, and organosulfur compounds at Au electrode in alkaline media [1,2]. the compounds of primary interest to us do not have strong UV/vis-active chromophores and, therefore, are not easily detected by direct conventional photometric techniques. Furthermore, detection of the majority of these compounds at Au electrodes under conditions of constant applied potential is characterized by loss of electrode response that is usually attributed to surface "fouling" as a result of (i) irreversible adsorption of intermediate oxidation products, in detection of polyalcohols, carbohydrates, and alkanolamines; and (ii) formation of inert surface oxides, in detections of amines, amino acids, and organosulfur compounds.

Detection of polyalcohols, carbohydrates, and alkanolamines can be achieved when a high electrode activity is maintained by application of pulsed potential waveforms in which the process of anodic detection is alternated with positive and negative potential excursions to achieve oxidative cleaning and reductive reactivation of the Au surface. This protocol is the basis of so-called "Pulsed Amperometric Detection (PAD)". Whereas this title implies the direct measurement of electrode current, instrumentation developed to achieve PAD frequently integrates the amperometric signal, or a proportional voltage signal, over a finite time period (t_{int}) to give a signal output with units of coulombs. Whereas this measurement strategy may be described

more correctly by the name "Pulsed Coulometric Detection (PCD)", the generic name "Pulsed Electrochemical Detection (PED)" is more commonly applied to any electrochemical detection methodology that benefits from application of pulsed potential waveforms regardless of the electronic strategy for signal measurement. Here, we report PED signals in units of nanocoulombs.

Neuburger and Johnson [3] demonstrated that the signal-to-noise ratio (S/N) in PED can be increased significantly by increasing t_{int} in the waveform. Furthermore, they recommended that discrimination against noise which is correlated with the line frequency. Subsequently, the value t_{int} = 200 ms has been commonly recommended to give optimal discrimination against noise correlated with both 60-Hz and 50-Hz line frequencies. LaCourse and Johnson [4] determined the optimal values for the various potential and time parameters in the PAD waveform to be applied for carbohydrate detection. Their optimization was based on a simplex procedure applied to data obtained by pulsed voltammetry at a rotated disk electrode (RDE). The result was an optimized waveform having frequency of *ca.* 1 Hz with t_{int} = 200 ms.

The advent of rapid and efficient separation techniques, for example, capillary electrophoresis (CE) and microcolumn liquid chromatography (MLC), has motivated us to apply PED waveforms at frequencies greater than 1 Hz to achieve a more accurate description of the narrow elution peaks expected to be obtained for these separation techniques. Previously, we described results of a kinetic study of the formation and dissolution of surface oxide at Au electrodes in 0.1 M NaOH [5]. We deduced that

formation of a monolayer of the hydrous surface oxide (AuOH) can be virtually complete within a period of ca. 20 ms, as compared to the recommended value of 180 ms in the optimized waveform of LaCourse and Johnson [4]. Furthermore, the kinetic data indicate that reductive dissolution of AuOH can be completed within a period of ca. 20 ms for $E_{red} \leq$ -0.4 V vs. SCE, as compared to 360 ms in the optimized waveform. Here we examine LC-PED signals for the separation of a mixture of five carbohydrates as a function of tint using minimal values for the oxidative cleaning and reductive reactivation periods.

EXPERIMENTAL

Reagents. Solutions were prepared from reagent grade chemicals as received. Water was purified by passage through two D-45 demineralizing cartridges (Culligan), followed by further treatment by a Milli-Q system (Millipore). Eluents were dearated by passing dispersed N_2 gas through the eluent reservoir.

Equipment. The liquid chromatograph consisted of an APM-1 pump (Dionex), a 7010 injection valve with a 20-μL sample loop (Rheodyne), and a CarboPac PA1 analytical column (4 x 250 mm, Dionex). Separations were achieved by isocratic elution with 0.1 M NaOH. The home-made detector dell consisted of a Au wire (0.4 mm diameter) in a wall-jet configuration [6] with a coiled Pt wire (*ca.* 2 cm^2) as the counter electrode. Potential-time (E-t) waveforms were applied and amperometric signals acquired using a Dionex Pulsed Electrochemical Detector. All electrode potentials were measured and are reported vs. a miniature saturated calomel electrode (SCE, Fisher Scientific). The analog output from the PED was digitally recorded using a 286 desk-top computer (Zenith) with a DT2821 interface (Data Translation) in conjunction with Asyst software (Asyst Software Technologies).

PAD waveform. The potential-time waveform applied in these studies is illustrated in Figure 1. The detection potential (E_{det}) was set at +0.15 V to correspond approximately with the potential of maximum signal for various

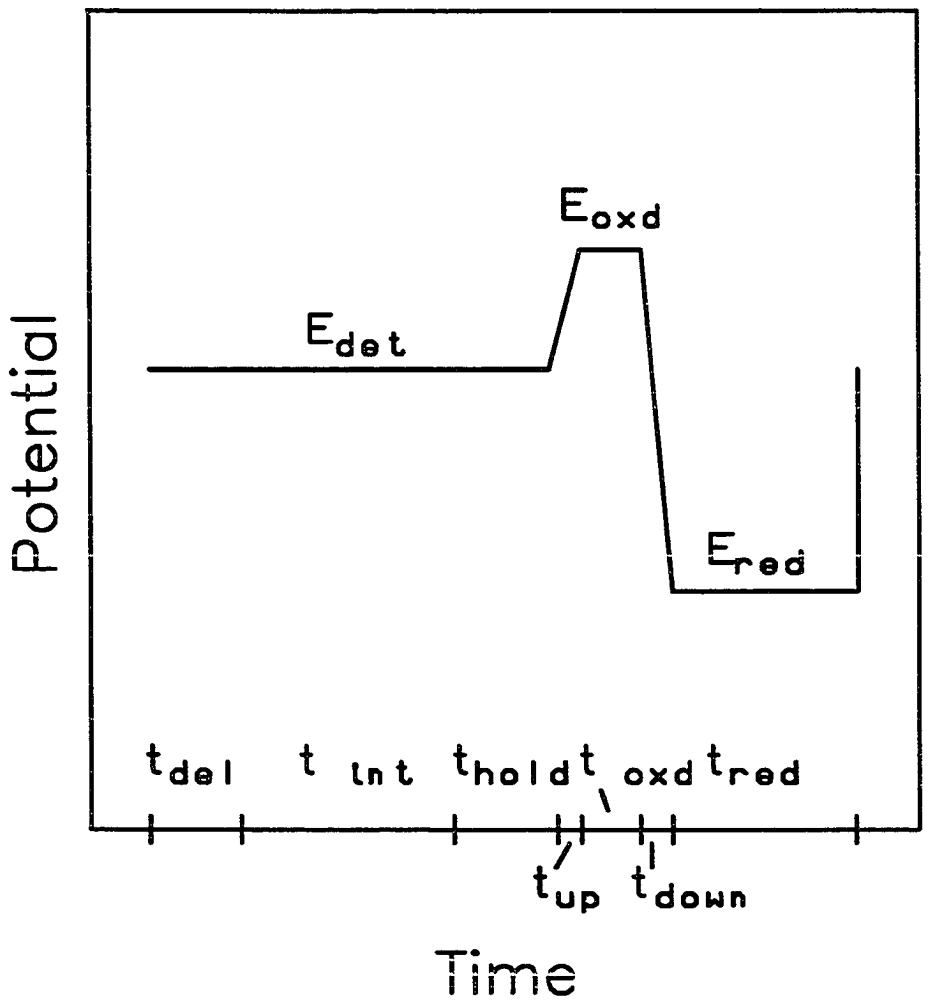

Figure 1. Diagram of PED waveform applied for detection of carbohydrates at Au electrode in 0.10 M NaOH.

Parameters: Edet = +0.15 V, (tdet = tdel + tint + thold),
Eoxd = +0.5 V, (tup = 10 ms, toxd = 20 ms),
Ered = -0.5 V, (tdown = 10 ms, tred = 50 ms).

carbohydrates as determined by cyclic voltammetry. The detection period (t_{det}) consisted of three component periods: (i) a brief delay period (t_{del}) prior to signal measurement to allow double-layer charging to subside and the analytical signal to decrease to a level which could be accurately monitored; (ii) the integration period (t_{int}) during which a voltage proportional to the amperometric signal was measured by digital integration; and a hold period (t_{hold}) following signal integration prior to application of the cleaning and reactivation pulses. The potential for oxidative cleaning (E_{oxd}) was chosen to be +0.5 V and was applied for a period (t_{oxd}) of 20 ms. The potential for reductive reactivation (E_{red}) was chosen to be -0.5 V and was applied for a period (t_{red}) of 60 ms. Whereas the prior kinetic study [5] indicated that t_{red} = 20 ms is sufficient for reduction of AuOH, the value of 60 ms was chosen to avoid an integration error obtained for shorter values of t_{red} in the Dionex Pulsed Electrochemical Detector (PED). This error arises when the integration period is greater than a predetermined fraction of the total waveform period. Transitions in the PAD waveform from E_{det} to E_{oxd}, during the period t_{up} (10 ms), and from E_{oxd} to E_{red}, during the period t_{down} (10 ms), were achieved by fast linear scans in the Dionex PED. Use of linear scans rather than potential steps to initiate the oxide formation and dissolution processes minimizes problems that could result from current overload as a consequence of large current spikes. The total waveform period (T_{tot}) was the sum of the seven component time periods.

Procedures. Data were obtained at ambient temperatures (25 $\pm$ 2°C). Electrodes were polished with 0.05-μm alumina in water on microcloth (Buehler) and then rinsed with deionized water. Polished electrodes were electrochemically conditioned by repetitive application of a three-step PAD waveform at the frequency of interest in the detector cell for ca. 30 min prior to injection of sample into the chromatographic column.

RESULTS AND DISCUSSION

Variation of the integration period. LC-PED data are shown in Figure 2 for separation of five carbohydrates as a function of t_{int} values increased from 30 to 850 ms corresponding to waveform frequencies decreased from 6.25 Hz to 1.02 Hz (see Table 1). Current scaling is maintained constant in Figure 2 to allow for ease in visual comparison of peak signal as a function of t_{int}. Clearly, as expected, the peak signal (P) for all five carbohydrates increased as a function of increased t_{int}, that is, decreased waveform frequency.

Figure 3 summarizes the values of P from Figure 2 as a function of t_{int}. According to Neuburger and Johnson [3], P is expected to increase as a linear function of t_{int} for a steady-state amperometric signal. The absence of an exact linear dependence of P upon tint in Figure 2 might be an indication that the electrode current following the step from E_{red} to E_{det} has not come to a steady-state value during the delay period (t_{del} = 30 ms) used in this experiment. Furthermore, electrode fouling during the combined periods $t_{del} + t_{int}$ also will contribute to a nonlinear P-t_{int} correspondence.

Estimation of detection limits for glucose. The experiment that produced Figure 2 was repeated for 20-μL injections containing 16 pmoles of glucose and the results are shown in Figure 4. It is apparent that the relative change in P as a function of t_{int} is virtually the same as shown in Figure 2. It is also apparent that the noise (N) in the baselines decreases only slightly with increasing t_{int}. The periodic nature of the

Table 1. Summary of waveform parameters in Figure 1 used to obtain data in Figures 2 through 4 as a function of integration period (t_{int})[a]

t_{int} (ms)	t_{det} (ms)	T_{tot} (ms)	frequency (Hz)
30	60	160	6.25
50	80	180	5.56
100	130	230	4.35
150	180	280	3.57
200	230	330	3.03
400	430	530	1.87
850	880	980	1.02

Potentials: E_{det} = +0.15 V, E_{oxd} = +0.5 V, E_{red} = -0.5 V. Time periods: t_{del} = 30 ms, t_{int} = variable, t_{hold} = 0 ms, t_{up} = 10 ms, t_{oxd} = 20 ms, t_{down} = 10 ms, t_{red} = 60 ms. $T_{tot} = t_{del} + t_{int} + t_{hold} + t_{up} + t_{oxd} + t_{down} + t_{red}$.

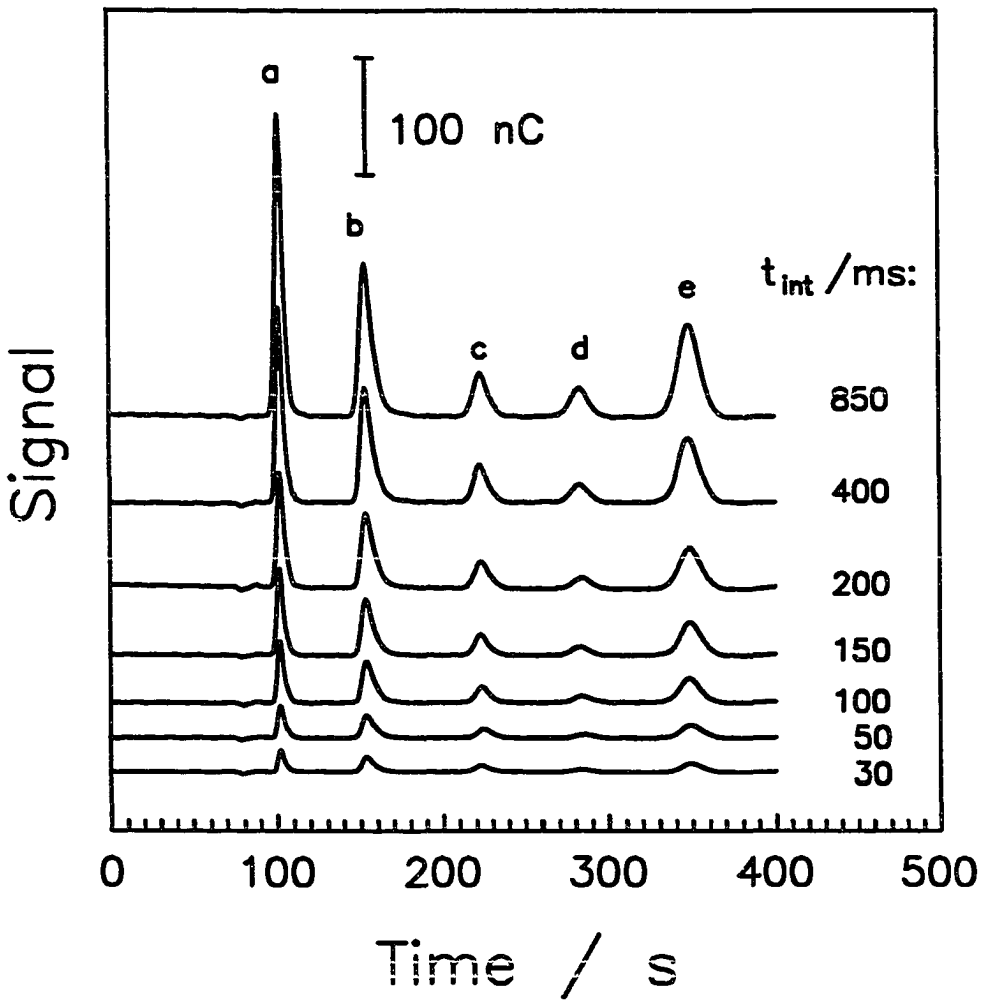

Figure 2. LC-PED results for mixture of five carbohydrates.
Waveform parameters: see Table 1.
Column: Dionex CarboPac PA1 (4 X 250 mm).
Elution: isocratic, 0.1 M NaOH 0.8 ml min^{-1}.
Injection: 20 μL.
Peaks: (a) 10 μM inositol, (b) 20 μM sorbitol, (c) 20 μM rhamnose, (d) 20 μM glucosamine, (e) 20 μM glucose.

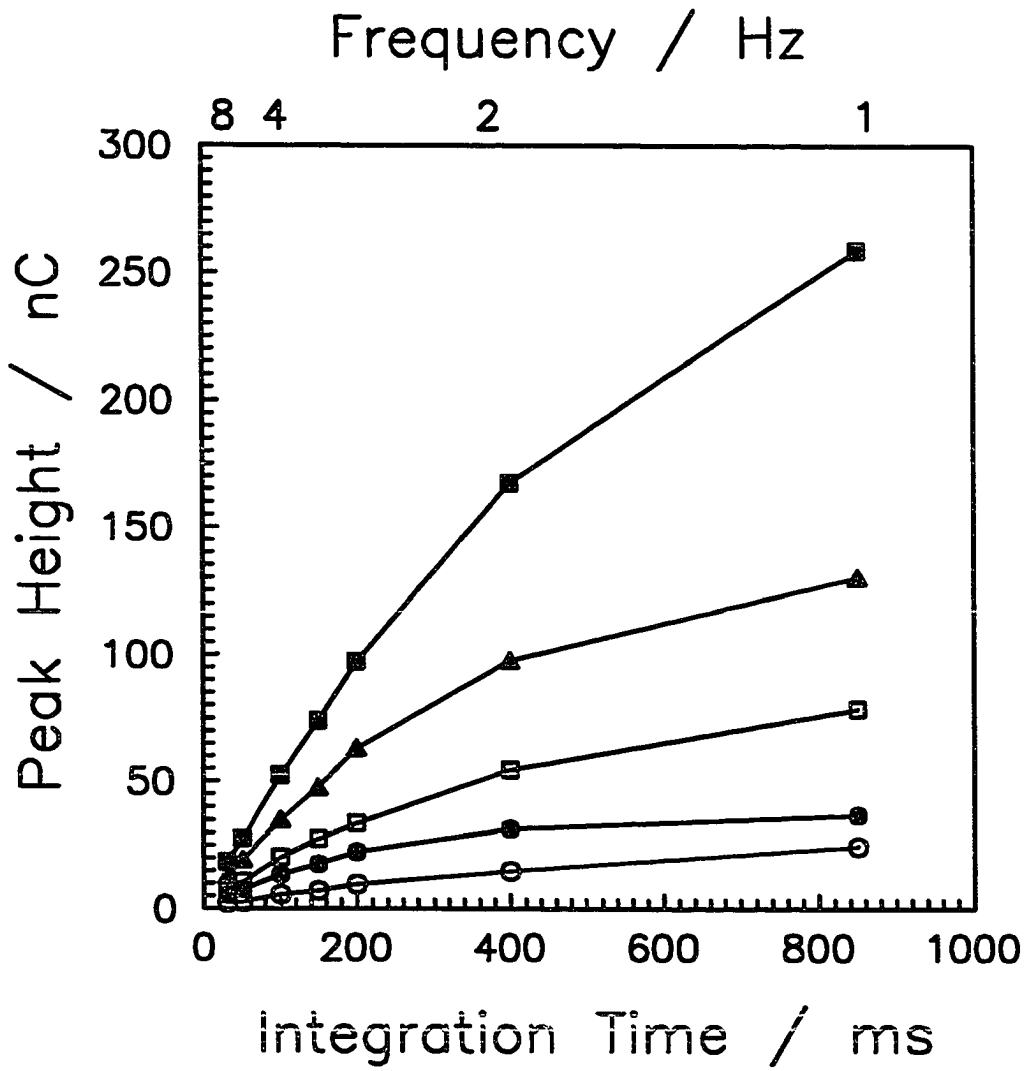

Figure 3. Summary of peak response in Figure 2 as a function of the integration period (t_{int}) and waveform frequency.

Curves: (■) 10 μM inositol, (▲) 20 μM sorbitol, (□) 20 μM rhamnose, (◒) 20 μM glucosamine, (○) 20 μM glucose.

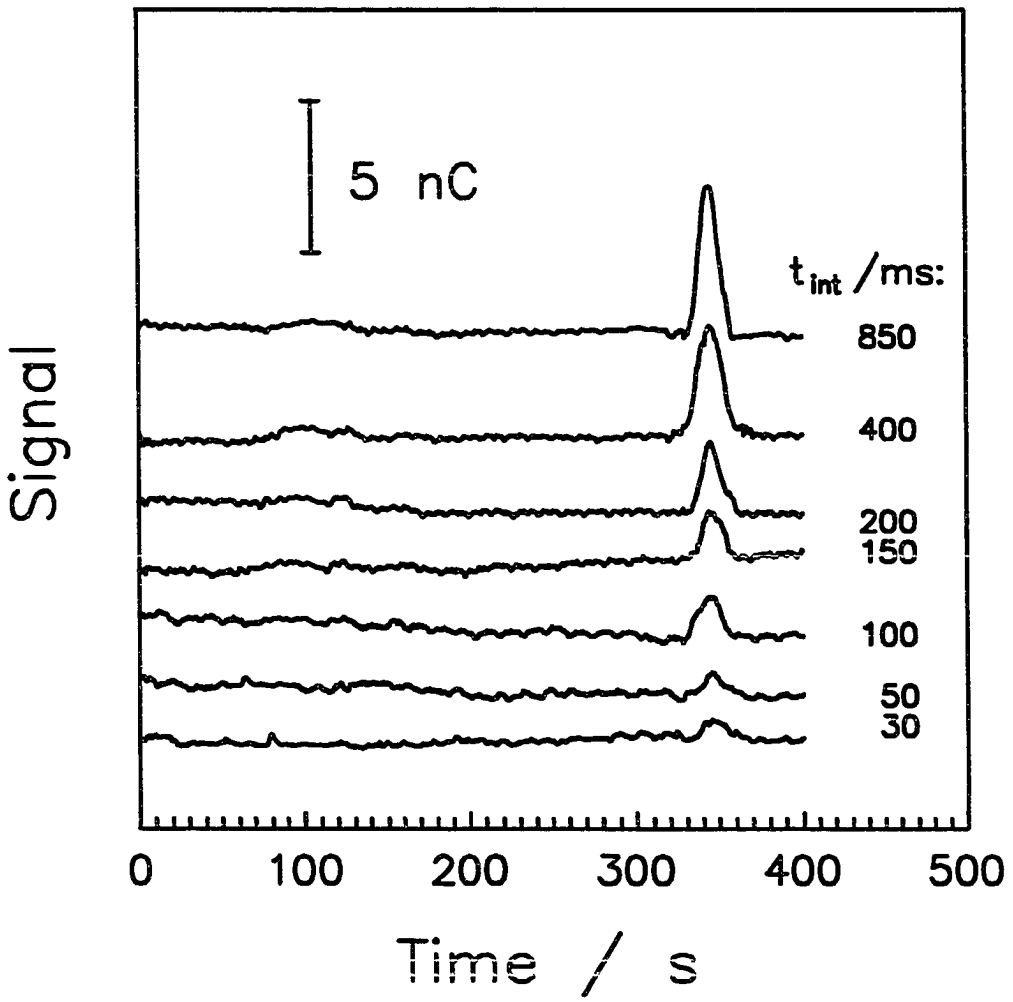

Figure 4. LC-PED results for 20 μL injections containing 16 pmoles glucose.
Waveform parameters: see Table 1.
Column: Dionex CarboPac PA1 (4 X 250 mm).
Elution: isocratic, 0.1 M NaOH 0.8 ml min^{-1}.

existent baseline noise is an indication that it originates from fluctuations in the flow rate of the mobile phase, for example, so-called "pump noise".

Figure 5 shows values of P (__) and P/N (----) from Figure 4 plotted as a function of t_{int}, where values of N were taken as 1/2 the peak-to-peak fluctuation in the baseline. It is apparent that P and P/N are nearly linear functions of t_{int} over the range $0 < t_{int} < 400$ ms, in agreement with the prediction of Neuburger and Johnson [3].

From these data, the limits of detection (LOD) for glucose in 20-μL injections corresponding to $P/N = 3$ in this apparatus were estimated for each waveform (see Table 1) and the results are given in Table 2. To summarize, the estimated LOD is

Table 2. Limits of detection based on P/N Values from data in Figure 5[a]

t_{int} (ms)	frequency (Hz)	L.O.D. (pmoles)
30	6.25	11
50	5.56	8.4
100	4.35	4.8
150	3.57	3.4
200	3.03	1.8
400	1.87	1.1
850	1.02	0.78

[a]Waveform: see table 1.

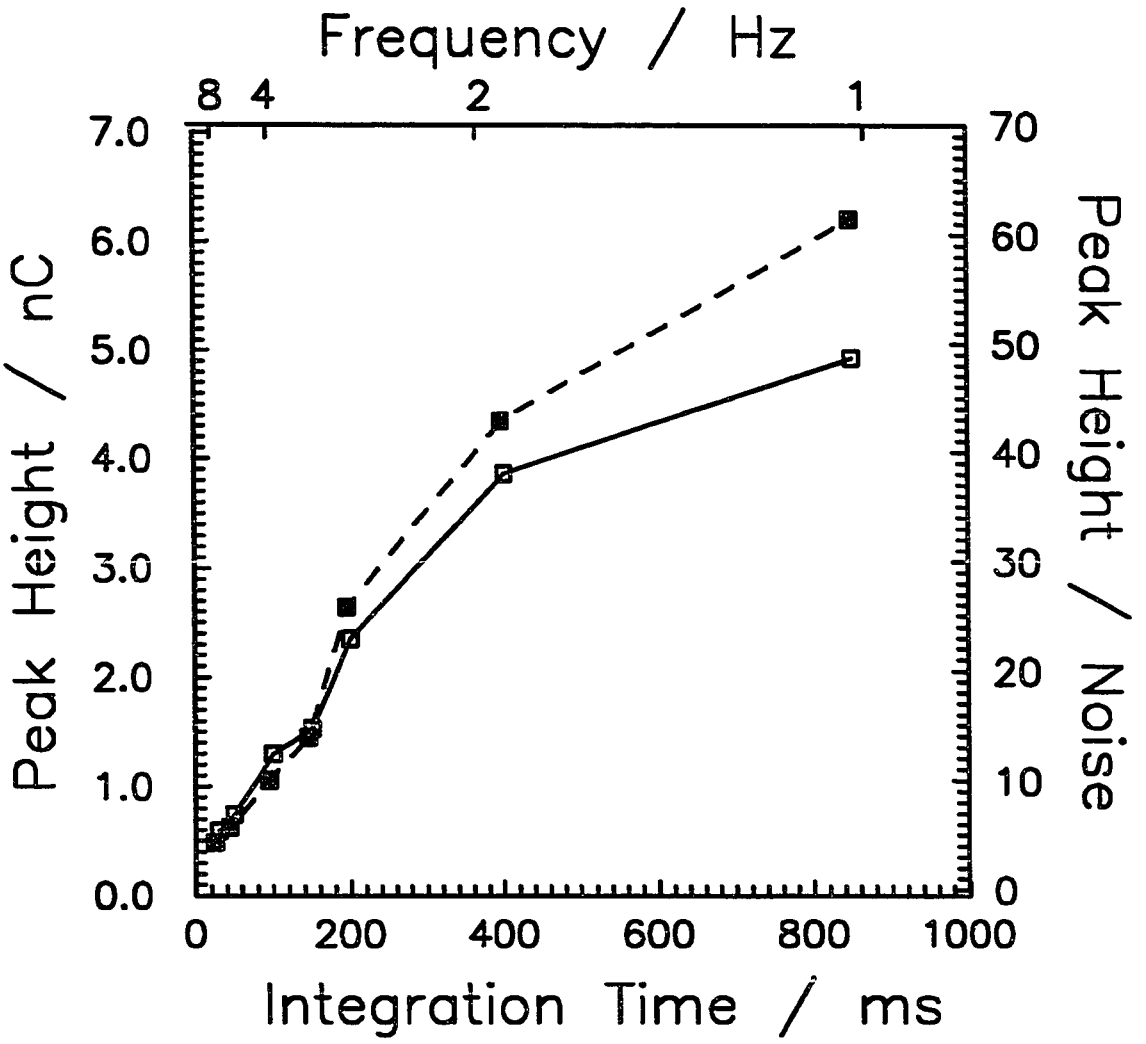

Figure 5. Summary of peak response (P) (__) and peak-to-noise ratio (P/N) (---) for data in Figure 4.

0.78 pmoles (*ca.* 0.04 μM) for t_{int} = 850 ms (1.02 Hz waveform), 1.8 pmoles (*ca.* 0.9 μM) for t_{int} = 200 ms (3.03 Hz), and 11 pmoles (*ca.* 0.6 μM) for t_{int} = 30 ms (6.25 Hz).

Variation of the hold period. We estimate that the choice of t_{oxd} = 20 ms corresponds to the minimum time for the generation of a monolayer of AuOH at E_{oxd} = +0.5 V in 0.1 M NaOH. therefore, we anticipate that fouling by adsorbed detection products and solution impurities must be kept at a minimum if oxidative cleaning is to be effective for this value of t_{oxd}, that is, low concentrations of carbohydrates. Because the extent of surface fouling is expected to be proportional to the total time period during which oxidative detection occurs (that is, $t_{det} = t_{del} + t_{int} + t_{hold}$), values of P were obtained as a function of t_{hold} for a constant value of t_{int} = 30 ms (see waveform summary in Table 3). The data are shown in Figure 6. The fact that P decreases slightly with increasing thold indicates that the electrode surface was slightly fouled during the total detection period (t_{det}). Hence, for these concentrations, the value of t_{oxd} = 20 ms apparently was not sufficient to accomplish complete oxidative cleaning of the electrode surface. Because there is no benefit in using $t_{hold} > 0$ ms, we certainly recommend $t_{hold} = 0$ in PAD waveforms to minimize the extent of electrode fouling. In spite of the evidence in Figure 6 that some fouling occurred for the concentrations used, peak signals were reproducible to better than 3 % relative standard deviation (rsd) for five injections for all waveforms and solutions tested in this study. Furthermore, there was

no long-term evidence of deterioration in peak response.

Table 3. Summary of waveform parameters in Figure 1 used to obtain data in Figure 6 as a function of hold period (thold)[a]

t_{hold} (ms)	t_{det} (ms)	T_{tot} (ms)	frequency (Hz)
0	60	160	6.25
40	100	200	5.00
90	150	250	4.00
170	230	330	3.00
340	400	500	2.00

[a]Potentials: E_{det} = +0.15 V, E_{oxd} = +0.5 V, E_{red} = -0.5 V. Time periods: t_{del} = 30 ms, t_{int} = 30 ms, t_{hold} = variable, t_{up} = 10 ms, t_{oxd} = 20 ms, t_{down} = 10 ms, t_{red} = 60 ms. $T_{tot} = t_{del} + t_{int} + t_{hold} + t_{up} + t_{oxd} + t_{down} + t_{red}$.

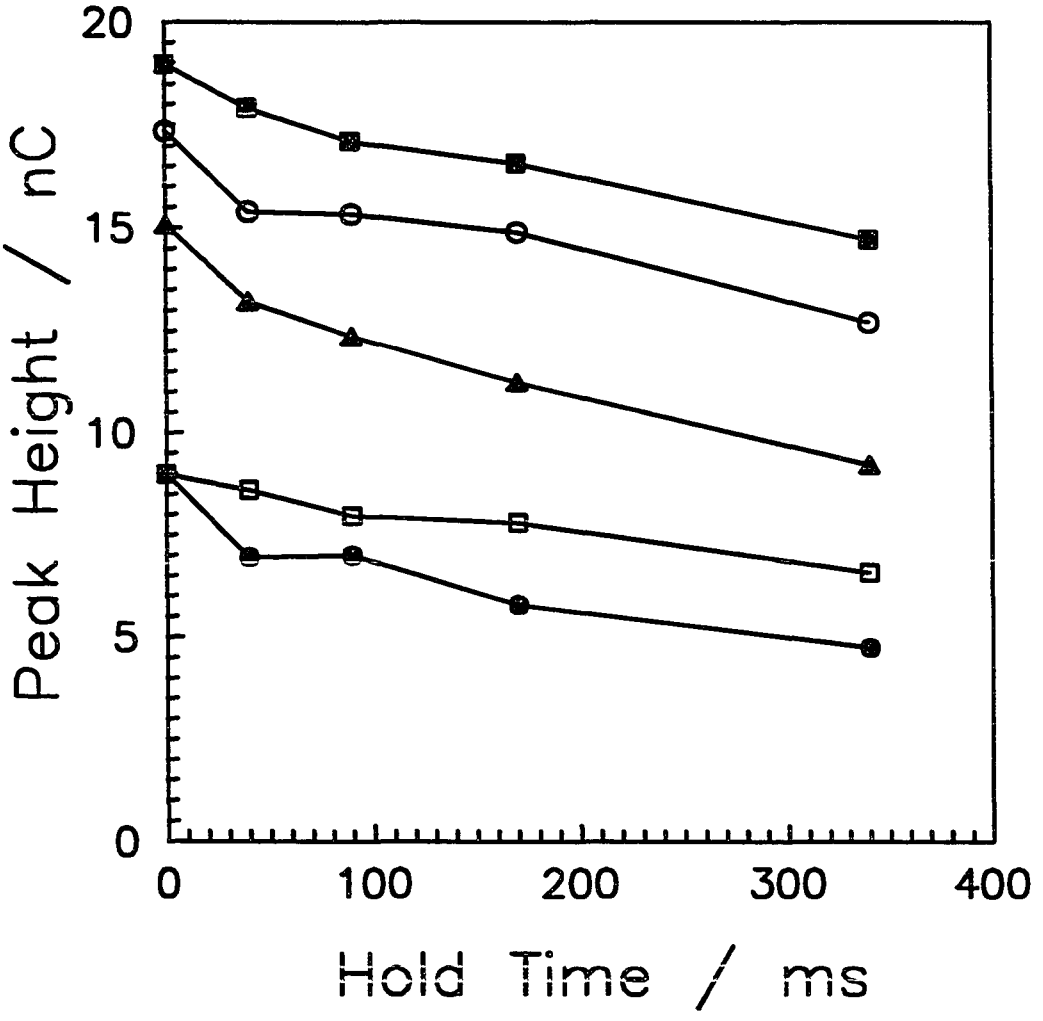

Figure 6. Summary of peak response as a function of the hold period (thold).
Waveform parameters: see Table 1.
Column: Dionex CarboPac PA1 (4 X 250 mm).
Elution: isocratic, 0.1 M NaOH 0.8 ml min^{-1}.
Injection: 20 μL.
Peaks: (■) 10 μM inositol, (○) 20 μM sorbitol, (▲) 20 μM rhamnose, (□) 20 μM glucosamine, (●) 20 μM glucose.

CONCLUSIONS

Pulsed waveforms can be applied in the Dionex PED system at a frequency of ca. 3 Hz by use of minimal values for oxidative cleaning (t_{oxd} = 20 ms) and reductive reactivation (t_{red} = 60 ms), while maintaining the normally recommended value for the integration period (t_{int} = 200 ms). Higher frequencies can be achieved for these minimal values of t_{oxd} and t_{red} only by decreasing tint with the result of sacrificing the peak signal (*P*) and the peak-to-noise ratio (*P/N*) in LC-PED. The extent of sacrifice can be anticipated approximately from Figure 5 for injections of 16 pmoles of glucose showing that *P* and *P/N* are nearly linear functions of tint for $t_{int} < 200$ ms.

In their optimization study, LaCourse and Johnson [4] demonstrated for 0.1 mM glucose in 0.1 M NaOH that signal strength at a Au RDE is decreased substantially at toxd < *ca.* 200 ms for $E_{oxd} \geq +0.6$ V. They concluded that small values of t_{oxd} are not sufficient to achieve complete oxidative cleaning of the electrode surface. Nevertheless, our data for five injections of solutions containing $\leq$ 20 μM of each component indicate the peak reproducibility is satisfactory (< 3 % rsd) for t_{oxd} = 20 ms without long-term deterioration of detection sensitivity.

Clearly, our results show that a sacrifice in LOD is to be expected when PED waveform frequency is increased. For example, on the basis of data for glucose given in Table 2, a frequency increase from 1 to 3 Hz results in an increase of LOD by *ca.* 2.3X; however, increasing frequency from 3 Hz to ca 6 Hz results in a further increase of LOD by 6X. The suitability of PED waveforms with frequency > 1 Hz for

applications to capillary electrophoresis (CE) and microcolumn liquid chromatography (MLC) will, of course, be dependent on peak widths which are strongly influenced by injection volume. A subsequent publication will examine the dependence of peak signal-noise characteristics and limits of detection on injection volume and waveform frequency.

ACKNOWLEDGEMENTS

This work was supported by grants from the National Science Foundation (CHE-8914700) and Dionex Corp.

REFERENCES

1. D.C. Johnson and W.R. LaCourse, *Anal. Chem.*, *62* (1990) 589A.

2. D.C. Johnson and W.R. LaCourse, *Electroanal.*, *4* (1992) 367.

3. G.G. Neuburger and D.C. Johnson, *Anal. Chim. Acta*, *192* (1987) 205.

4. W.R. LaCourse and D.C. Johnson, *Anal. Chem.*, *65* (1993) 50.

5. R. Roberts and D.C. Johnson, *Electroanal.*, *4* (1992) 741.

6. P.J. Vandeberg, J.L. Kawagoe and D.C. Johnson, *Anal. Chim. Acta*, *260* (1992) 1.

PAPER 4

FAST-PULSED ELECTROCHEMICAL DETECTION AT NOBLE METAL ELECTRODES: A STUDY OF THE FREQUENCY-DEPENDENT RESPONSE FOR CARBOHYDRATES SEPARATED BY CAPILLARY ELECTROPHORESIS[4]

[4]R.E. Roberts and D.C. Johnson, unpublished.

ABSTRACT

Optimum pulsed potential waveforms applied for the detection of carbohydrates separated by high performance anion exchange chromatography are operated at frequencies of *ca.* 1 Hz. However, the rapid and efficient separation of carbohydrates by capillary electrophoresis requires waveforms of greater frequency to adequately describe elution peaks. A capillary electrophoresis system is described for use with the Dionex Pulsed Electrochemical Detector. Waveform frequencies greater than 1 Hz are obtained by minimizing the oxidative and reductive cleaning times, and a frequency of 2.7 Hz can be achieved without changing the 200-ms integration period usually prescribed for the detection of carbohydrates. Further decrease in the integration period results in a decrease in the predicted signal strength, possibly due to insufficient cleaning of fouling species by the minimized cleaning cycle. The 2.7 Hz waveform is used to determine the concentration of glucose in human blood samples.

INTRODUCTION

In our laboratory, we are interested in the direct and sensitive detection of many polar aliphatic molecules following their separation by liquid chromatography. Species such as carbohydrates and polyalcohols lack a strong UV-vis chromophore, and require derivatization prior to photometric detection. Constant potential detection of carbohydrates and polyalcohols at Au electrodes results in reduced electrode response over time, due to the accumulation of adsorbed reaction products and inert oxides at the electrode surface. Pulsed electrochemical detection (PED) allows reproducible and sensitive detection of carbohydrates by incorporating anodic and cathodic potential excursions to oxidatively clean and reductively reactivate the electrode surface before application of the detection potential. This cycle of detection and cleaning pulses forms the basis of PED and typically is applied at a frequency of 1-Hz. Pulsed electrochemical detection has become the preferred method for the detection of carbohydrates. Several reviews of PED have been published that describe principles and applications in liquid chromatography (1,2).

Most applications of capillary electroporesis rely on UV-vis or fluorometric detection, because these are the only detectors available in commercial systems. Borate complexes of carbohydrates have been known to have a strong UV absorbance (3), and several researchers have exploited this by using borate in their running buffers for the detection of carbohydrates (4) and derivitized carbohydrates (5,6). Additionally, carbohydrates have been detected by using indirect UV absorbance (7) and indirect

fluorescence (8). Typically, these detections have high concentration detection limits (*ca.* 1 mM) because of the short path length in CE systems.

Electrochemical detection in CE is not dependent on the inner dimensions of the capillary, and has been used primarily for the detection of reversible redox species. However, the constant-potential detection of carbohydrates separated by CE has been described at conventional sized Cu electrodes (9) and Cu microwire electrodes (10). Although PED is well developed for liquid chromatography, few applications of PED coupled with CE separations have appeared in the literature. Lunte, O'Shea, and LaCourse (11) have described a system for CE-PED of carbohydrates using a Nafion-coated decoupling junction and 300 - 350 × 50-μm Au microwire electrodes. Lu and Cassidy (12) also described CE-PED of several carbohydrates using a Au microdisk electrodes with on-column PED of carbohydrates. In both of these studies, waveforms of *ca.* 1.6 Hz were used for the description of electrophoretic peaks.

We are concerned whether the 1-Hz waveforms commonly used in liquid chromatography are sufficient for detection of narrow elution peaks of carbohydrates separated by capillary electrophoresis. Guidelines for CE detection suggest that 25 - 30 points are sufficient for description of an analyte peak (13). Therefore, a 10-s CE peak would require a PED waveform frequency of *ca.* 2.5 - 3.0 Hz to attain reproducible results.

Customarily, electrode current in PED is sampled over an integration period (t_{int}) that is an integer multiple (n) of 16.7 ms (1/60 Hz) to discriminate against 60-Hz line

noise (*i.e.*, t_{int} = 16.7n). Neuberger and Johnson (14) reported a significant increase in the signal to noise ratio (S/N) for PED as the value of n is increased. Typically, a value of t_{int} = 200 ms (n = 12) is recommended to provide optimal discrimination against both 50 and 60-Hz line noise. Pulsed-voltammetry experiments at a Au rotated-disk electrode (RDE) were used by LaCourse and Johnson to determine the optimum PED waveform parameters for detection of carbohydrates separated by LC (15). Their work suggests that a 1-Hz waveform with t_{int} = 200 ms provide optimum sensitivity for the detection of carbohydrates.

In previous work, fast-PED waveforms were used for the detection of carbohydrates separated by anion-exchange chromatography (16). Oxidative and reductive cleaning parameters in these studies were based upon a prior kinetic study of oxide formation and dissolution at Au electrodes in alkaline solutions (17). In the present work, the frequency- dependent response for carbohydrates separated by capillary electrophoresis was investigated. An empirical investigation of the cleaning cycle parameters t_{oxd}, E_{oxd}, and t_{red} was conducted to optimize the values for oxidative and reductive cleaning pulses in fast-PED waveforms. Once the cleaning cycle was minimized, the waveform frequency was varied by changing t_{int} in integer multiples of 16.7 ms. A 2.7-Hz waveform (*i.e.*, t_{int} = 200 ms) was used to determine the concentration of glucose in blood 30 min and 14 hr after a high carbohydrate meal.

EXPERIMENTAL

Reagents. Sample carbohydrates (Sigma) were used as received. All water was purified by passage through two D-45 demineralizing cartridges (Culligan) and further purified in a Milli-Q system (Millipore). Sodium hydroxide solution (80 mM) was prepared from a 50% stock solution (Fisher).

Equipment. Electrophoretic separations were carried out using a 30-kV reversible-polarity high-voltage power supply (Spellman, Model CZE1000). The high-voltage input was contained in a plexiglass box with an interlock switch for operator safety. Platinum wires (ca. 40 mm × 1 mm) were used as the electrodes in the positive and negative (ground) buffer reservoirs. The positive buffer reservoir was contained in the plexiglass box and the ground buffer reservoir and electrochemical detection cell were located outside of this enclosure. Electrochemical detection was accomplished using a PED detector (Dionex). Data acquisition and control of the high voltage power supply were maintained by a Zenith 286 computer with a DT2821 interface board (Data Translation). Asyst software (Data Translation) was used to write programs for data acquisition and instrument control.

Fused-silica capillaries, 30-μm i.d. × 350-μm o.d. (Polymicro Technologies Inc.) were used for all separations. The high voltage power supply was decoupled from the electrochemical detector by forming a porous junction *ca.* 2.5 cm from the end of the capillary. This was accomplished in a manner similar to Whang and Chen (18). Figure

1 shows the details of the construction of the porous junction. The polyimide coating was removed from a 1-cm section of capillary with a flame, then cleaned with methanol followed by deionized water. Capillaries then were affixed to a rigid plastic backing using UHU Bond All glue (Faber Castell), and allowed to dry overnight. A ceramic capillary-cleaving tool (Polymicro Technologies) was used to score capillaries within the polyimide-free region. One drop (*ca.* 10 - 20 μl) of 10% w/v cellulose acetate in acetone was coated around the capillary in the vicinity of the score mark. Once dry, the capillary was fractured within this sheath by applying gentle pressure lateral to the capillary in the proximity of the score mark. Another coat of cellulose acetate solution was then applied to the fracture, and allowed to dry overnight.

To aid the insertion of the working electrode into the end of the capillary, the exit was etched in the manner used by Sloss and Ewing (19). The end of the capillary was immersed in a solution of 49% HF for about 10 minutes, to allow the HF solution to siphon into the capillary and etch the exit in a conical shape. The capillary exits were then immersed in a solution of 0.1 M NaOH and allowed to siphon for *ca.* 30 min to neutralize any remaining HF. The result was that the internal diameter of the capillary exit was increased to *ca.* 70 μm and tapered to 30 μm within 100 - 200 μm. This made it much easier to guide the microwire into the capillary exit.

The porous junction assembly was sealed in a polyethylene buffer reservoir as shown in Figure 1. Two vertical incisions were made on opposite sides of the beaker and the capillary was then placed between these slits, and sealed with silicon sealant

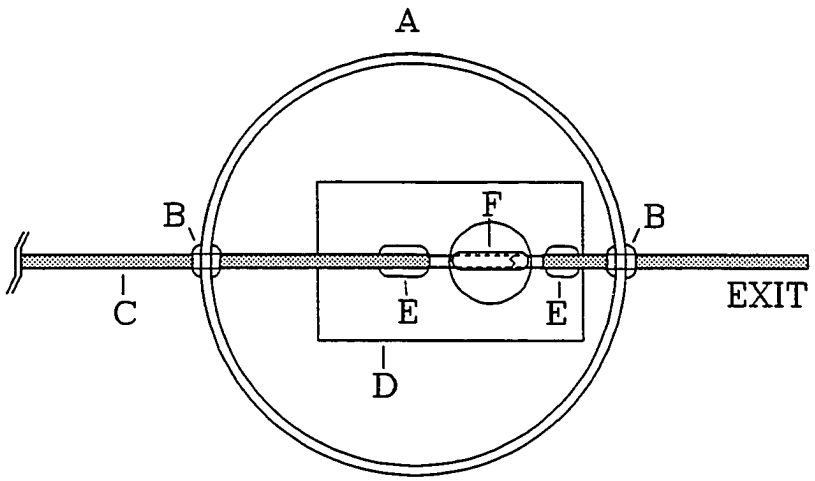

Top View

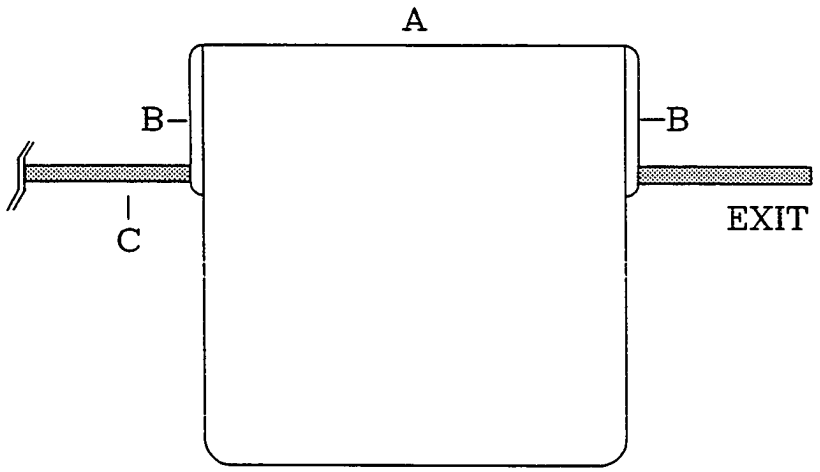

Side View

Figure 1. Schematic diagram of the buffer reservoirs. (A) Polyethylene buffer reservoir, (B) Silicone sealant, (C) Fused-silica capillary, (D) Plastic support, (E) Epoxy, (F) Cellulose acetate coated fracture.

(Hartz). Before use, capillaries were preconditioned by rinsing with deionized water, followed by running buffer (80 mM NaOH) for at least 1 hour before use. After use, the capillaries were rinsed with deionized water for *ca.* 30 min, then dried for *ca.* 30 min with air.

Typically, ultramicroelectrodes are constructed by sealing metal wires or carbon fibers in glass micropipets by melting the glass or by using some form of sealant (20). However, microcylinder electrodes can be constructed by sealing Au microwires in melted PEEK tubing as shown in Figure 2. These were constructed by inserting 4 - 5 cm of 25-μm or 50-μm microwire into 0.010 inch i.d. PEEK tubing (Upchurch). One end of this tubing was then melted on a warm soldering iron, and sealed around the wire with a quick twisting motion. The other end of the micro wire was then attached to a *ca.* 15-cm section of 28-gauge copper wire with Nickel Print (GC Electronics). This assembly was sealed into the barrel of a 1-mL tuberculin syringe with silicon sealant to provide support in the three-axis micropositioner (Edmund Scientific) used to maneuver the microelectrodes into the capillary exit.

Figure 3 shows a picture of the experimental apparatus. The detection cell was an inverted plastic volummetric flask cap. A miniature SCE (Fisher) was used as a reference electrode in this work, and a coiled Pt wire (ca. 0.5 cm^2) was used as the counter electrode. The end of the capillary was placed in the detection cell, and the microwire electrode was manipulated into the end of the capillary.

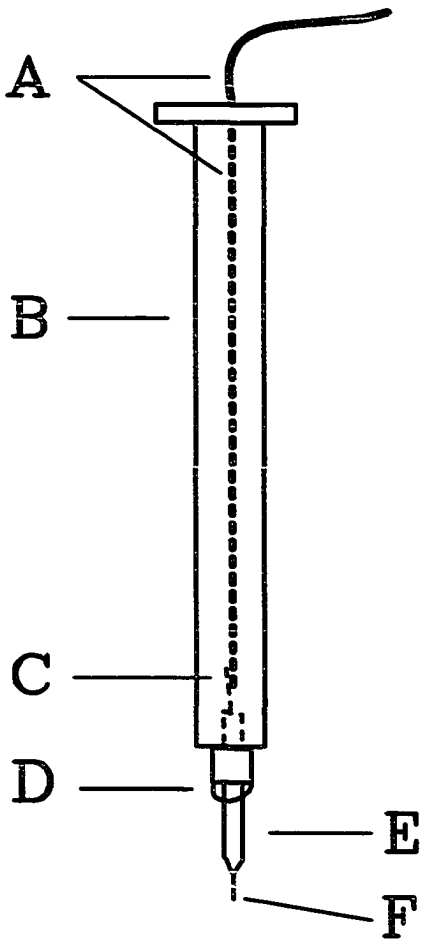

Figure 2. Schematic diagram of Au microwire electrode construction. (A) Cu wire, (B) Syringe barrel, (C) Nickel print, (D) Silicone sealant, (E) PEEK tubing, (F) Au microwire.

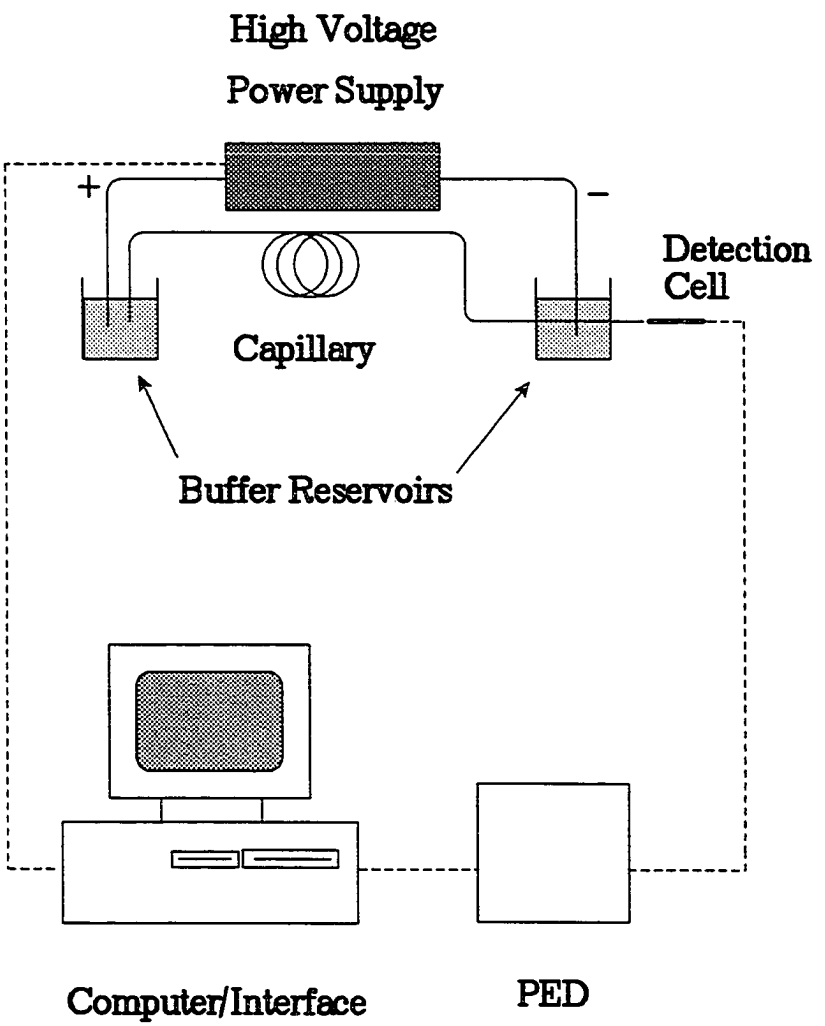

Figure 3. Experimental apparatus for CE-PED.

Sample preparation. All carbohydrate samples were prepared in 80 mM NaOH. For the determination of glucose in human blood, 100 μL of blood was diluted to 5 ml in 80 mM NaOH with 100- μM inositol as an internal standard for interday comparison of results. The blood was filtered through a 0.22-μm syringe filter (Fisher) prior to analysis.

Waveforms. The basic waveform used in the following studies is shown in Figure 4. It consists of a fixed detection step of E_{det} = 0.15 V, $t_{det} = t_{del} + t_{int}$, where t_{del} = 30 ms and t_{int} = 200 ms. There were also 10-ms delays between the detection step and the oxidative cleaning step and between the oxidatative cleaning step and the reductive cleaning step, which we refer to as t_{up} and t_{down}, respectively. In each of the following studies one of the cleaning parameters, t_{oxd}, E_{oxd} or t_{red}, were varied independently to determine the optimum cleaning parameters for the detection of carbohydrates. The integration period then was varied to determine the frequency-dependent response for carbohydrates separated by CE.

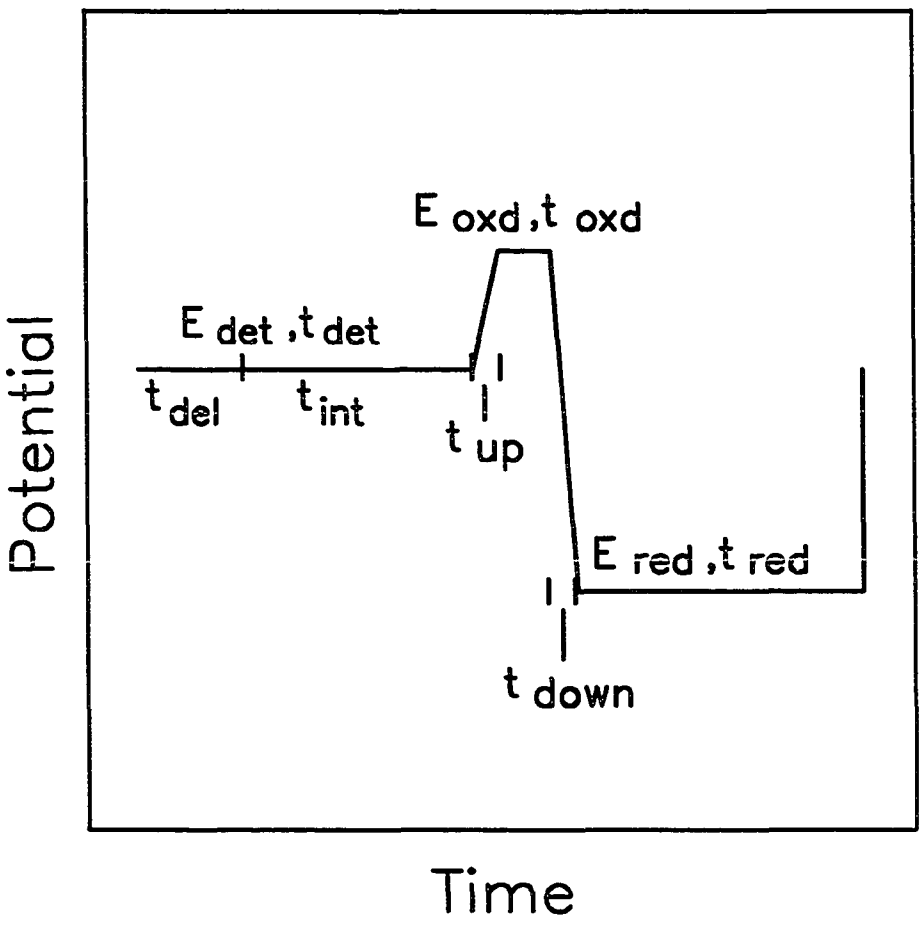

Figure 4. Potential-time (E-t) waveform applied for detection of carbohydrates at Au microelectrode in 80 mM NaOH. E_{det} = detection potential; t_{det} = detection time; t_{del} = delay time; t_{int} = integration time; t_{up} = ramp time; E_{oxd} = oxidation potential; t_{oxd} = oxidation time; t_{down} = ramp time; E_{red} = reduction potential; t_{red} = reduction time.

RESULTS AND DISCUSSION

System performance. Capillaries appeared to be stable, and retention times (t_r) for carbohydrates varied less than 2% within one day. However, values of t_r varied as much as 10% for day-to-day comparisons. This may be due to increases in the inner diameter by slight dissolution of the fused silica capillary, causing an increase in the conductivity of the capillary. Hydration of the cellulose acetate junction and slight variations in the buffer concentration also may contribute to this day-to-day variation. The greatest variation in retention times was noticed between different capillaries, where variations of t_r was $\pm$ 15%. This is primarily due to finite differences in the lengths of the electrophoresis and decoupling sections of capillary. Additionally, differences in the thickness of cellulose acetate coatings were visible under a microscope.

Within one day, peak response (P) varied less than 3% for the detection of carbohydrates. However, day-to-day reproducibility was $\pm$ 10%. This is probably due to variation in the insertion of the microwire electrode into the end of the capillary, and differences in peak widths caused by variation in t_r values. For interday comparisons, the use of an internal standard is recommended. In this work inositol was used because it produced a peak that was well-resolved from glucose.

Variation of the oxidative cleaning time, t_{oxd}. In these experiments the basic waveform described above was used with a fixed reductive cleaning step of E_{red} = -0.5 V and t_{red} = 450 ms, while the value of t_{oxd} was varied for E_{oxd} = 0.5 V. Relatively

large sample plugs (12.5 nL) of 100-μM glucose were introduced in this and the two following studies, to provide sufficient peak-width for reproducibility, and to test the cleaning parameters under adverse conditions. Figure 5 illustrates the effect of increasing t_{oxd} over the range 20 - 200 ms. Clearly, as t_{oxd} is increased, the signal for the detection of glucose increases significantly between 20 - 40 ms. However, there is only a moderate increase in signal for $t_{oxd} > 60$ ms. This increase is probably due to more effective cleaning provided by the longer anodic polarization of the electrode. It is interesting to note the similarity between this curve and curves observed for chronocoulometry experiments for the formation of oxide at an Au electrode without any analyte (17). These show that a majority of oxide is formed at Au electrodes within 20 ms after application of an anodic potential. Further formation of oxide occurs more gradually at $t_{oxd} > 20$ ms. Hence, the most rapid cleaning probably occurs over the first 20 ms, with a gradual increase in the amount of cleaning that occurs at longer times. It may be inferred that the fast cleaning at short times is accomplished primarily by the formation of surface AuOH species, while the more tenacious fouling species may require removal by formation AuO.

Variation of the oxidative cleaning potential, E_{oxd}. In the above study, we observed that the values of $E_{oxd} = 0.5$ V with $t_{oxd} = 20$ ms may not be sufficient for optimal sensitivity in "Fast-PED" waveforms. However, the cleaning efficiency can be

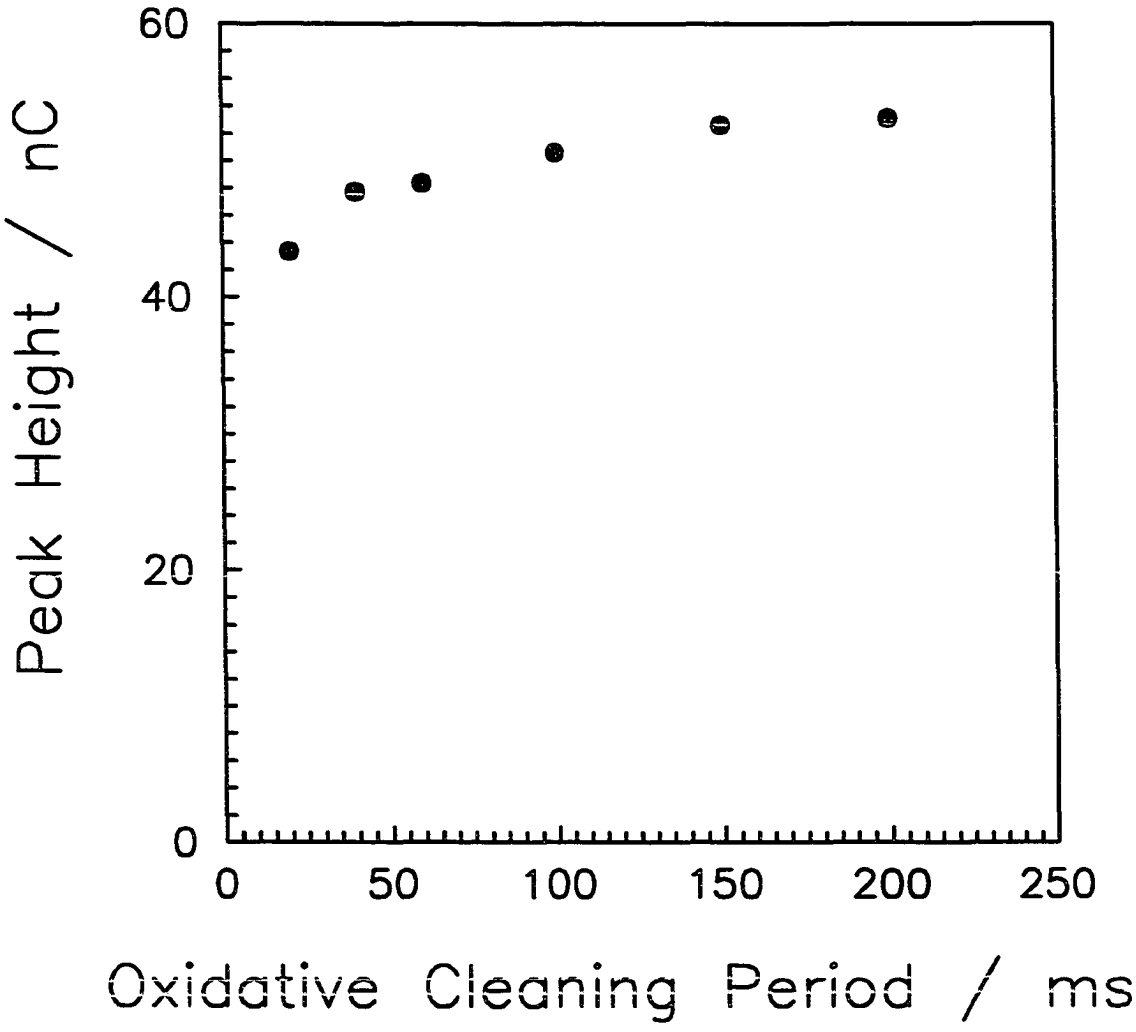

Figure 5. Effect of increasing t_{oxd} upon the signal for the detection of 1.25 pmol glucose (12.5 nL, 100 μM).

increased by using more positive values of E_{oxd} for t_{oxd} = 20 ms. The waveform had the same detection (E_{det}, t_{det}) and reductive (E_{red}, t_{red}) cleaning steps as above; however, E_{oxd} was varied for t_{oxd} = 20 ms. Figure 6 illustrates that as E_{oxd} is increased in the PED waveform the signal for the detection of glucose increases. Furthermore, this appears to be linear for $0.5 < E_{oxd} < 0.8$ V. Hence, the optimum value of E_{oxd} for further work was chosen at 0.8 V.

Variation of the reductive cleaning period, t_{red}. In the previous studies, the reductive cleaning pulse (E_{red}, t_{red}) was maintained at 450 ms, while E_{oxd} or t_{oxd} was varied independently, and was assumed to be sufficient to provide adequate reduction of oxide during the PED waveform. Because we are interested in PED waveforms with frequencies greater than 1 Hz, the value of t_{red} was varied to observe the effect on the signal for the detection of glucose. Figure 7 shows that the signal increases slightly as t_{red} is increased, and has a shape similar to q-t curves for formation of surface oxide at Au electrodes in 0.1 M NaOH (17). Hence, using a value of $t_{red} > 50$ ms will result in greater sensitivity for the detection of carbohydrates. The increase in signal is probably due to more efficient reduction of oxide at longer values of t_{red}. It is also possible that depletion of glucose from the diffusion layer is evident for short t_{red} values. Hence, more signal is observed when more time is allowed for transport of glucose back into the diffusion layer prior to detection. It can be seen in Figure 7, that by decreasing t_{red} from 450 to 100 ms, a 51% decrease in the total time for the waveform t_{tot} ($t_{tot} = t_{del}$

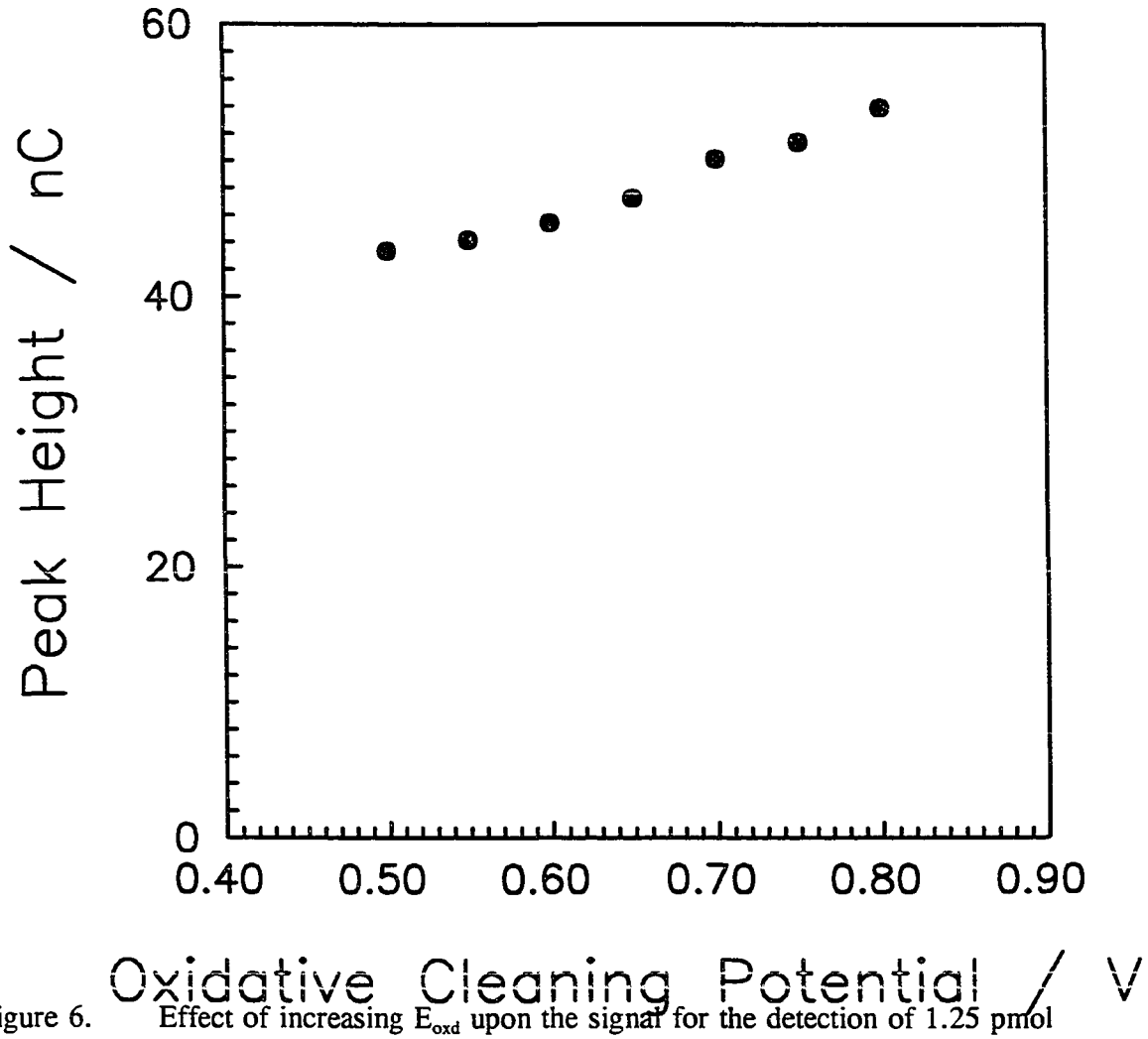

Figure 6. Effect of increasing E_{oxd} upon the signal for the detection of 1.25 pmol glucose (12.5 nL, 100 μM).

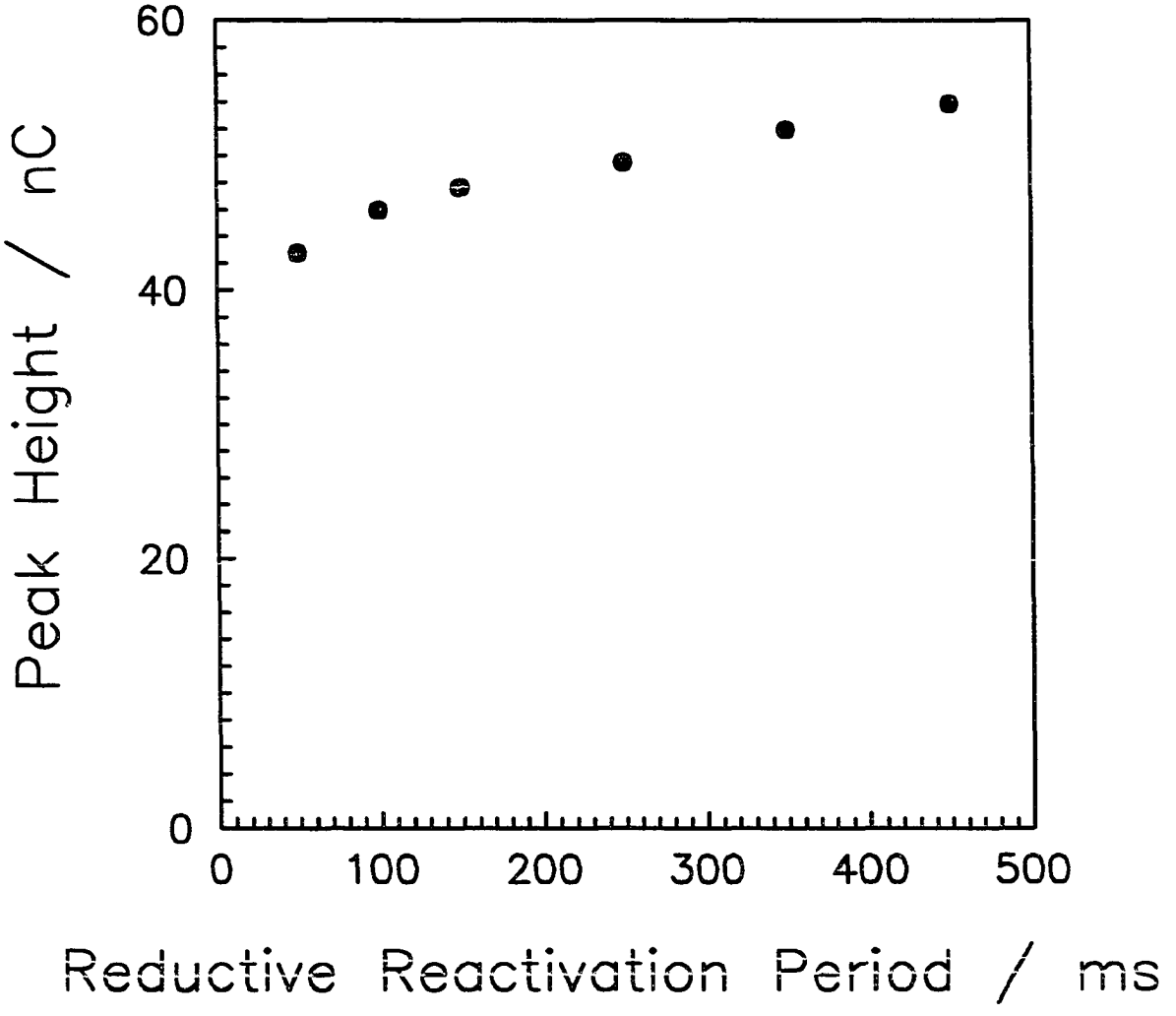

Figure 7. Effect of increasing t_{red} upon the signal for the detection of 1.25 pmol glucose (12.5 nL, 100 μM).

+ t_{int} + t_{up} + t_{oxd} + t_{down} + t_{red}; t_{del} = 30 ms, t_{int} = 200 ms, t_{up} = 10 ms, t_{oxd} = 20 ms, t_{down} = 10 ms), while the signal only decreases by 14%. Therefore, a value of 100 ms was chosen for t_{red} to maintain waveforms with frequencies greater than 1 Hz.

On the basis of these studies, the optimum cleaning potentials E_{oxd} and E_{red} for t_{det} = 230 ms are +0.80 V and -0.50 V, respectively. The cleaning times t_{oxd} and t_{red} are 20 ms and 100 ms, respectively. All further investigations use these values for electrode cleaning. Hence, a waveform where t_{int} = 200 (n = 12), would correspond to a waveform frequency of 2.7 Hz, and for n = 3, an upper waveform frequency of 4.54 Hz is possible.

Variation of the integration period, t_{int}. The optimized fast-PED waveform parameters for determination of the dependence of response for carbohydrate detection on t_{int} are shown in Table 1. These waveforms were used for the detection of a mixture of seven carbohydrates separated by capillary electrophoresis, and these data are shown in Figure 8 at four values of t_{int}. Lunte, O'Shea and LaCourse (11) reported that they were not able to resolve glucose, fructose and sucrose using a 75 μm i.d. $\times$ 95 cm length capillary using 10 mM NaOH/8 mM Na_2CO_3 as the running buffer. However these sugars are well resolved in the present investigation, with *ca.* 50,000 theoretical plates for each sugar. It is apparent that as t_{int} is increased, and the waveform frequency decreased, the peak signal increases. This is expected because of the greater amount of charge passed for longer values of t_{int}.

Table 1. Summary of PED waveform parameters used to obtain data in Figures 8 through 12 as a function of integration period (tint)[a]

t_{int} (ms)	t_{det} (ms)	T_{tot} (ms)	Frequency (Hz)
50	80	220	4.54
100	130	270	3.70
150	180	320	3.12
200	230	370	2.70
300	330	470	2.12
400	430	570	1.75
800	830	970	1.03

[a]Potentials: E_{det} = +0.15 V, E_{oxd} = +0.8 V, E_{red} = -0.5 V. Time Periods: t_{del} = 30 ms, t_{int} = variable, t_{up} = 10 ms, t_{oxd} = 20 ms, t_{down} = 10 ms, t_{red} = 100 ms; $T_{tot} = t_{del} + t_{int} + t_{up} + t_{down} + t_{red}$.

Figure 9 summarizes the values of Peak Height (P) as a function of t_{int}. Neuberger and Johnson predicted a linear relationship for a plot of P *vs.* t_{int} for steady state measurements (14). A linear relationship is observed for the plots of P *vs.* t_{int} for $t_{int} \leq 200$ ms. However, for $t_{int} > 200$ ms the signal is less than would be expected. This suggests that minimized values for oxidative and reductive cleaning may not be adequate for longer values of t_{int} resulting in greater fouling of the electrode surface. It is also possible that the long integration period may result in depletion of glucose in the

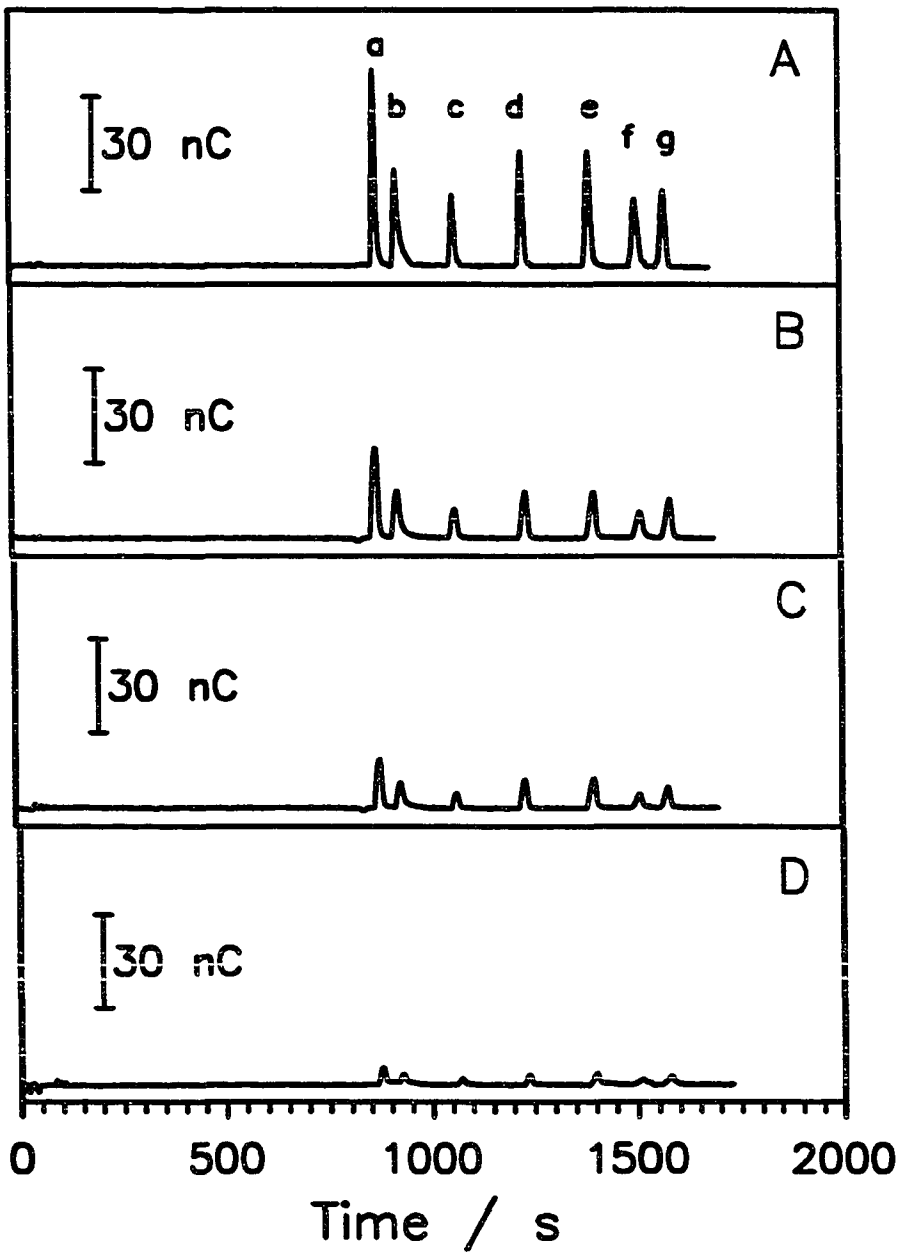

Figure 8. CE-PED results for a mixture of seven carbohydrates. Waveforms: (A) 1.03 Hz, (B) 2.12 Hz, (C) 3.12 Hz, (D) 4.54 Hz (see table 1), Column: 30 μm i.d. x 350 μm i.d. x 65 cm, Decoupling column: 30 μm i.d. x 350 μm i.d. x 2.5 cm. Buffer: 80 mM NaOH, Injection: 400 fmol each (4 nL, 100 μM). Separation: 12kV @ 35 μA, Peaks 100 μM each: (a) inositol, (b) sorbitol, (c) sucrose, (d) fucose, (e) glucose, (f) fructose, (g) xylose.

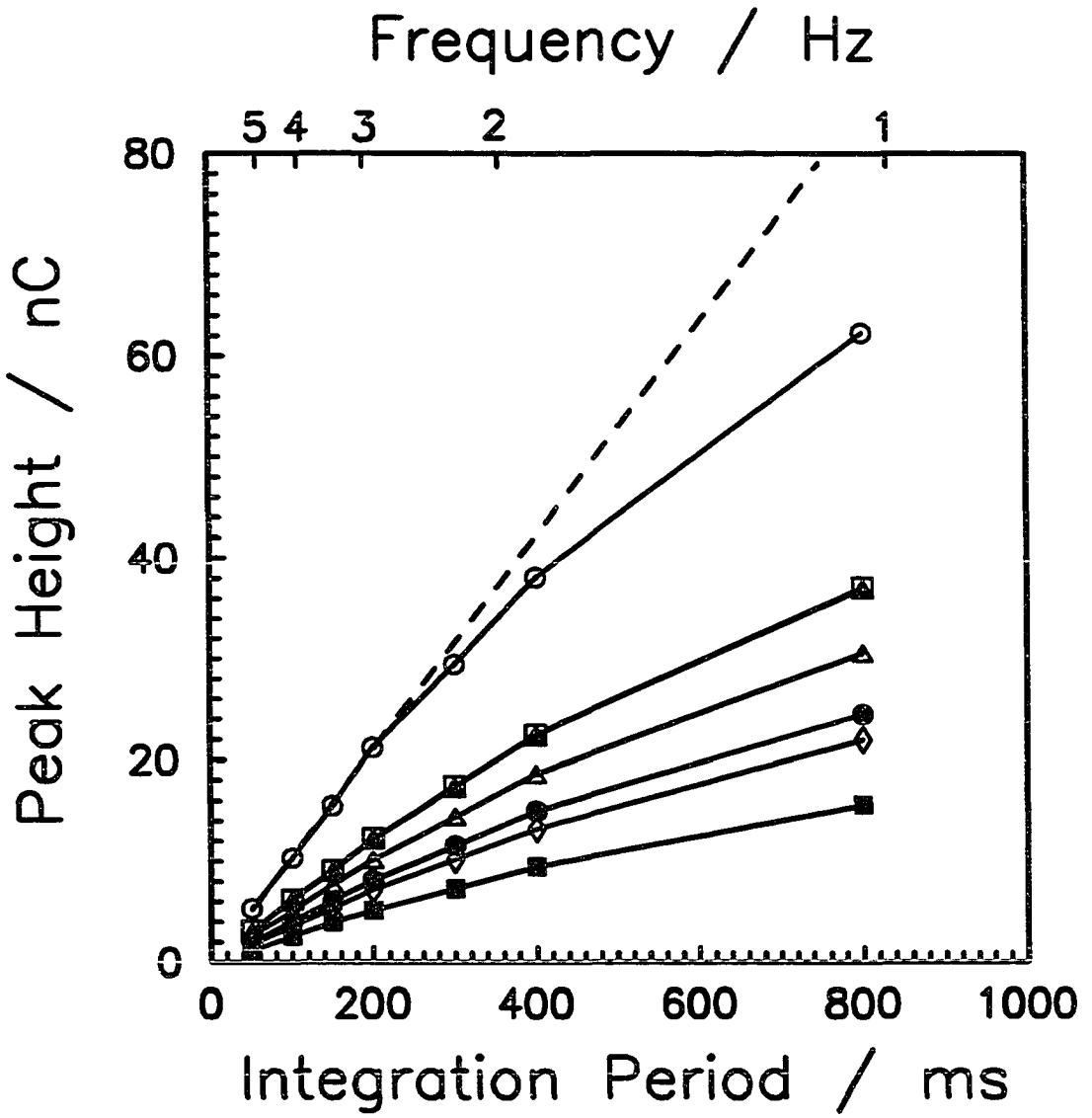

Figure 9. Summary of CE-PED response for data in Figure 8, and waveforms in Table 1, as a function of the integration period (t_{int}) and waveform frequency. Curves: (○) inositol, (△) sorbitol, (●) sucrose, (▲) fucose, (□) glucose, (■) fructose, (◇) xylose.

diffusion layer, and there is insufficient time during the cleaning cycle to replenish the concentration of glucose in the diffusion layer. However, peak heights were reproducible to greater than 3% for eight runs (*ca.* 4 hr).

Figure 10 summarizes the values of signal-to-noise ratio (P/N) for glucose as a function of t_{int}. The noise in the system was independent of t_{int}, suggesting that the source of the noise was probably not 60-Hz line noise, and may be related to electronic noise in the PED detector or high-voltage power supply. Limits of detection (LOD) for glucose at each frequency were estimated at S/N = 3, and these data are presented in Table 2. From these data, we can expect the limit of detection for t_{int} = 200 ms

Table 2. Summary of detection limits (S/N = 3)for glucose as a function of function of integration period (t_{int}) and waveform frequency[b].

t_{int} (ms)	t_{tot} (ms)	Frequency (Hz)	LOD (fmol)
50	220	4.54	31.8
100	270	3.70	19.2
150	320	3.12	14.7
200	370	2.70	8.7
300	470	2.12	6.1
400	570	1.75	6.0
800	970	1.03	2.9

[a]See Table 1 for waveform parameters.

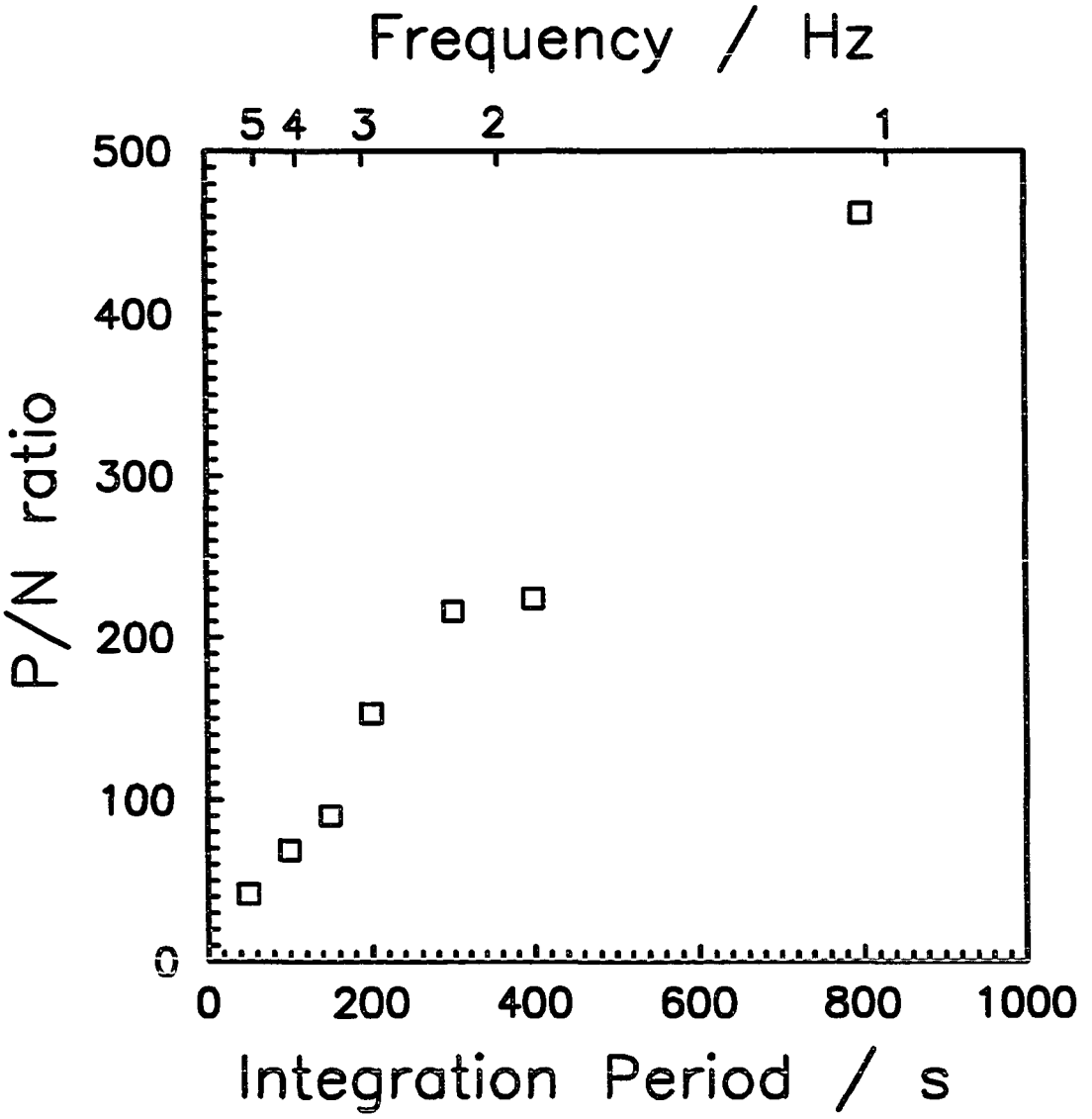

Figure 10. Summary of peak height to noise ratio (P/N) for glucose data in Figure 9.

(2.70 Hz) to be *ca.* 7.9 fmol (4 nL).

As mentioned above, we are concerned that a 1-Hz waveform may not provide enough data points to accurately describe narrow CE peaks. Figure 11 shows a CE peak for a 5-s, 10-kV injection of inositol, separated at 15 kV. It is apparent that the 1-Hz waveform does not provide the 25 - 30 data points suggested (13) for reproducible description of peaks in CE. However, curve B illustrates that waveform frequencies equal to or greater than 2 Hz would provide an adequate data acquisition rate for this CE separation. As was seen in the previous two figures, the use of higher waveform frequencies (shorter t_{int}) results in a sacrifice of signal strength.

Determination of glucose in human blood. Glucose is the primary sugar present in blood, and its quantitation can be diagnostic for disorders such as diabetes. The normal fasting concentration of glucose in human blood is 100 mg/100 mL $\pm$ 20% (21), and can rise by as much as 75 mg/100 mL for normal individuals, after eating a meal high in glucose (22). In the following study, the concentration of glucose in human blood *ca.* 30 min after a meal high in glucose (2 cans of coke, 2 large cookies), was compared to that after a 14 hour fast (no cokes, no cookies). As mentioned above, the day-to-day reproducibility for retention times and peak response was $\pm$ 10%, requiring the use of an internal standard for accurate comparison of results. Inositol was found to have a response factor of 1.69 $\times$ that of glucose, and 100 μM was added as an internal standard. Figure 12A contains typical results for application of CE-PED, with the 2.7

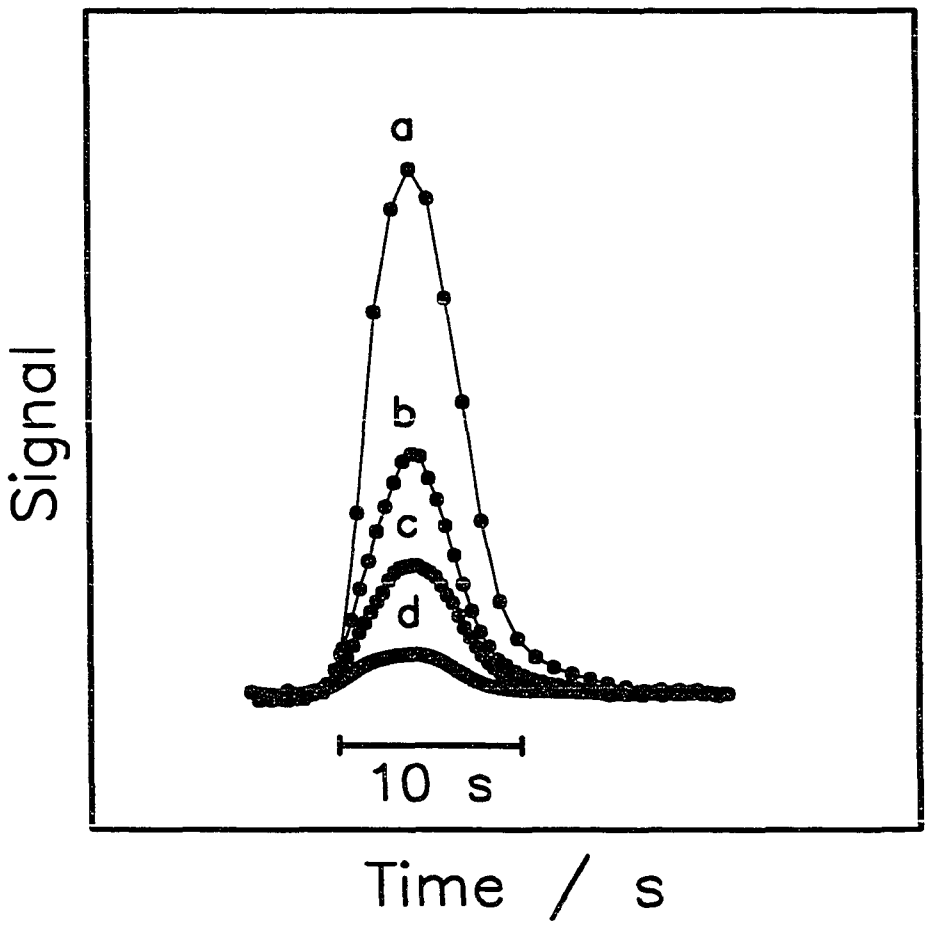

Figure 11. CE-PED results for narrow inositol peak produced by 4 s, 12 kV injection, and separation at 15 kV. Waveform Frequencies: (a) 1.03 Hz, (b) 2.12 Hz, (c) 3.12 Hz, (d) 4.54 Hz, (see table 1).

Hz detection waveform (see Table 1), to the determination of the concentration of glucose in human blood after the high carbohydrate meal. The concentration of glucose in this blood sample was determined to be 137 $\pm$ 4 mg/100 ml. Figure 12B shows the analysis of human blood, from the same individual, after a 14-hr fast. The response for glucose, relative to the inositol peak, is diminished and the concentration was determined to be 97 $\pm$ 2 mg/100 ml.

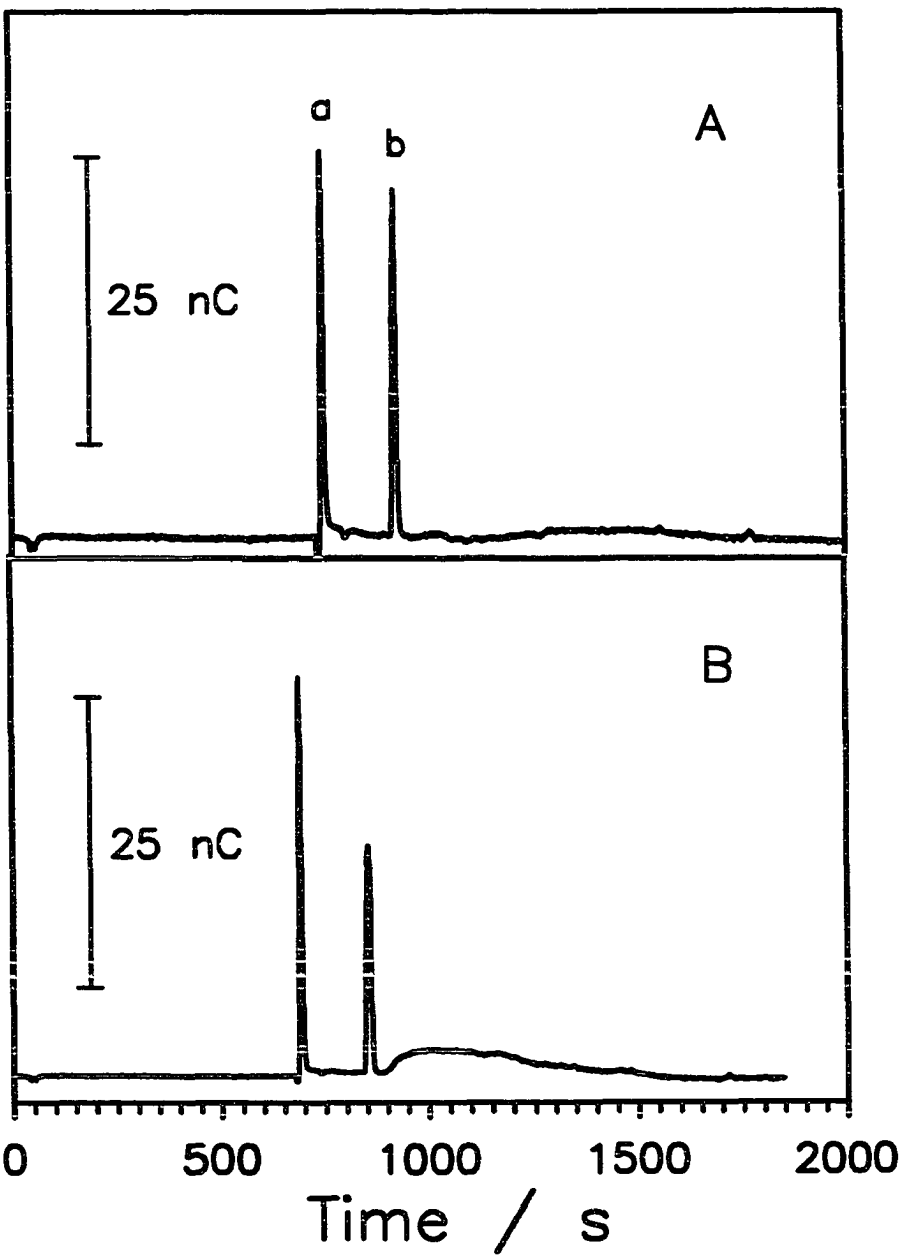

Figure 12. CE-PED results for the analysis of glucose in human blood. Column: (see Figure 7). Waveform: 2.7 Hz (see Table 1). Injection: 8 s, 12 kV, Separation: 15 kV, (A) Blood sample 30 min after high glucose meal. Peaks: (a) 100 μM inositol (internal standard), (b) glucose. (B) Blood sample after 14 hr fast.

CONCLUSIONS

Pulsed waveforms can be applied in the Dionex PED system at a frequency of *ca.* 3 Hz for the analysis of carbohydrates separated by capillary electrophoresis. By using minimal values for oxidative cleaning (t_{oxd} = 20 ms) and reductive reactivation (t_{red} = 100 ms), the normally recommended value for the integration period (t_{int} = 200 ms) can be used to attain a waveform frequency of 2.7 Hz. By decreasing the value of t_{int}, higher waveform frequencies can be achieved, with the result of sacrificing the peak signal (*P*) and the peak-to-noise ratio (*P/N*) in CE-PED. The extent of sacrifice can be anticipated approximately from Figure 10 and Table 2.

From our data, it is apparent that increased waveform frequency will result in a sacrifice in LOD for the detection of carbohydrates in CE-PED. On the basis of data for glucose given in Figure 10 and Table 2, a frequency increase from 1 to 2.7 Hz (decrease in t_{int} from 800 ms to 200 ms) results in an increase of LOD by *ca.* 3 ×; however, increasing frequency from 2.7 Hz to *ca.* 4.54 Hz (decrease in t_{int} from 200 ms to 50 ms) results in a further increase of LOD by 3.7 ×. The suitability of PED waveforms with frequency > 1 Hz for applications to CE is demonstrated in Figure 11, where the resolution of a *ca.* 12 s electrophoretic peak for inositol is shown at four frequencies. Clearly, waveform frequencies greater than 1 Hz will be a necessity as separation technology is improved.

ACKNOWLEDGEMENTS

This work was supported by grants from the National Science Foundation (CHE-8914700) and Dionex Corp.

REFERENCES

1. D.C. Johnson and W.R. LaCourse, *Anal. Chem., 62* (1990) 589A.

2. D.C. Johnson and W.R. LaCourse, *Electroanalysis, 4* (1992) 367.

3. H. Weigel, Adv. *Carbohydr. Chem., 18* (1963) 61.

4. S. Hoffstetter-Kuhn, A. Paulus, E. Gassmann, and H.M. Widmer, *Anal. Chem., 63* (1991) 1541.

5. S. Honda, S. Iwase, A. Makino, S. Fujiwara, *Anal. Biochem., 176* (1989) 72.

6. S. Honda, S. Suzuki, A. Nose, K. Yamamoto, K. Kakehi, *Carbohydr. Res., 215* (1991) 193.

7. A.E. Vorndran, P.J. Oefner, H. Scherz, and G.K. Bonn, *Chromatographia, 33* (1992) 163.

8. T.W. Garner and E.S. Yeung, *J. Chromatogr., 515* (1990) 639.

9 J. Ye and R.P. Baldwin, *Anal. Chem., 65* (1993) 3525.

10. L.A. Colon, R.Dadoo, and R.N. Zare, *Anal. Chem., 65* (1993) 476.

11. T.J. O'Shea, S.M. Lunte, and W.R. LaCourse, *Anal. Chem., 65* (1993) 948.

12 W. Lu and R.M. Cassidy, *Anal. Chem., 65* (1993) 2878.

13. R. Weinberger, *Practical Capillary Electrophoresis*, Academic Press, San Diego, CA, 1993, p. 282.

14. G.G. Neuberger and D.C. Johnson, *Anal. Chim. Acta, 192* (1987) 205.

15. W.R. LaCourse and D.C. Johnson, *Anal. Chem., 65* (1993) 50.

16. R.E. Roberts and D.C. Johnson, *Electroanalysis, 6* (1994) 269.

17. R.E. Roberts and D.C. Johnson, *Electroanalysis, 4* (1992) 741.

18. C-W. Whang and I-C. Chen, *Anal. Chem., 65* (1993) 2461.

19. S. Sloss and A.G. Ewing, *Anal. Chem.*, *65* (1993) 577.

20. R.M. Wightman and D.O. Wipf, In *Electroanalytical Chemistry*, A.J. Bard, Ed., Marcel Dekker, Inc., New York, 1989, pp 328-334.

21. L. Stryer, *Biochemistry*, W.H. Freeman and Co., New York, 1988, p. 637.

22. W.G. Exton, and A.R. Rose, *Am. J. Clin. Path.*, *4* (1934) 381.

GENERAL CONCLUSIONS

The advent of rapid and efficient separation techniques such as microbore-LC and CE has made it necessary to evaluate the sampling frequency provided by the conventional PED waveform. Because a sufficient number of points must be acquired to accurately and reproducibly describe the peaks as they elute PED waveforms with frequencies greater than one Hz needed to be developed. The processes of oxide formation and reduction are used in LC-PED and CE-PED to maintain a reproducible response. Therefore, it was important to understand the kinetics of these processes when minimizing the waveform to achieve high frequency PED waveforms.

Chronocoulometric investigations of oxide formation at Au and Pt electrodes in 0.1 M NaOH indicate that a virtual monolayer of hydrous oxide can be formed at both metals within 20 - 30 ms. Reduction of a monolayer of this hydrous oxide at Au electrodes in 0.1 M NaOH was found to be complete within 50 - 100 ms, and independent of potential for $E_{red} < -0.4$ V. However, reduction of the hydrous oxide was incomplete for $t_{red} < 1000$ ms at Pt electrodes in 0.1 M NaOH. Therefore, Au electrodes are recommended for the use of fast-PED for the detection of carbohydrates.

Pulsed waveforms can be applied in the Dionex PED system at a frequency as great as *ca.* 5 Hz for the analysis of carbohydrates separated by either liquid chromatography or capillary electrophoresis. By using minimal values for oxidative cleaning ($t_{oxd} = 20$ ms) and reductive reactivation ($t_{red} = 100$ ms), the normally recommended value for the integration period ($t_{int} = 200$ ms) can be used to attain a

waveform frequency of ca. 3 Hz. Higher waveform frequencies can be achieved by decreasing the value of t_{int}. At these higher frequencies, there is a sacrifice in the peak signal (*P*) and the peak-to-noise ratio (*P/N*) in CE-PED as a consequence of smaller t_{int}. The extent of sacrifice can be anticipated approximately from Figures 5 and 10 and Tables 2 and 2.

Data for the detection of carbohydrates in CE-PED, demonstrate that increased waveform frequency will result in a sacrifice in LOD. On the basis of data for glucose given in Figure 10 and Table 2, a frequency increase from 1 to 2.7 Hz (decrease in t_{int} from 800 ms to 200 ms) results in an increase of LOD by *ca.* 3 ×; however, increasing frequency from 2.7 Hz to *ca.* 4.54 Hz (decrease in t_{int} from 200 ms to 50 ms) results in a further increase of LOD by 3.7 ×. The suitability of PED waveforms with frequency > 1 Hz for resolution of a *ca.* 12 s electrophoretic peak for inositol is demonstrated in Figure 11. As separation technology is improved, waveform frequencies greater than 1 Hz will be a necessity.

LITERATURE CITED

1. G. Zubay, *Biochemistry*, Addison-Wesley Publishinng Co., Reading, MA, 1986, p. 437.

2. N. Sharon, *Sci. Amer.*, *243(5)* (1980) 90.

3. L. Stryer, *Biochemistry*, third ed., W.H. Freeman and Co., New York, 1988, p. 331.

4. E. Percival, in *The Carbohydrates*, 2nd ed., W. Pigman and D. Horton, Eds., Academic Press, New York 1972, ch 40.

5. W. Pigman and D. Horton, in *The Carbohydrates*, 2nd ed., W. Pigman and D. Horton, Eds., Academic Press, New York, 1972, ch 1.

6. Product literature, Grain Processing Corporation, Muscatine, IA.

7. S. Hanessian and T.H. Haskell, in *The Carbohydrates*, 2nd ed., W. Pigman and D. Horton, Eds., Academic Press, New York, 1972, ch 31.

8. L. Stryer, *Biochemistry*, third ed., W.H. Freeman and Co., New York, 1988, p. 759.

9. R.W. Jeanloz, in *The Carbohydrates*, 2nd ed., Pigman and Horton Eds, Academic Press, New York, 1972, ch35.

10. N. Sharon and H. Lis, *Sci. Amer.*, *268(1)* (1993) 82.

11. S. Borman, *Chem. Eng. News, 70(49)* (1992) 25.

12. *Modern Nutrition in Health and Disease*, eighth ed., M.E. Shils, J.A. Olsen, and M. Shike, Eds., Lea and Febiger, Malvern, PA, 1994, p. 1259.

13. A. Cantrow and M. Trumper, *Clinical Biochemistry*, seventh ed., W.B. Saunders and Co., Philadelphia, PA, 1975, pp 82-89.

14. S.C. Churms, *J. Chromatogr.*, *500* (1990) 555.

15. M. Ghebregzabher, S. Rufini, B. Monaldi, M. Lato, *J. Chromatogr.*, *127* (1976) 133.

16. R.M. Scott, *Clinical Analysis by Thin-Layer Chromatography Techniques*, Ann Arbor-Humphrey Science Publishers, Inc., Ann Arbor, MI, 1969.

17. L.Hough and JKN Jones, *Methods Carbohydr. Chem.*, 1962, *1*, 21.

18. D.A.T. Southgate, *Determination of Food Carbohydrates*, second ed., Elsevier, New York, 1993, Ch. 3.

19. D.A.T. Southgate, *Determination of Food Carbohydrates*, second ed., Elsevier, New York, 1993, p. 49.

20. R.C. Crippen, *GC/LC, Instrumetnts, Derivatives in Identifying Polutants and Unknowns*, Pergammon Press, 1983, p. 90.

21. R.A. Laine, W.J. Esselman, and C.C. Sweeley, in *Methods in Enzymology*, 1972, *28*(B).

22. J.-M. Dethy, B.Callaert-Deveen, M. Janssens, A. Lenaers, *Anal. Biochem.*, *143* (1984) 119.

23. J. Lehrfeld, *J. Chromatogr.*, *120* (1976) 141.

24. F. Nachtmann and K.W. Bunda, *J. Chromatogr.*, *48* (1976) 1576.

25. T. Okada and T. Kuwamoto, *Anal. Chem.*, *58* (1986) 1375.

26. S. Hughes and D.C. Johnson, *J. Agric. Food Chem.*, *30* (1982) 712.

27. W.R. LaCourse, W.A. Jackson, and D.C. Johnson, *Anal. Chem.*, *61* (1989) 2466.

28. W.A. Jackson, W.R. Lacourse, D.A. Dobberpuhl, and D.C. Johnson, *Anal. Chem.*, *61* (1989) 607.

29. J.A. Polta and D.C. Johnson, *J. Liq. Chromatogr.*, *6* (1983) 1727.

30. L. Welch, W.R. LaCourse, D.A. Mead Jr., D.C. Johnson, T. Hu, *Anal. Chem.*, *61* (1989) 555.

31. A. Ngoviwatchai and D.C. Johnson, *Anal. Chim. Acta*, *215* (1989) 1.

32. P.J. Vandeberg, J.L. Kawagoe, D.C. Johnson, *Anal. Chim. Acta*, *260* (1992) 1.

33. P. J. Vandeberg and D.C. Johnson, *Anal. Chem.*, *65* (1993) 2713.

34. P.J. Vandeberg and D.C. Johnson, *Anal. Chim. Acta*,

35. D.G. Williams and D.C. Johnson, *Anal. Chem.*, *64* (1992) 1785.

36. D.C. Johnson and W.R. LaCourse, *Anal. Chem.*, *62* (1990) 589A.

37. W.R. LaCourse and D.C. Johnson, Carbohydr. Res., *215* (1991) 159.

38. D.C. Johnson and W.R. LaCourse, *Electroanalysis*, *4* (1992) 367.

39. D.C. Johnson, D. Dobberpuhl, R. Roberts, P. Vandeberg, *J. Chromatogr.*, *640* (1993) 79.

40. W.G. Kuhr and C.A. Monning, *Anal. Chem.*, *64* (1992) 389R.

41. W.G. Kuhr, *Anal. Chem.*, *62* (1990) 403R.

42. P.D. Grossman and J.C. Colburn, *Capillary Electrophoresis: Theory and Practice*, Academic Press, Inc., San Diego, CA, 1992.

43. R. Weinberger, Practical Capillary Electrophoresis, Academic Press, Inc., San Diego, CA, 1993.

44. P. Jandik and G. Bonn, Capillary Electrophoresis of Small Molecules and Ions, VCH Publishers, Inc., New York, 1993.

45. R. Kuhn and S. Hoffstetter-Kuhn, Capillary Electrophoresis: Principles and Practice, Springer-Verlag, New York, 1993.

46. R.A. Wallingford and A.G. Ewing, *Anal, Chem.*, *59* (1987) 1762.

47. B.L. Hogan and E.S. Yeung, Anal Chem., *64* (1992) 2841.

48. T.T. Lee and E.S. Yeung, Anal Chem., 1992, *64*, 3045.

49. H. Weigel, Adv. Carbohydr. Chem., *18* (1963) 61.

50. S. Hoffstetter-Kuhn, A. Paulus, E. Gassmann, and H.M. Widmer, *Anal. Chem.*, *63* (1991) 1541.

51. S. Honda, S. Iwase, A. Makino, S. Fujiwara, *Anal. Biochem.*, *176* (1989) 72.

52. S. Honda, S. Suzuki, A. Nose, K. Yamamoto, K. Kakehi, *Carbohydr. Res.*, *215* (1991) 193.

53. A.E. Vorndran, E. Grill, C. Huber, P.J. Oefner, G.K. Bonn, *Chromatographia*, *34* (1992) 109.

54. J. Liu, O. Shirato, and M. Novotny, *Anal. Chem.*, *63* (1991) 413.

55. A.E. Vorndran, P.J. Oefner, H. Scherz, and G.K. Bonn, *Chromatographia*, *33* (1992) 163.

56. T.W. Garner and E.S. Yeung, *J. Chromatogr.*, *515* (1990) 639.

57. P.D. Curry Jr., C.E. Engstrom-Silverman, and A.G. Ewing, *Electroanalysis*, *3* (1991) 587.

58. A.G Ewing, J.M. Mesaros and P.F. Gavin, *Anal. Chem.*, *66* (1994) 527A.

59. X. Huang and R.N. Zare, *Anal. Chem.*, *59* (1987) 1762.

60. T.J. O'Shea, R.D. Greeenhagen, S.M. Lunte, C.E. Lunte, M.R. Smyth, D.M. Radzik, N.J. Watanabe, *J. Chromatogr.*, *593* (1992) 305.

61. W. Lu and R.M. Cassidy, *Anal. Chem.*, *66* (1994) 200.

62. L.A. Knecht, E.J. Guthrie and J.W. Jorgenson, *Anal. Chem.*, *56* (1984) 479.

63. T.M. Olefirowicz and A.G. Ewing, *Anal. Chem.*, *62* (1990) 1872.

64. J. Ye and R.P. Baldwin, *Anal. Chem.* *65* (1993) 3525.

65. L.A. Colon, R.Dadoo, and R.N. Zare, *Anal. Chem.*, *65* (1993) 476.

66. T.J. O'Shea, S.M. Lunte, and W.R. LaCourse, *Anal. Chem.*, *65* (1993) 948.

67. W. Lu and R.M. Cassidy, *Anal. Chem.*, *65* (1993) 2878.

68. R. Weinberger, *Practical Capillary Electrophoresis*, Academic Press, San Diego, CA, 1993, p. 282.

69. G.G. Neuberger and D.C. Johnson, *Anal. Chim. Acta*, *192* (1987) 205.

70. W.R. LaCourse and D.C. Johnson, *Anal. Chem. 65* (1993) 50.

ACKNOWLEDGEMENTS

I would like to express my gratitude to Dr. Johnson for his support and guidance throughout my graduate studies. I am also fortunate to have had the opportunity to work with the many talented members of Electrochemistry Group #1. In particular, I would like to thank Dobbs, Pete, Doug, Tiger and Joe for their friendship and assistance.

I give special thanks to my wife Carla for her perseverance during the hard times in my studies. Without her understanding and love none of this would have been possible.

I would also like to thank my close friends Dave, John, and Luther for the many diversions we pursued during our stay at Iowa State. Without them my life would have been boring. (I might have finished sooner, but I wouldn't have had any fun)

Finally, I would also like to thank my family and Carla's family for their love and support throughout my studies.